

Asteroseismology of 36 *Kepler* subgiants – I. Oscillation frequencies, linewidths and amplitudes

Yaguang Li,^{1,2,3*} Timothy R. Bedding,^{2,3} † Tanda Li,^{2,3} Shaolan Bi¹ ‡
Dennis Stello,^{4,2,3} Yixiao Zhou⁵ and Timothy R. White^{2,3}

¹Department of Astronomy, Beijing Normal University, Beijing 100875, China

²Sydney Institute for Astronomy (SIfA), School of Physics, University of Sydney, NSW 2006, Australia

³Stellar Astrophysics Centre, Department of Physics and Astronomy, Aarhus University, Ny Munkegade 120, DK-8000 Aarhus C, Denmark

⁴School of Physics, University of New South Wales, 2052, Australia

⁵Research School of Astronomy and Astrophysics, Australian National University, Canberra, ACT 2611, Australia

Accepted in xxx. Received in yyy; in original form zzz

ABSTRACT

The presence of mixed modes makes subgiants excellent targets for asteroseismology, providing a probe for the internal structure of stars. Here we study 36 *Kepler* subgiants with solar-like oscillations and report their oscillation mode parameters. We performed a so-called peakbagging exercise, i.e. estimating oscillation mode frequencies, linewidths, and amplitudes with a power spectrum model, fitted in the Bayesian framework and sampled with a Markov Chain Monte Carlo algorithm. The uncertainties of the mode frequencies have a median value of 0.180 μ Hz. We obtained seismic parameters from the peakbagging, analysed their correlation with stellar parameters, and examined against scaling relations. The behaviour of seismic parameters (e.g. $\Delta\nu$, ν_{\max} , ϵ_p) is in general consistent with theoretical predictions. We presented the observational p–g diagrams: $\gamma_1 - \Delta\nu$ for early subgiants and $\Delta\Pi_1 - \Delta\nu$ for late subgiants, and demonstrate their capability to estimate stellar mass. We also found a $\log g$ dependence on the linewidths and a mass dependence on the oscillation amplitudes and the widths of oscillation excess. This sample will be valuable constraints for modelling stars and studying mode physics such as excitation and damping.

Key words: stars: solar-type – stars: oscillations (including pulsations) – stars: low-mass

1 INTRODUCTION

Some of the first detections of solar-like oscillations, using ground-based spectroscopy, were in subgiant stars such as η Boo (Kjeldsen et al. 1995; Christensen-Dalsgaard et al. 1995; Guenther & Demarque 1996; Kjeldsen et al. 2003; Di Mauro et al. 2003b; Guenther 2004; Carrier et al. 2005), β Hyi (Bedding et al. 2001; Carrier et al. 2001; Di Mauro et al. 2003a; Fernandes & Monteiro 2003; Bedding et al. 2007; Brandão et al. 2011), ν Ind (Bedding et al. 2006; Carrier et al. 2007) and μ Her (Bonanno et al. 2008; Pinheiro & Fernandes 2010; Grundahl et al. 2017). Observations by the space telescopes *CoRoT* and *Kepler* enabled high-quality photometry with high duty cycle. These include subgiants such as HD 49385

(Deheuvels & Michel 2010; Paxton et al. 2013), HD 169392A (Mathur et al. 2013), KIC 11026764 (“Gemma”; Metcalfe et al. 2010), KIC 11395018 (“Boogie”; Mathur et al. 2011), KIC 10920273 and KIC 10273246 (“Scully” and “Mulder”; Campante et al. 2011), the α -enhanced star KIC 7976303 (Ge et al. 2015) and the binary twin system KIC 7107778 (Li et al. 2018).

Beginning with η Boo, it was realised that subgiants show mixed modes (Christensen-Dalsgaard et al. 1995), which are now recognised as a feature in all evolved stars. Main-sequence (MS) dwarfs with solar-like oscillations host a convective envelope, which excites and propagates pressure (p) modes. In subgiants, the so-called mixed modes that result from coupling between the pressure mode cavity and gravity (g) mode cavity carry information from the core and have observable amplitudes on the surface.

The mixed modes have long been realised to have strong diagnostic potential because the frequencies of g modes,

* yaguang.li@mail.bnu.edu.cn

† tim.bedding@sydney.edu.au

‡ bisl@bnu.edu.cn

which we denote by γ , evolve quite rapidly (Christensen-Dalsgaard et al. 1995). Bedding (2014) suggested a new asteroseismic diagram, the p–g diagram, which plots γ versus the large separation of p modes $\Delta\nu$. By comparing observed values of γ and $\Delta\nu$ with stellar models on this diagram, a stellar mass can be estimated. Benomar et al. (2012) showed that the coupling strength (see Section 3 below) is a strong indicator of evolutionary stage in subgiants. These suggestions of the diagnostic power of mixed modes were confirmed with modelling. When modelling Gemma (KIC 11026764), Metcalfe et al. (2010) showed that the asteroseismic age could be constrained to a precision of 15% that was set by the choice of input physics. Li et al. (2019) modelled μ Her and demonstrated that the asteroseismic age did not significantly change as a function of the mixing-length parameter, or the initial helium abundance. In addition to global parameters, the mixed modes also shed light on the interior physics of stars, for example, constraining the buoyancy frequency profile (Li et al. 2019), internal angular momentum transport (Deheuvels et al. 2014; Eggenberger et al. 2019) and convective core overshooting (Deheuvels et al. 2016).

A complete analysis of oscillation modes has been made for *Kepler* observations of 35 planet-host stars (Davies et al. 2016) and 66 MS stars (Lund et al. 2017), the so-called LEGACY sample. However, similar analyses for subgiants has only been done on a subset of *Kepler* data (e.g. Appourchaux et al. 2012). Therefore it is valuable to gather and analyse subgiants with the full set of *Kepler* observations, given the great promise of mixed modes. In this paper, we fit the oscillation modes and analyse the fitted frequencies, linewidths and amplitudes from the fit. In a companion paper (Paper II, T. Li et al. submitted), we perform a detailed modelling to these stars with the constraints of frequencies obtained here.

2 OBSERVATIONS

We considered *Kepler* targets observed in short cadence mode, which samples at an integration time $\Delta t = 58.89$ s, or frequency $f_s = 1/\Delta t = 16980.8 \mu\text{Hz}$. There are about 5000 stars observed in this mode, and we detected about 50 subgiants. In this context, we define subgiants as stars showing oscillations of mixed modes, recognised as mode bumping (see Section 3.1 for a detailed discussion), which starts around the time of hydrogen exhaustion in the core. However, we required that the density of the mixed modes should be low enough, such that $\Delta\Pi_1 > \Delta\nu/\nu^2$, where $\Delta\Pi_1$ is the period spacing of dipolar g modes. This occurs around the subgiant phase. Only subgiants with high signal-to-noise ratios (S/N) were selected to avoid any ambiguity of the correct assignment of the spherical degree l of each mode (see Section 3.1 below). Further, we required the observation duration, denoted by t_{obs} , to be at least two months. This resulted in a total of 36 subgiants that we analyse here.

The atmospheric parameters (T_{eff} and $[\text{Fe}/\text{H}]$) were adopted from the KIC DR25 release (Mathur et al. 2017). Table 1 lists the 36 stars in our sample along with t_{obs} , nicknames used in previous papers and references to any previous studies. Figure 1 shows the targets in the $\Delta\nu - T_{\text{eff}}$ plane. They extend from the MS turnoff phase to the bottom

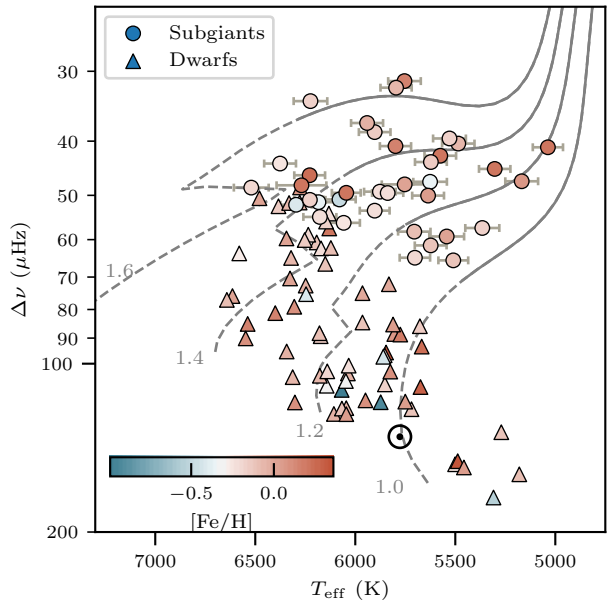


Figure 1. Asteroseismic H-R diagram showing $\Delta\nu$ vs. T_{eff} for the 36 subgiants shown as black circles colour-coded by metallicity. For comparison, the LEGACY sample (Lund et al. 2017) is together shown in triangles labelled as dwarfs. The Sun is marked by the usual symbol. The theoretical evolutionary tracks with solar metallicity (Stello et al. 2013) are shown before (dashed lines) and after (solid lines) the exhaustion of central hydrogen, with each track labelled with mass in solar units.

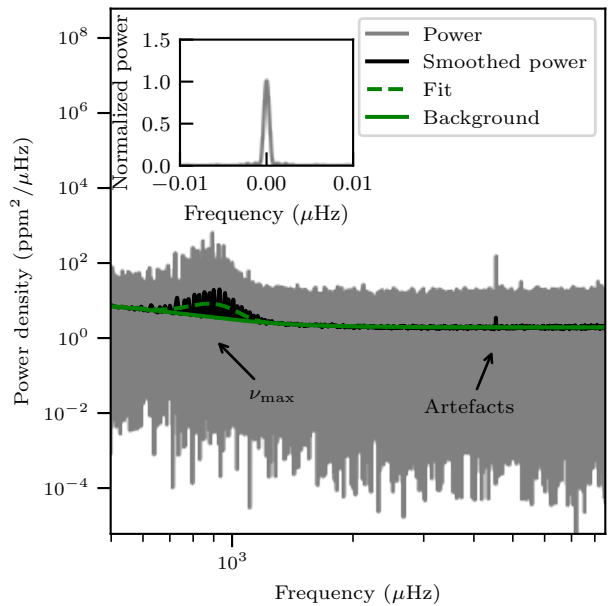


Figure 2. Power spectrum density of Gemma (KIC 11026764). The original (grey), smoothed (black) and fitted power spectra (green) are shown. The peaks around $4500 \mu\text{Hz}$ are artifacts (Gilliland et al. 2010). The inset shows the normalised spectral window.

Table 1. Observational properties.

KIC	Nickname	t_{obs} (d)	T_{eff} (K)	$\log g$ (cgs; dex)	[Fe/H] (dex)	References
2991448	—	204	5623 ± 80	3.98 ± 0.02	-0.10 ± 0.15	—
3852594	—	540	6296 ± 78	4.02 ± 0.14	-0.40 ± 0.15	—
4346201	—	108	6058 ± 81	3.97 ± 0.01	-0.24 ± 0.17	—
5108214	—	222	5799 ± 78	3.81 ± 0.07	0.16 ± 0.15	—
5607242	—	1031	5485 ± 81	3.76 ± 0.06	-0.06 ± 0.15	a
5689820	—	506	5037 ± 76	3.76 ± 0.06	0.21 ± 0.15	b
5955122	Rhapsody	988	5877 ± 79	3.87 ± 0.01	-0.22 ± 0.15	a
6064910	—	532	6376 ± 80	3.83 ± 0.01	-0.26 ± 0.17	—
6370489	—	97	6184 ± 80	3.92 ± 0.01	-0.36 ± 0.15	—
6442183	Dougal	822	5702 ± 76	4.00 ± 0.01	-0.20 ± 0.15	c, d
6693861	—	565	5626 ± 84	3.84 ± 0.02	-0.36 ± 0.15	—
6766513	—	534	6227 ± 78	3.93 ± 0.02	-0.18 ± 0.15	—
7174707	—	1031	5168 ± 82	3.71 ± 0.12	0.07 ± 0.15	—
7199397	—	1182	5903 ± 79	3.76 ± 0.07	-0.14 ± 0.15	e
7668623	—	112	6228 ± 77	3.87 ± 0.02	0.24 ± 0.15	—
7747078	—	986	5903 ± 74	3.90 ± 0.01	-0.22 ± 0.15	a
7976303	John	962	6079 ± 81	3.89 ± 0.06	-0.48 ± 0.15	a
8026226	Gypsy	305	6224 ± 84	3.70 ± 0.06	-0.18 ± 0.17	a
8524425	Katrina	1006	5543 ± 87	3.97 ± 0.01	0.02 ± 0.17	a
8702606	—	980	5529 ± 82	3.76 ± 0.06	-0.16 ± 0.15	a, b
8738809	—	341	6045 ± 72	3.90 ± 0.01	0.20 ± 0.12	—
9512063	—	110	5838 ± 78	3.88 ± 0.02	-0.22 ± 0.15	—
10018963	Klaas	936	6177 ± 82	3.93 ± 0.01	-0.22 ± 0.17	a
10147635	—	761	5941 ± 80	3.75 ± 0.02	-0.02 ± 0.15	—
10273246	Mulder	705	6269 ± 124	4.41 ± 0.07	0.21 ± 0.15	f
10593351	—	528	5754 ± 82	3.66 ± 0.06	0.16 ± 0.15	—
10873176	—	122	6520 ± 87	3.90 ± 0.01	-0.20 ± 0.28	—
10920273	Scully	532	5365 ± 85	3.78 ± 0.12	-0.16 ± 0.15	f
10972873	—	878	5705 ± 81	3.96 ± 0.02	-0.08 ± 0.15	—
11026764	Gemma	985	5636 ± 80	3.89 ± 0.06	0.04 ± 0.15	a
11137075	Zebedee	530	5510 ± 74	4.00 ± 0.01	-0.12 ± 0.12	c
11193681	—	1026	5575 ± 79	3.79 ± 0.06	0.21 ± 0.15	a
11395018	Boogie	562	5753 ± 114	3.65 ± 0.18	0.02 ± 0.15	a, g
11414712	Jingle	943	5622 ± 80	3.80 ± 0.06	-0.14 ± 0.15	a
11771760	—	1030	5796 ± 78	3.67 ± 0.06	-0.06 ± 0.17	a
12508433	—	999	5303 ± 78	3.83 ± 0.06	0.20 ± 0.15	a, b

Note: (a) Appourchaux et al. (2012); (b) Deheuvels et al. (2014); (c) Tian et al. (2015); (d) Appourchaux et al. (2014); (e) Davies et al. (2016); (f) Campante et al. (2011); (g) Mathur et al. (2011).

of red giant branch. The MS stars in the *Kepler* LEGACY sample (Lund et al. 2017) are also shown.

We used light curves measured from simple aperture photometry (SAP) by the Kepler Science Center¹. We corrected instrumental effects with the KASOC FILTER². For a full description of this reduction procedure, see García et al. (2011) and Handberg & Lund (2014). Briefly, it constructs moving-median high-pass filters, one with $\tau_{\text{long}} = 1/2$ d, and one with $\tau_{\text{short}} = 1/24$ d. Trends longer than $1/\tau_{\text{long}} \sim 23$ μHz are removed, and any sharp feature that could produce drastically different signals for the two filters are eliminated. The light curves were converted into relative flux in ppm (parts per million) and we calculated power spectra by a Lomb-Scargle Periodogram algorithm (Lomb 1976; Scargle 1982), equivalent to a sine-wave fitting, as implemented in ASTROPY (Astropy Collaboration et al. 2013, 2018). The power density spectra were constructed by multiplying the power by the total observing time (Kjeldsen & Bed-

ding 1995). Figure 2 uses Gemma (KIC 11026764) as an example to illustrate the power density spectrum and the spectral window. The former is comprised of a background and a group of peaks with a Gaussian-like envelope centred on ν_{max} . Although there are small gaps in the original data, they have a negligible influence on the shape of oscillation modes. This can be seen from the fact that the spectral window has sidelobes with very low power.

3 PARAMETER ESTIMATION

3.1 Mode identification

Each oscillation mode is associated with three quantum numbers (n, l, m). The first step in mode identification is to assign an l -degree to each peak. In the asymptotic regime ($n \gg l$) of p modes (Tassoul 1980; Gough 1986), this is straightforward because modes follow regular patterns. The frequencies are approximately equally spaced by $\Delta\nu$:

$$\nu_p(n_p, l) \approx \Delta\nu \left(n_p + \frac{l}{2} + \epsilon_p \right) - \delta\nu_{0l}, \quad (1)$$

¹ <https://archive.stsci.edu/kepler/>

² <https://github.com/tasoc/corrections>

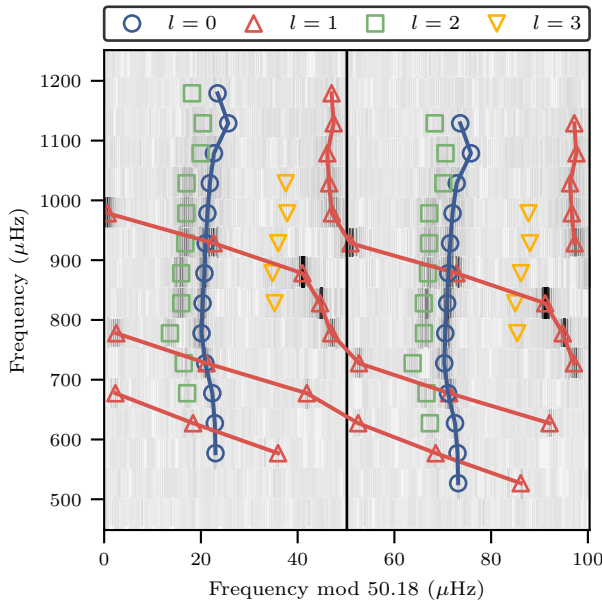


Figure 3. Replicated échelle diagram for Gemma (KIC 11026764). By shifting one $\Delta\nu$ downwards for the right replicate, the dipolar modes can be traced by a single line with one mode per horizontal row. The grey scale denotes the square-root of S/N to enhance contrast. The symbols represent extracted frequencies.

where $\Delta\nu$ is the separation between adjacent radial modes, ϵ_p is the offset of the pattern, and the small separation $\delta\nu_{0l}$ defines the frequency differences between $l = 0$ and l . The g modes, which we do not observe directly, are approximately equally spaced in period in the asymptotic regime:

$$\Pi_g(n_g, l) = \nu_g^{-1}(n_g, l) \approx \Delta\Pi_l(n_g + \epsilon_g), \quad (2)$$

where $\Delta\Pi_l$ and ϵ_g are the period spacing and offset for g modes. Shibahashi (1979) derived an asymptotic relation for mixed modes. Specifically, for dipolar modes ($l = 1$) the mixed mode frequencies ν_m satisfy

$$\tan\theta_p = q \tan\theta_g, \quad (3)$$

where

$$\theta_p = \frac{\pi}{\Delta\nu} (\nu_m - \nu_p), \quad (4)$$

$$\theta_g = \frac{\pi}{\Delta\Pi_1} \left(\frac{1}{\nu_m} - \frac{1}{\nu_g} \right), \quad (5)$$

and q is a coupling factor determined by the width of the evanescent zone. Less-evolved subgiants have large period spacings, with one g mode often coupling with several p modes. The coupled modes can be bumped very far away from their regular p-mode spacings. By replicating échelle diagrams horizontally, a line can trace all mixed modes, which helps mode identification (Bedding 2012; Benomar et al. 2012). See Figure 3 for an illustration. Using this method, we were able to make unambiguous identifications for mixed dipolar modes, which still have a detectable amplitude even when they are bumped by a large amount. However, that is not the case for quadrupolar ($l = 2$) modes

due to their weaker couplings. Therefore, in most cases we only expect to detect one mixed quadrupolar mode in each order, even though sometimes two should be present. The same is true for octupolar ($l = 3$) modes. To sum up, the dipolar mixed modes follow Equation 3 closely, and the radial, quadrupolar and octupolar modes are distributed regularly, approximately as described by Equation 1.

We first obtained a crude estimate of $\Delta\nu$ by tuning the horizontal width of the échelle diagram such that the ridge of radial modes was vertical. To identify modes in each star, we smoothed the power spectrum and folded by $\Delta\nu$ to create a collapsed power spectrum. This was cross-correlated with a template spectrum comprising three peaks, two narrower ($l = 0$ and $l = 2$) and one wider ($l = 1$), to simulate the ridges. The value of ϵ_p , which defines the location of $l = 0$, could be correctly identified according to the lag at which the correlation coefficient was the largest. The modes satisfying $(\nu/\Delta\nu \bmod 1) \in [\epsilon_p - 0.04, \epsilon_p + 0.04]$, $[\epsilon_p - 0.12, \epsilon_p - 0.04]$ and $[\epsilon_p + 0.31, \epsilon_p + 0.39]$ were labelled as $l = 0, 2$ and 3 , respectively. These ranges were first empirically chosen. The reason is that $\delta\nu_{0l}$ approximately follows a linear trend with $\Delta\nu$ and the slope is consistent with the ranges defined by those numbers (see Section 4). All other modes were provisionally assigned as $l = 1$, noting that some $l = 0, 2$ and 3 modes could actually be $l = 1$. We used the relative height ($l = 1$ modes are typically higher) and the regularity of those modes (Eq. 1) to help resolve the ambiguity. All labels were further confirmed in échelle diagrams using the method mentioned above. We identified all modes within $\pm 8\Delta\nu$ around ν_{\max} . The identified peaks were used as inputs for the peakbagging.

3.2 Power spectrum model

We now describe the model used to fit the power spectrum. First, we consider the background caused by granulation, modelled as a sum of Lorentzian profiles:

$$B(\nu) = \sum_{i=1}^n \frac{2\sqrt{2}}{\pi} \frac{a_i^2/b_i}{1 + (\nu/b_i)^{c_i}}. \quad (6)$$

The number of power profiles was set to be $n = 1$ or 2 (Harvey 1985; Kallinger et al. 2014), subject to the goodness of fit, which is sufficient to account for the background near ν_{\max} . Second, we describe the signal of oscillations. For a mode with quantum number (n, l, m) , we adopted a power spectrum model

$$L_{nlm}(\nu) = \frac{\mathcal{E}_{lm}(i^*) 2A_{nl}^2 / (\pi\Gamma_{nl})}{1 + 4(\nu - \nu_{nl} + m\nu_{s,nl})^2 / \Gamma_{nl}^2} \quad (7)$$

to account for oscillations, where the frequency ν_{nl} , linewidth Γ_{nl} , amplitude A_{nl} , and rotational splitting $\nu_{s,nl}$ varies with n and l (Anderson et al. 1990). The relative height within a multiplet depends on the inclination angle i^* of the star and is modulated by a visibility function:

$$\mathcal{E}_{lm}(i^*) = \frac{(l - |m|)!}{(l + |m|)!} \left[P_l^{|m|}(\cos i^*) \right]^2, \quad (8)$$

where $P_l^{|m|}$ are Legendre functions (Gizon & Solanki 2003). The final model to fit the whole power spectrum was

$$M(\nu) = \eta^2(\nu) \left[\sum_{n=n_{\min}}^{n_{\max}} \sum_{l=0}^3 \sum_{m=-l}^l L_{nlm}(\nu) + B(\nu) \right] + W. \quad (9)$$

We used a frequency-independent constant W to account for white/photon noise. The apodisation of the signal due to the integration time $\Delta t = 58.89$ s was

$$\eta^2(\nu) = \frac{\sin^2(\pi\nu\Delta t)}{(\pi\nu\Delta t)^2}. \quad (10)$$

The free parameters to fit the power spectrum were $\theta = \{\nu_{nl}, A_{nl}, \Gamma_{nl}, \nu_{s,nl}, i^*, a_i, b_i, c_i, W\}$.

3.3 Fitting method

We estimated the model parameters in the Bayesian framework (Handberg & Campante 2011). Given data D , model M and prior information I , the parameters θ were estimated via posterior probability using Bayes' theorem:

$$p(\theta|D, M, I) = \frac{p(\theta|M, I)p(D|\theta, M, I)}{p(D|M, I)}. \quad (11)$$

The posterior probability can be seen as a product of the prior and the likelihood function, divided by the Bayesian evidence, which is the marginalisation of that product over all parameter space.

We utilised three kinds of prior functions. The first was a uniform prior, which sets the prior probability as a constant over a parameter range:

$$p(\theta|M, I) = \begin{cases} \frac{1}{\theta_{\max} - \theta_{\min}}, & \theta_{\min} < \theta < \theta_{\max} \\ 0, & \text{otherwise} \end{cases} \quad (12)$$

We used uniform priors for most parameters. For example, the priors on the frequencies, ν_{nl} , were set to be $3\,\mu\text{Hz}$ ranges centred around their initial guessed values. The inclination angle was assigned a uniform prior across $[-\pi/2, \pi]$ and folded to $[0, \pi/2]$ after sampling. We also tested an isotropic prior for the inclination, but found no significant bias on mode parameters. The second is a modified Jeffreys prior, which was set for the linewidths and amplitudes:

$$p(\theta|M, I) = \begin{cases} \frac{1}{\theta + \theta_{\text{uni}}} \frac{1}{\log((\theta_{\text{uni}} + \theta_{\max})/\theta_{\text{uni}})}, & 0 < \theta < \theta_{\max} \\ 0, & \text{otherwise} \end{cases} \quad (13)$$

We tested the impact of adopting uniform priors for these two particular parameters. The amplitudes do not present obvious bias while the linewidths are typically overestimated using the uniform priors. Despite the present bias, more than 95% modes in our sample agree within $1-\sigma$. For the splitting frequency, $\nu_{s,nl}$, we used the third prior, a flat prior with a half Gaussian:

$$p(\theta|M, I) = \begin{cases} 0, & \theta < S \\ C, & S \leq \theta < U \\ C \cdot \exp\left[-\frac{(\theta - U)^2}{2\sigma^2}\right], & \theta \geq U \end{cases} \quad (14)$$

where $C = (U - S + \sqrt{\pi/2}\sigma)^{-1}$. We applied this prior to $\nu_{s,nl}$ with $S = 0\,\mu\text{Hz}$, $U = 1\,\mu\text{Hz}$ and $\sigma = 0.5\,\mu\text{Hz}$ (Deheuvels et al. 2014).

Gaussian noise in the time domain translates to a χ^2 distribution with 2 degrees of freedom in the frequency domain (in power). Assuming all frequency bins, indexed by

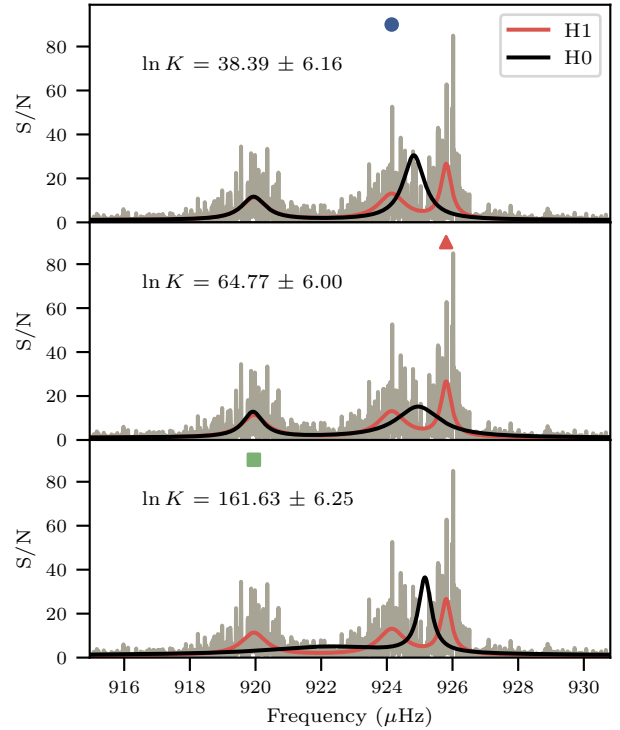


Figure 4. Significance tests for three modes of Gemma (KIC 11026764). Each panel presents the fits of the mode marked by the symbol, under H1 and H0 hypotheses separately. All three modes show very strong detections according to the Kass & Raftery (1995) scale.

i in the power spectrum, are statistically independent, the logarithm of the likelihood function is

$$\ln p(D|\theta, M, I) = - \sum_i \left[\ln M_i(\theta) + \frac{D_i}{M_i(\theta)} \right]. \quad (15)$$

We used an H1 (odds ratio) approach to test whether a frequency range contains a mode (Appourchaux et al. 2012; Corsaro & De Ridder 2014; Davies et al. 2016). H1 is the hypothesis that a range of a power spectrum contains the mode, while H0 is the null hypothesis. In short, we computed the Bayes factor $\ln K = \ln p(D|M_1, I) - \ln p(D|M_0, I)$ and assessed it based on the Kass & Raftery (1995) scale:

$$\ln K = \begin{cases} < 0 & \text{favours H0} \\ 0 - 1 & \text{not worth more than a bare mention} \\ 1 - 3 & \text{positive} \\ 3 - 5 & \text{strong} \\ > 5 & \text{very strong.} \end{cases} \quad (16)$$

3.4 Fitting details

Based on the methods mentioned in the previous sections, we fitted the data as follows:

- (i) The power spectrum was initially fitted with Equation 9 but the sum of Lorentzians was replaced by a single Gaussian profile centred around ν_{\max} (see Figure 2). The

background spectrum was determined from this fit. By dividing the signal by the background, we obtained the S/N spectrum, which fluctuates around 1.

(ii) We selected seven modes with the highest amplitudes to fit simultaneously and to determine the inclination angle by maximising the posterior probability.

(iii) The power spectrum was divided into segments and modes were fitted in each segment separately with a fixed inclination determined in step (ii). The sizes of the segments were based on the proximity of consecutive mode frequencies. Any two modes closer than $10 \mu\text{Hz}$ were grouped into the same segment. There was a minimum of one and a maximum of five modes per segment. The estimation of each parameter was obtained by marginalising the posterior probability and calculating median and 68 per cent credible limit values.

(iv) The Bayes factor was calculated for each mode to evaluate its significance, by comparing the Bayesian evidence with or without that mode in the model. Figure 4 shows the fit of the three modes in a segment. All of them have very strong detections.

We developed python software called SOLARLIKEPEAK-BAGGING³, providing a wrapper for the Markov Chain Monte Carlo (MCMC) sampling algorithm implemented in EMCEE (Goodman & Weare 2010; Foreman-Mackey et al. 2013), also featuring customisable Bayesian statistics, models, and other fitting algorithms. For the above fits, the sampler was chosen either to be an affine-invariant ensemble sampler (step ii) or a parallel-tempering sampler with 20 temperatures (step iii), depending on whether the Bayes factor was calculated. We initialised 500 walkers with values adopted from a least-squares fit, then burned-in for 1000 steps and iterated for 2000 steps. After each run, we checked convergence and the goodness of sampling by several metrics, including auto-correlation time, acceptance fraction, the evolution of model parameters, and the shapes of the marginal probability distributions.

3.5 Fitting results

We present mode frequencies, amplitudes and linewidths for $m = 0$ modes in Table 2. The rotational splittings will be comprehensively studied in a future paper. Figure 5 shows the power spectrum of Gemma (KIC 11026764) with fitted mode frequencies overlaid. We present the plots of the other stars in the Appendix.

In Figure 6, we show the histograms of uncertainties. The median value of frequency uncertainties is $0.180 \mu\text{Hz}$. As expected, the uncertainty is a function of S/N. The typical uncertainty is $0.1 \mu\text{Hz}$ for S/N=3. The median uncertainties of linewidths are 31.7% and amplitudes are 10.1%.

As a check, we can consider the classical maximum likelihood estimator (MLE; Libbrecht 1992; Toutain & Apourchaux 1994; Ballot et al. 2008). This calculates uncertainties by inverting the Hessian matrix whose elements are the second derivatives of the likelihood function to the parameters. The Cramér-Rao bound states that an unbiased MLE reaches the lowest variance bound, so any other unbiased estimators are expected to obtain a larger variance.

³ <https://github.com/parallelpro/SolarlikePeakbagging>

Libbrecht (1992) derived an analytical form of the uncertainty. We found the estimated uncertainties derived from the MCMC-based posterior distributions were typically larger than those obtained from the above analytical forms, by factors of 1.15 (frequency), 1.18 (linewidth) and 1.41 (height), respectively. Thus the uncertainties are safe to use for modelling.

4 MODE FREQUENCIES

We fitted the radial mode frequencies with Equation 1 to estimate $\Delta\nu$ and ϵ_p . The errors were considered within the Bayesian framework thus they were propagated from the priors and likelihoods. The likelihood function was selected to reflect the residuals between data and the models, weighted by uncorrelated uncertainties from both dependent and independent variables, as normal distributions.

The p mode offset ϵ_p is sensitive to the lower and upper turning points of a mode (e.g. Gough 1986). It has been demonstrated to vary with T_{eff} and $\Delta\nu$ (White et al. 2011b; Hon et al. 2018), and was used to resolve ambiguous mode identification problems found in F-type dwarfs (White et al. 2012) and to discriminate between red-giant-branch (RGB) and helium-core-burning (HeB) stars (Kallinger et al. 2012). The upper turning point lies at the surface, where T_{eff} and $\log g$ are relevant quantities, so it may be conjectured that ϵ_p is related to both of them. In Figure 7 we present ϵ_p as a function of T_{eff} . As Ong & Basu (2019) pointed out, ϵ_p depends on the method of measurement, so we recalculated the ϵ_p of the MS dwarfs from Lund et al. (2017) using our approach. As the figure shows, the general trend of ϵ_p in subgiants follows a similar pattern as for dwarfs. We also identify a dependence on $\log g$: stars with similar T_{eff} but smaller $\log g$ have lower ϵ_p . The dwarf stars, which have higher $\log g$, sit above the subgiants on the $\epsilon_p - T_{\text{eff}}$ diagram. In the bottom panel of Figure 8, we present ϵ_p as a function of $\Delta\nu$. The obvious offset between observations and stellar models stems from the improper modelling of near-surface layers (Christensen-Dalsgaard et al. 1988).

We show the small separations $\delta\nu_{02}$ versus $\Delta\nu$ in Figure 8, the so-called C–D diagram (Christensen-Dalsgaard 1984; Mazumdar 2005). The evolutionary tracks with different masses are well separated on the main sequence. By comparing to models, the diagram is useful for estimating mass and age when $\delta\nu_{02}$ and $\Delta\nu$ are known. We note that the $\epsilon_p - \Delta\nu$ diagram could be used for a similar purpose, provided the surface effect is well accounted for. However, the tracks become more degenerate in the subgiant phase (White et al. 2011a,b). We performed a linear fit to the subgiants:

$$\delta\nu_{02} = (0.088 \pm 0.001)\Delta\nu + (0.070 \pm 0.059) \mu\text{Hz}. \quad (17)$$

We point out that some obvious outliers from the fitted line are present. They are affected by bumped $l = 2$ modes, which lift the average distance of a quadrupolar mode to a radial mode. Bedding et al. (2010) fitted the same relation to a sample of red giants, which have a steeper slope (as shown by the dashed line in Figure 8). This difference is also visible from the calculation of stellar models. Similarly, we fitted $\delta\nu_{03}$ using ten stars that have detected $l = 3$ modes:

$$\delta\nu_{03} = (0.152 \pm 0.002)\Delta\nu + (2.578 \pm 0.102) \mu\text{Hz}. \quad (18)$$

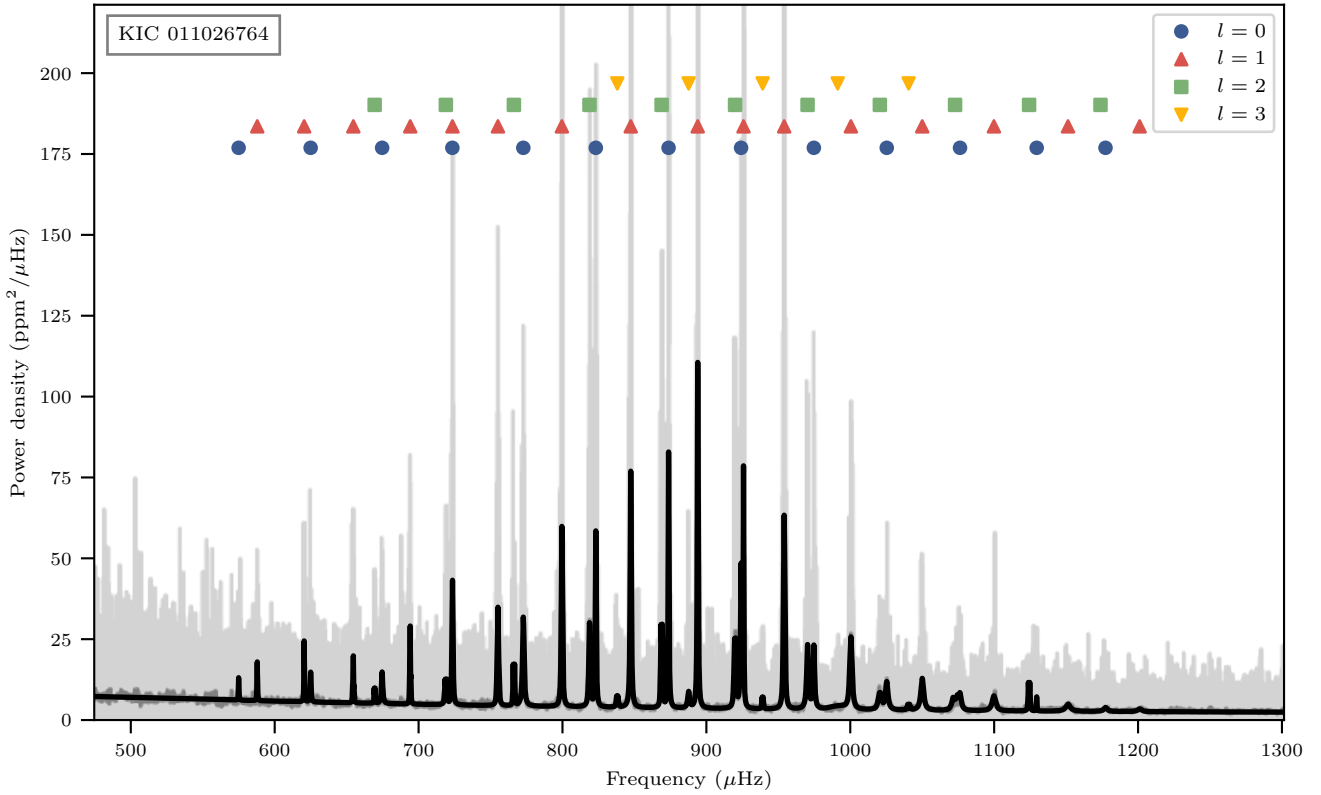


Figure 5. Power spectrum of Gemma (KIC 11026764). The fitted power spectrum (black) is overlaid on the original power spectrum (light grey).

Table 2. Mode parameters obtained from the peakbagging. These are $m = 0$ modes. Only the first 10 rows are shown. The full table is available online.

KIC	l	ν_{nl} (μHz)	Γ_{nl} (μHz)	A_{nl} (ppm)	$\ln K$
2991448	0	889.34 ± 0.312	0.79 ± 0.96	5.72 ± 1.53	2.16 ± 0.75
2991448	0	949.46 ± 1.111	8.02 ± 2.37	12.95 ± 1.61	3.61 ± 0.98
2991448	0	1011.17 ± 0.202	1.15 ± 0.46	9.47 ± 1.23	20.49 ± 4.32
2991448	0	1072.78 ± 0.099	0.76 ± 0.24	14.78 ± 1.49	39.42 ± 2.54
2991448	0	1134.18 ± 0.113	0.89 ± 0.28	14.21 ± 1.38	47.86 ± 2.81
2991448	0	1195.89 ± 0.547	3.29 ± 1.72	13.37 ± 2.38	5.40 ± 2.13
2991448	0	1257.81 ± 0.969	3.53 ± 2.63	10.04 ± 2.96	2.68 ± 1.52
2991448	0	1319.52 ± 1.294	3.00 ± 3.56	5.09 ± 3.29	0.18 ± 1.20
2991448	1	857.88 ± 0.384	0.97 ± 0.79	5.88 ± 1.62	-0.21 ± 0.69
2991448	1	915.60 ± 0.153	0.81 ± 0.32	9.62 ± 1.27	19.19 ± 1.16

Finally, we use the radial modes to determine ν_{\max} because they are purely acoustic, since there are no radial g modes for them to couple with. By fitting the amplitudes versus frequencies of radial modes with a Gaussian function, ν_{\max} was obtained as the Gaussian's centre. The height of the Gaussian, A_{\max} , together with the width, are analysed in Section 7. We fitted the well-established $\Delta\nu - \nu_{\max}$ relation (e.g. Stello et al. 2009; Huber et al. 2009) to our subgiants:

$$\Delta\nu = a(\nu_{\max}/\mu\text{Hz})^b \mu\text{Hz}, \quad (19)$$

and determined the best fitted parameters as $a = 0.158 \pm 0.036$ and $b = 0.847 \pm 0.034$. Huber et al. (2011) determined $a = 0.22$ and $b = 0.797$ from a sample consisting of both MS stars and red giants. We plot the two relations in Figure 9.

The most noticeable effect is that the subgiants lie above the dwarfs, which can be understood from simple scaling arguments. The asteroseismic scaling relations (Brown et al. 1991; Kjeldsen & Bedding 1995) state that $\Delta\nu \propto \sqrt{\rho} \propto M^{1/2} R^{-3/2}$, and $\nu_{\max} \propto g/\sqrt{T_{\text{eff}}} \propto MR^{-2} T_{\text{eff}}^{-1/2}$. Dividing the two relations, we obtain $\Delta\nu/\nu_{\max} \propto M^{-1/2} R^{1/2} T_{\text{eff}}^{-1/2}$. The subgiants and dwarfs have similar M and T_{eff} , but subgiants are more inflated, which ultimately leads to higher $\Delta\nu/\nu_{\max}$. Indeed, this spread is the signal upon which the widely-used scaling relations for mass and radius are based (Stello et al. 2008; Kallinger et al. 2010).

Table 3. Global Oscillation parameters.

KIC	$\Delta\nu$ (μHz)	ϵ_p	ν_{\max} (μHz)	A_{\max} (ppm)	Width (μHz)	$\delta\nu_{02}$ (μHz)	$\delta\nu_{03}$ (μHz)	γ_1 (μHz)	$\Delta\Pi_1$ (s)
2991448	61.35 ± 0.05	1.486 ± 0.013	1115 ± 16	9.83 ± 0.45	187.3 ± 21.9	5.38 ± 0.41	—	1022.0 ± 0.3	—
3852594	51.95 ± 0.06	1.270 ± 0.018	912 ± 8	13.00 ± 0.35	181.3 ± 12.7	—	—	—	—
4346201	56.00 ± 0.04	1.169 ± 0.014	1123 ± 107	8.07 ± 0.48	366.5 ± 129.1	5.26 ± 0.53	—	812.2 ± 2.6	—
5108214	40.81 ± 0.02	1.309 ± 0.007	712 ± 7	9.51 ± 0.35	197.2 ± 11.8	3.38 ± 0.24	—	—	411 ± 23
5607242	40.39 ± 0.01	1.444 ± 0.003	684 ± 2	10.76 ± 0.27	114.4 ± 3.7	3.77 ± 0.14	8.77 ± 0.13	—	176 ± 16
5689820	41.02 ± 0.01	1.561 ± 0.002	683 ± 4	13.85 ± 0.47	100.1 ± 5.0	3.81 ± 0.21	9.24 ± 0.39	—	154 ± 2
5955122	49.22 ± 0.01	1.340 ± 0.004	861 ± 4	9.04 ± 0.14	175.5 ± 5.6	4.02 ± 0.23	—	1143.9 ± 10.0	—
6064910	43.82 ± 0.08	1.160 ± 0.032	649 ± 197	12.75 ± 0.98	456.8 ± 275.9	—	—	—	390 ± 5
6370489	51.22 ± 0.03	1.394 ± 0.010	907 ± 13	9.50 ± 0.44	220.6 ± 19.7	5.21 ± 0.37	—	937.6 ± 0.8	—
6442183	64.65 ± 0.01	1.490 ± 0.002	1166 ± 3	7.82 ± 0.13	206.1 ± 4.3	5.42 ± 0.21	12.33 ± 0.09	1005.6 ± 0.1	—
6693861	47.26 ± 0.01	1.402 ± 0.005	818 ± 9	10.76 ± 0.38	147.9 ± 12.3	4.89 ± 0.13	—	—	—
6766513	50.91 ± 0.04	1.151 ± 0.013	945 ± 18	9.03 ± 0.43	288.3 ± 29.2	4.09 ± 0.50	—	799.3 ± 0.4	—
7174707	47.19 ± 0.01	1.492 ± 0.003	819 ± 4	11.22 ± 0.30	118.4 ± 4.9	5.35 ± 0.23	10.14 ± 0.18	—	172 ± 5
7199397	38.54 ± 0.01	1.353 ± 0.005	661 ± 6	9.87 ± 0.21	148.9 ± 6.5	3.53 ± 0.25	—	—	228 ± 45
7668623	46.05 ± 0.05	1.033 ± 0.019	889 ± 18	8.77 ± 0.39	216.8 ± 25.4	5.40 ± 0.60	—	675.2 ± 1.1	—
7747078	53.22 ± 0.01	1.475 ± 0.002	931 ± 5	8.14 ± 0.13	187.7 ± 5.8	4.30 ± 0.24	—	1031.7 ± 0.2	—
7976303	50.85 ± 0.01	1.346 ± 0.003	866 ± 4	9.21 ± 0.13	182.3 ± 4.7	5.09 ± 0.22	—	979.4 ± 0.6	—
8026226	33.85 ± 0.02	1.231 ± 0.010	611 ± 90	8.03 ± 0.54	334.5 ± 160.0	3.15 ± 0.31	—	—	343 ± 25
8524425	59.23 ± 0.01	1.539 ± 0.001	1069 ± 3	8.96 ± 0.15	184.2 ± 4.4	5.09 ± 0.22	10.15 ± 0.72	1049.6 ± 0.1	—
8702606	39.55 ± 0.01	1.416 ± 0.002	667 ± 2	10.74 ± 0.20	116.8 ± 2.5	3.97 ± 0.08	8.70 ± 0.25	—	167 ± 17
8738809	49.44 ± 0.02	1.178 ± 0.008	905 ± 9	8.40 ± 0.31	217.6 ± 11.4	3.86 ± 0.24	—	852.4 ± 0.2	—
9512063	49.55 ± 0.02	1.340 ± 0.008	890 ± 23	7.93 ± 0.53	238.1 ± 62.7	4.55 ± 0.27	—	—	—
10018963	54.66 ± 0.01	1.352 ± 0.003	1035 ± 6	7.55 ± 0.12	246.5 ± 5.9	4.63 ± 0.19	—	786.0 ± 0.3	—
10147635	37.08 ± 0.01	1.303 ± 0.006	672 ± 15	8.84 ± 0.39	190.9 ± 19.6	3.26 ± 0.25	—	683.9 ± 0.3	—
10273246	47.98 ± 0.02	1.391 ± 0.006	881 ± 8	10.58 ± 0.36	189.8 ± 10.4	4.19 ± 0.28	—	977.8 ± 1.0	—
10593351	31.18 ± 0.01	1.354 ± 0.006	543 ± 5	12.77 ± 0.47	133.8 ± 7.1	3.49 ± 0.24	—	—	350 ± 23
10873176	48.43 ± 0.11	1.314 ± 0.037	845 ± 11	14.34 ± 0.90	117.6 ± 11.8	—	—	—	—
10920273	57.19 ± 0.02	1.435 ± 0.007	1035 ± 13	10.73 ± 0.40	185.4 ± 22.0	5.19 ± 0.22	—	—	—
10972873	58.07 ± 0.01	1.469 ± 0.003	1033 ± 5	8.84 ± 0.17	186.3 ± 6.1	5.26 ± 0.21	10.57 ± 0.13	1041.7 ± 0.1	—
11026764	50.07 ± 0.01	1.454 ± 0.003	866 ± 3	8.08 ± 0.13	171.5 ± 4.0	4.74 ± 0.19	10.09 ± 0.23	926.4 ± 0.1	—
11137075	65.35 ± 0.01	1.510 ± 0.003	1177 ± 7	9.66 ± 0.29	181.7 ± 11.0	6.31 ± 0.18	—	1143.6 ± 0.1	—
11193681	42.48 ± 0.01	1.497 ± 0.004	737 ± 4	10.21 ± 0.20	151.5 ± 5.6	3.81 ± 0.16	—	—	—
11395018	47.76 ± 0.02	1.330 ± 0.006	852 ± 10	10.35 ± 0.25	171.7 ± 15.9	4.32 ± 0.18	—	—	MNRAS 000 , 000–000 (2018)
11414712	43.62 ± 0.01	1.444 ± 0.002	750 ± 3	8.73 ± 0.15	146.4 ± 3.4	4.11 ± 0.13	10.07 ± 0.20	—	204 ± 17
11771760	32.10 ± 0.02	1.262 ± 0.008	526 ± 5	12.20 ± 0.35	106.7 ± 7.7	3.02 ± 0.13	—	—	191 ± 10
12508433	44.84 ± 0.00	1.490 ± 0.002	790 ± 2	11.14 ± 0.21	111.7 ± 2.0	3.89 ± 0.17	9.32 ± 0.23	—	164 ± 9

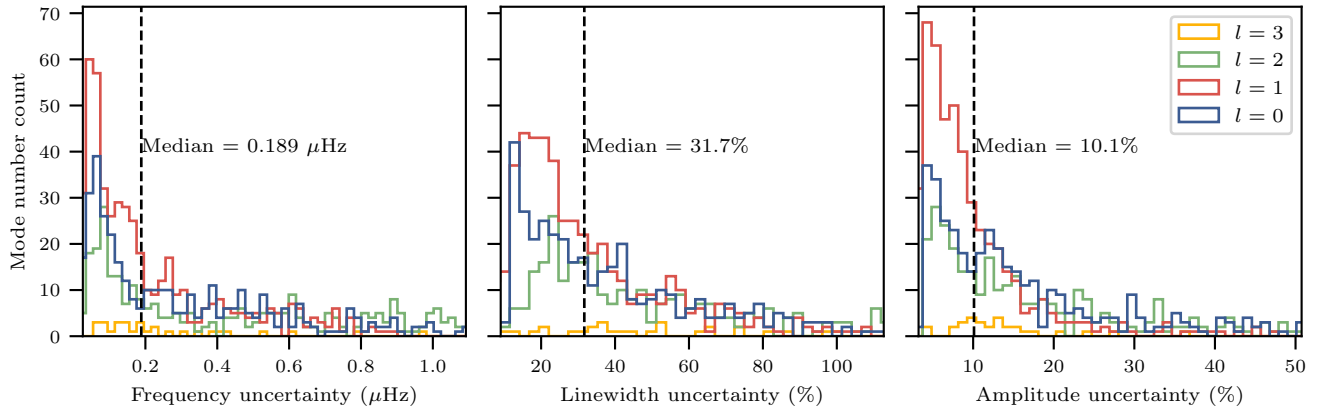


Figure 6. Histograms of the uncertainties for measured mode frequencies (left), linewidths (middle) and amplitudes (right). The linewidths and amplitudes are shown in relative uncertainty.

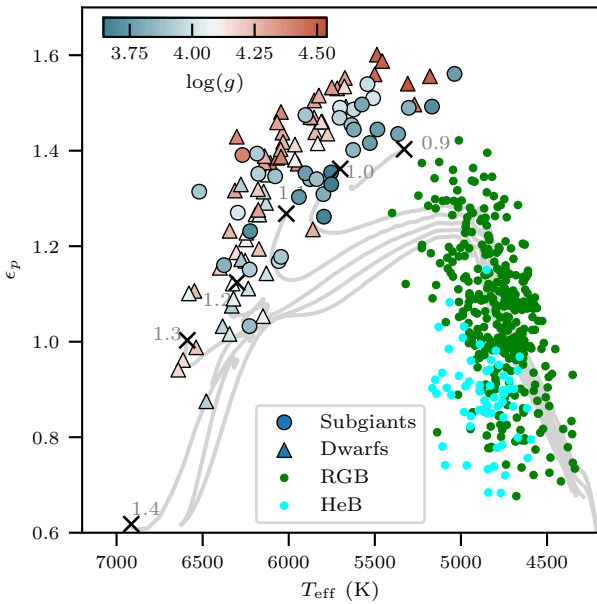


Figure 7. ϵ_p vs. T_{eff} with colour-coded $\log g$. The measurement of red giants were adopted from Huber et al. (2010). The theoretical evolutionary tracks (White et al. 2011b) are labelled with mass in solar units. The crosses mark the zero-age MS.

5 THE P–G DIAGRAM

We now focus on the frequencies of the underlying g modes, which we denote by γ (Aizenman et al. 1977). Adjusting the model parameters to fit the observed frequencies can be difficult and time-consuming. As pointed out by Bedding (2014), the information contained in the mixed modes can be used more elegantly, by considering the frequencies of the avoided crossings themselves. The suggestion was that, before fitting models to the observed mixed modes, one can first consider the underlying g modes. These are not directly detected but their frequencies can be inferred from the locations of the avoided crossings.

This discussion suggests a new asteroseismic diagram (Bedding 2014), inspired by the classical C–D diagram, in which the frequencies of the avoided crossings γ are plotted against the large separation of the p modes. This p–g diagram, so named because it plots g mode frequencies versus p mode frequencies, could prove to be an instructive way to display results of many stars and to make a first comparison with theoretical models (Bedding 2014; Campante et al. 2011).

For example, the échelle diagram in Figure 3 shows three avoided crossings of dipole modes, at about 950, 750 and 650 μHz . We recognise these as the frequencies of the γ modes, that is, the pure g modes that would exist in the core cavity if there was no coupling to the p modes in the envelope (Aizenman et al. 1977). Much of the diagnostic information contained in the mixed modes can be captured in this way. This is because the overall pattern of the mixed modes is determined by the mode bumping at each avoided crossing, and these patterns are determined by the g modes trapped in the core. For related discussion on this point, see Deheuvels & Michel (2010) and Benomar et al. (2013).

We determined the g mode frequencies, γ , from fitting $l = 1$ mixed mode frequencies $\nu_{n,l=1}$. Specifically, Lorentzian profiles were fitted to $\nu_{n+1,l=1} - \nu_{n,l=1}$ versus $(\nu_{n+1,l=1} + \nu_{n,l=1})/2$. A dip is present wherever there is an avoided crossing. This is because the presence of mixed modes makes two adjacent modes closer in frequency. We identified the centres of the Lorentzian profiles as the g mode frequencies, γ . The errors were estimated following a Monte Carlo procedure by adding Gaussian errors to mode frequencies, repeating the fitting for 1000 times, and adopting the standard deviation of γ from the distribution. If multiple avoided crossings (at least three) are present, we further estimated $\Delta\Pi_1$ by calculating the average differences between $1/\gamma$. The results are shown in Table 3. Some stars do not have reported γ_1 or $\Delta\Pi_1$ because they tend to have uncertain identifications of the first g mode, and they also present a small number of avoided crossings.

For less-evolved subgiants in which the first ($n_g = 1$) g mode frequency, γ_1 , is present, we made the $\gamma_1 - \Delta\nu$ diagram in Figure 10. This provides an indicative measurement

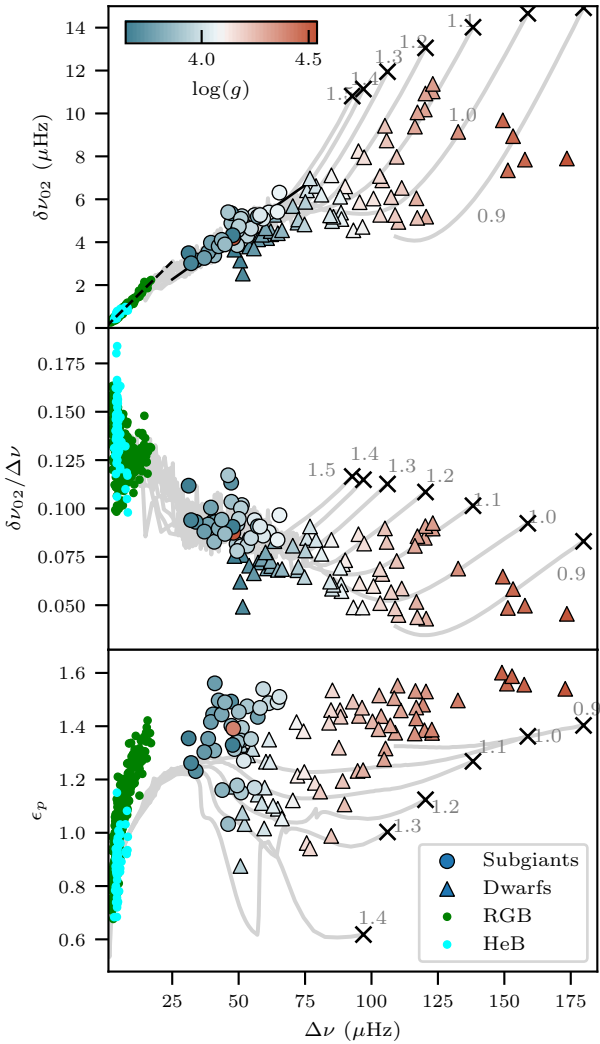


Figure 8. Top and middle: C–D diagrams, which show the small separation $\delta\nu_{02}$ as a function of $\Delta\nu$, with colour-coded $\log g$. The solid line is a linear fit to the subgiants, and the dashed line is a similar fit to low-luminosity red giants (Bedding et al. 2010). Bottom: ϵ_p vs. $\Delta\nu$. The measurement of dwarfs and red giants were adopted from Lund et al. (2017) and Huber et al. (2010), respectively. The theoretical evolutionary tracks (White et al. 2011b) are labelled with mass in solar units with crosses marking the zero-age MS.

of stellar mass when evolutionary tracks are simultaneously plotted, unlike the C–D diagram where stellar tracks are degenerate. The stars evolve diagonally, so γ_1 and $\Delta\nu$ can determine not only mass, but age as well.

Another important diagnostic diagram is to plot the period spacings of g modes $\Delta\Pi_1$ in Equation 2 versus $\Delta\nu$ (another p–g diagram). The diagram has been proved useful for distinguishing RGB and HeB stars because the two types of stars cluster at different locations (Bedding et al. 2011; Mosser et al. 2012b; Stello et al. 2013; Vrard et al. 2016). We made the diagram in Figure 11 for more-evolved subgiants. These stars have more than one avoided crossing, which makes measuring $\Delta\Pi_1$ feasible, although we note that

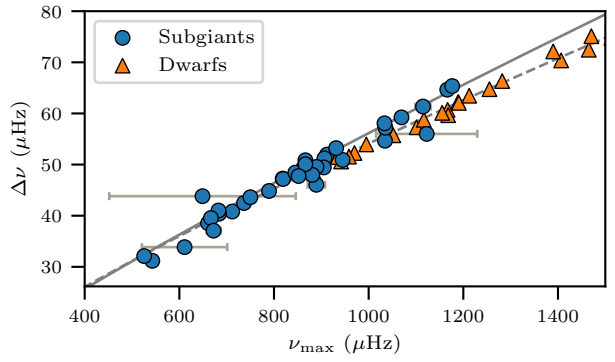


Figure 9. $\Delta\nu - \nu_{\max}$ diagram. The solid line is the best-fitted curve for subgiants. The dashed line is a similar fit, but obtained from a sample of MS dwarfs and red giants (Huber et al. 2011). The measurement of dwarfs were adopted from Lund et al. (2017).

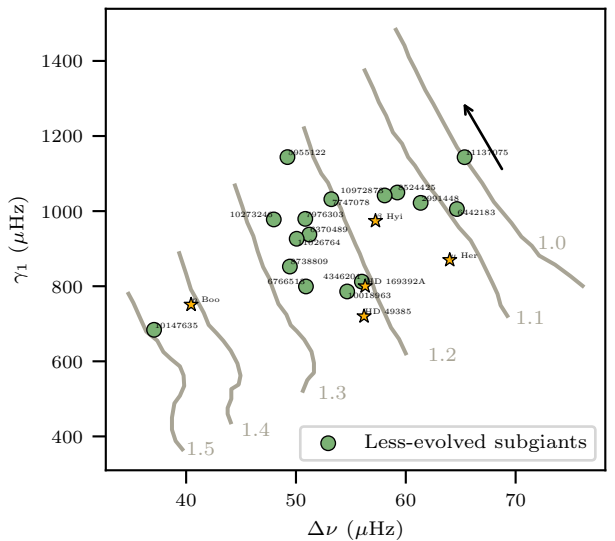


Figure 10. The p–g diagram using the lowest-order dipolar g mode γ_1 vs. $\Delta\nu$ for less-evolved subgiants. We also include five stars observed by ground-based telescopes and *CoRoT*, shown in the star symbols. The theoretical evolutionary tracks (Paper II) are labelled with mass in solar units, with the black arrow pointing in the direction of evolution.

these are lower-order g modes so we are not in the asymptotic regime. For subgiants, stellar models predict $\Delta\Pi_1$ is rather independent of $\Delta\nu$, especially for higher-mass subgiants, such that they evolve almost vertically (Benomar et al. 2013; Gai et al. 2017).

Finally, we note that using the two diagrams to infer mass and age provides a method independent of asteroseismic scaling relations. This is discussed in more detail in Paper II.

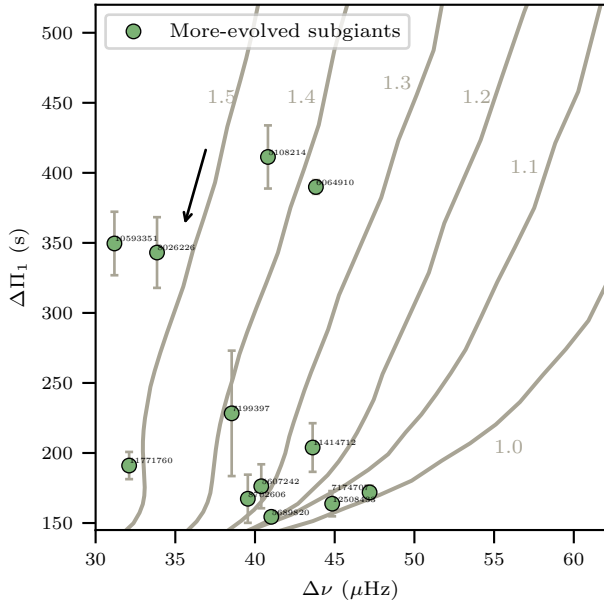


Figure 11. The dipolar g mode period spacing $\Delta\Pi_1$ vs. $\Delta\nu$ for more-evolved subgiants. The theoretical evolutionary tracks (Choi et al. 2016) are labelled with mass in solar units, with the black arrow pointing in the direction of evolution.

6 MODE LINETHICKNESS

6.1 Linethickness as a function of frequency

The modes of solar-like oscillations are damped by convection. For these observations, the modes have lifetimes much shorter than the length of time series, which results in a broadened Lorentzian shape in the power spectrum. The modes are hence ‘resolved’. The linewidth (full-width-at-half-maximum) of that shape can be translated to the lifetime through $\tau = (\pi\Gamma)^{-1}$, or damping rate $\eta = \pi\Gamma$. This is important to constrain the physics of the super-adiabatic layers near the surface, including the mechanism of how the kinetic energy of oscillations is dissipated into turbulent convection. The answer requires a detailed treatment of convection, but it is difficult to formulate with current convection theories (Gough 1980; Balmforth 1992a; Gabriel 1996; Houdek et al. 1999; Grigahcène et al. 2005; Xiong et al. 2015). However, the theories are able to reproduce the frequency-dependence of the linewidths seen in the observations, provided the free parameters in the modelling are carefully calibrated, in red giants (Aarslev et al. 2018) and in MS stars (Houdek et al. 2019). 3D hydrodynamical convection simulations may offer a promising path, by eliminating the degrees of freedom in the theory and provide a numerical solution (e.g. Belkacem et al. 2019; Zhou et al. 2019).

Appourchaux et al. (2014) first parametrised the $\Gamma - \nu$ relation in a given star and Lund et al. (2017) improved the fitting details. Here, we followed their procedure to fit the linewidths of radial modes, as follows:

$$\ln \Gamma(\nu; \theta) = \alpha \ln(\nu/\nu_{\max}) + \ln \Gamma_\alpha + \frac{\ln \Delta\Gamma_{\text{dip}}}{1 + \left[\frac{2 \ln(\nu/\nu_{\text{dip}})}{\ln(W_{\text{dip}}/\nu_{\max})} \right]^2},$$

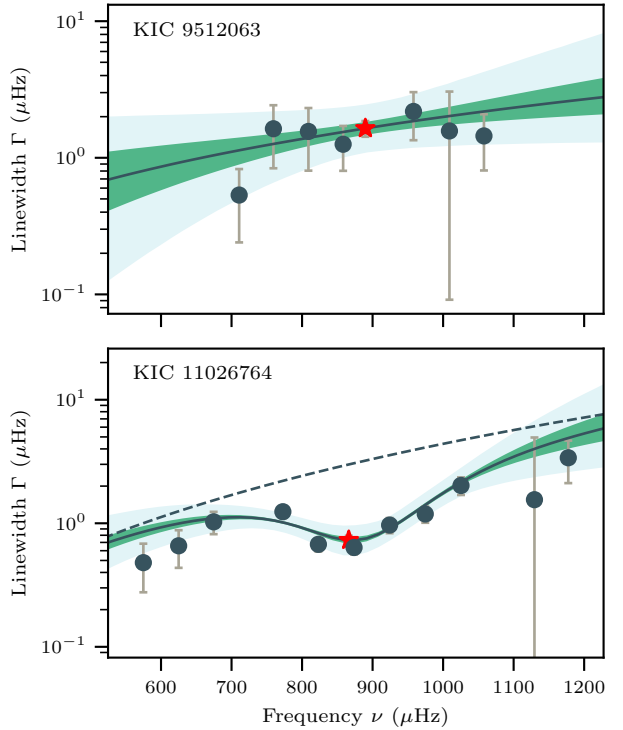


Figure 12. Linewidths as a function of frequencies for KIC 9512063 (top) and Gemma (KIC 11026764, bottom), denoted by the filled circles. The solid lines are the fits of Equation 20, with KIC 9512063 using the first two terms (the power-law), and Gemma using the full terms. The dashed line is the power-law component in Gemma’s fit. The shaded green regions show 1- σ and 3- σ credible intervals for the fit. The red star symbols around $900 \mu\text{Hz}$ are the estimations of linewidth at ν_{\max} , obtained from the MCMC samples.

(20)

where the free parameters are $\theta = (\alpha, \Gamma_\alpha, \Delta\Gamma_{\text{dip}}, W_{\text{dip}})$. This $\Gamma - \nu$ relation follows a power-law but saturates near ν_{\max} to form a plateau (or a dip) centred on ν_{dip} , with width W_{dip} and height $\Delta\Gamma_{\text{dip}}$. The dip could originate from a resonance of the thermal timescale in the superadiabatic layer and mode frequency (Balmforth 1992a; Belkacem et al. 2011). To fit the parameters, we optimised the likelihood function:

$$\ln L \propto \sum_i [\ln \Gamma_i - \ln \Gamma(\nu_i; \theta)]^2 / \sigma_{\ln \Gamma_i}^2. \quad (21)$$

The modes used in this fit were radial modes satisfying Bayes factors $\ln K > 1$. The priors of $\Delta\Gamma_{\text{dip}}$ and W_{dip} deserve a further mention. As suggested by Lund et al. (2017), the values of $\Delta\Gamma_{\text{dip}}$ were bound to be between 0 and 1 to reduce correlations between the parameters. W_{dip} can have two solutions, one larger than ν_{\max} , and one smaller. We kept the convention from Lund et al. (2017) to use the larger one. We estimated the FWHM (full-width-at-half-maximum) of the dip through $\text{FWHM} = \nu_{\text{dip}} \left| \sqrt{W_{\text{dip}}/\nu_{\max}} - \sqrt{\nu_{\max}/W_{\text{dip}}} \right|$ (Appourchaux et al. 2016), and the amplitude of the dip as $A_{\text{dip}} = \exp |\ln \Delta\Gamma_{\text{dip}}|$ (Lund et al. 2017). Figure 12 shows the fit for Gemma (KIC 11026764), which shows a dip around ν_{\max} . Note that some stars do not present the evid-

Table 4. Fit parameters of the Γ - ν relation.

KIC	$\Gamma(\nu_{\max})$	α	Γ_α (μHz)	$\Delta\Gamma_{\text{dip}}$ (μHz)	ν_{dip} (μHz)	W_{dip} (μHz)	FWHM (μHz)	A_{dip} (μHz^{-1})
2991448	0.73 ± 0.22	1.35 ± 1.38	56.96 ± 55.33	0.01 ± 0.01	1100 ± 11	1477 ± 93	311 ± 72	80 ± 87
3852594	4.42 ± 1.18	1.35 ± 0.64	5.95 ± 0.40	—	—	—	—	—
5607242	0.43 ± 0.16	4.24 ± 0.71	2.35 ± 1.17	0.12 ± 0.04	698 ± 7	898 ± 76	191 ± 60	8 ± 3
5689820	0.13 ± 0.05	1.71 ± 1.65	12.70 ± 30.15	0.01 ± 0.05	731 ± 67	2534 ± 1580	1029 ± 565	69 ± 233
5955122	1.67 ± 0.41	3.17 ± 0.94	11.83 ± 28.40	0.10 ± 0.12	874 ± 37	1729 ± 554	621 ± 298	10 ± 12
6064910	5.13 ± 1.33	0.16 ± 0.17	6.59 ± 0.38	—	—	—	—	—
6442183	0.64 ± 0.13	2.93 ± 0.41	2.79 ± 1.44	0.20 ± 0.07	1166 ± 12	1572 ± 181	350 ± 136	5 ± 2
6693861	0.59 ± 0.46	5.39 ± 2.75	42.11 ± 58.02	0.01 ± 0.03	838 ± 39	1529 ± 337	532 ± 195	71 ± 174
7174707	0.42 ± 0.22	1.70 ± 1.41	18.61 ± 39.44	0.02 ± 0.07	806 ± 27	1723 ± 473	613 ± 238	54 ± 211
7199397	1.15 ± 0.26	2.23 ± 0.34	1.41 ± 0.07	—	—	—	—	—
7747078	1.04 ± 0.16	3.15 ± 1.56	10.96 ± 34.76	0.09 ± 0.18	958 ± 66	2006 ± 751	753 ± 389	11 ± 20
7976303	1.76 ± 0.26	2.11 ± 1.09	8.63 ± 34.46	0.18 ± 0.28	933 ± 121	2790 ± 2583	1155 ± 1027	6 ± 9
8524425	0.60 ± 0.65	4.64 ± 1.13	2.97 ± 3.81	0.21 ± 0.13	1096 ± 35	1603 ± 284	447 ± 199	5 ± 3
8702606	0.31 ± 0.09	3.14 ± 0.95	12.17 ± 32.95	0.04 ± 0.10	660 ± 26	1547 ± 512	572 ± 239	23 ± 55
9512063	1.21 ± 0.63	1.75 ± 0.92	1.48 ± 0.18	—	—	—	—	—
10018963	2.37 ± 0.42	2.60 ± 0.22	2.37 ± 0.09	—	—	—	—	—
10147635	2.79 ± 0.73	3.71 ± 0.43	2.43 ± 0.16	—	—	—	—	—
10273246	1.68 ± 0.46	5.07 ± 1.08	8.51 ± 21.03	0.23 ± 0.31	1359 ± 695	5690 ± 2432	2919 ± 1719	4 ± 6
10593351	2.03 ± 0.64	3.04 ± 0.44	2.29 ± 0.17	—	—	—	—	—
10873176	3.26 ± 1.59	3.67 ± 2.10	3.42 ± 0.76	—	—	—	—	—
10920273	0.57 ± 0.25	8.48 ± 3.66	21.88 ± 44.10	0.03 ± 0.07	1082 ± 35	1577 ± 443	459 ± 311	33 ± 81
10972873	0.67 ± 0.14	3.69 ± 1.40	13.36 ± 38.59	0.05 ± 0.14	1062 ± 52	2204 ± 932	823 ± 483	18 ± 46
11026764	0.73 ± 0.17	2.17 ± 0.43	1.99 ± 0.36	0.31 ± 0.06	882 ± 10	1065 ± 51	183 ± 43	3 ± 1
11137075	0.53 ± 0.22	10.02 ± 1.98	49.24 ± 55.66	0.01 ± 0.01	1224 ± 25	1912 ± 173	601 ± 115	110 ± 173
11193681	0.86 ± 0.22	3.06 ± 0.37	1.20 ± 0.06	—	—	—	—	—
11395018	0.67 ± 0.15	1.72 ± 1.56	35.73 ± 51.69	0.02 ± 0.03	822 ± 21	1497 ± 200	469 ± 115	45 ± 70
11414712	0.69 ± 0.16	2.66 ± 0.26	0.94 ± 0.04	—	—	—	—	—
11771760	0.63 ± 0.17	0.79 ± 0.52	1.05 ± 0.07	—	—	—	—	—
12508433	0.27 ± 0.06	3.92 ± 1.66	26.15 ± 44.41	0.01 ± 0.03	796 ± 56	2294 ± 556	890 ± 230	73 ± 154

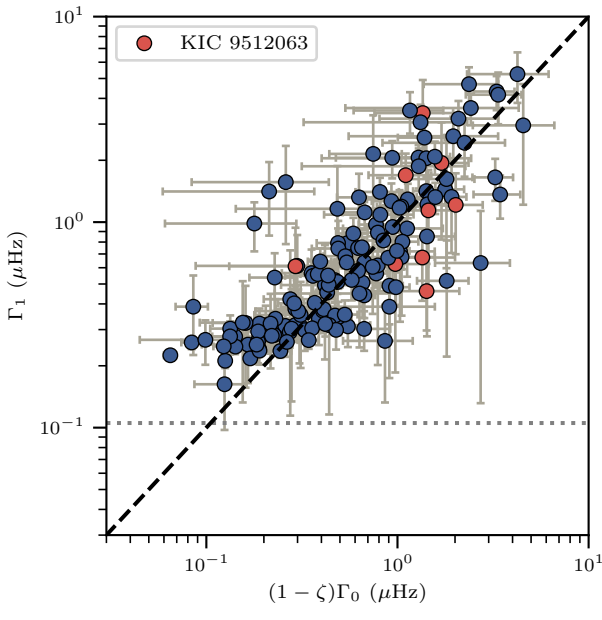


Figure 13. Linewidths of dipole mixed modes vs. those of radial modes modified with the stretch function ζ . The dashed line indicates the 1:1 relation. The horizontal dotted line denotes the nominal frequency resolution, $1/t_{\text{obs}}$, of KIC 9512063, which is around $0.1 \mu\text{Hz}$; the largest among the sample.

ence of a dip. Their linewidths increase monotonically with frequencies. We only fitted those stars with the first two terms of Equation 20. Figure 12 also shows an example, KIC 9512063, where the large random errors obscure the presence of either a dip or a plateau. Table 4 lists the fitted parameters for all stars.

The dipole modes have a more complicated Γ - ν relation. The dipole modes with more g mode characteristics have larger inertia and are less affected by damping from the surface than are radial modes, hence resulting in smaller linewidths. Benomar et al. (2014) suggested using linewidths to measure mode inertias, which could also be obtained from the asymptotic formalism of mixed modes (Goupil et al. 2013; Shibahashi 1979). Mosser et al. (2018) introduced a stretch function ζ , which is the degree of mode trapping characterised by the ratio of mode inertia inside the g-mode cavity to that throughout the star. The linewidths of mixed modes, Γ_1 , relate to those of radial modes, Γ_0 , as follows (Mosser et al. 2011, 2015; Vrard et al. 2016; Hekker & Christensen-Dalsgaard 2017; Mosser et al. 2018):

$$\Gamma_1 = \Gamma_0(1 - \zeta), \quad (22)$$

where

$$\zeta(\nu) = \left[1 + \frac{q}{N(\nu)} \frac{1}{q^2 \cos^2 \theta_p(\nu) + \sin^2 \theta_p(\nu)} \right]^{-1}, \quad (23)$$

$$N(\nu) = \frac{\Delta\nu}{\nu^2 \Delta\Pi_1}, \quad (24)$$

Table 5. Fit parameters of the $\Gamma(\nu_{\max})$ scaling relation.

Phase	Γ_0	c_1	c_2
MS	1.10 ± 0.01	13.41 ± 0.10	0.05 ± 0.02
Subgiants	0.50 ± 0.04	13.71 ± 0.19	-0.65 ± 0.06
RGB	0.25 ± 0.00	2.78 ± 0.09	0.09 ± 0.00
HeB	0.47 ± 0.02	1.70 ± 0.13	0.19 ± 0.01

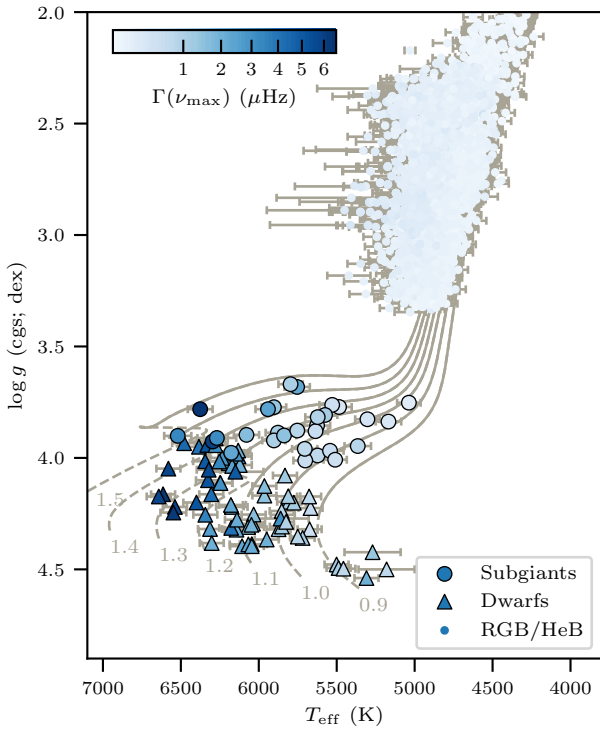


Figure 14. Kiel diagram with colour-coded $\Gamma(\nu_{\max})$. The measurements of dwarfs and red giants are adopted from Lund et al. (2017) and Vrard et al. (2018), respectively. The theoretical evolutionary tracks (Choi et al. 2016) before and after the MS turnoff are shown in the dashed and solid lines, respectively, with each track labelled with mass in solar units.

and

$$\theta_p(\nu) = \pi \left\{ \frac{\nu}{\Delta\nu} - \left[n_p + \frac{l}{2} + \epsilon_p - d_{0l} + \frac{\alpha_p}{2} \left(n_p - \frac{\nu_{\max}}{\Delta\nu} \right)^2 \right] \right\}, \quad (25)$$

Using the above definition of θ_p , together with Equation 3 and 5, we fitted the asymptotic parameters $\{\epsilon_p, \alpha_p, d_{0l}, \Delta\nu, \Delta\Pi_1, \epsilon_g\}$ to the dipole mode frequencies estimated from the peakbagging. The value of ζ was then straightforwardly obtained. In Figure 13, we compare Γ_1 with $\Gamma_0(1-\zeta)$ and find good agreement. That is, the widths of the dipole modes are smaller than those of the radial modes, as expected. This suggests that the asymptotic theory agrees well with the observation.

6.2 Scaling relations for linewidths

Scaling relations for linewidths were studied only recently, focusing on the linewidths around ν_{\max} , denoted by $\Gamma(\nu_{\max})$. Chaplin et al. (2009) used non-adiabatic pulsation computations and ground-based observations to study the linewidths across different stages of evolution. They showed that the linewidths scale with fundamental stellar parameters, primarily T_{eff} . This dependence on surface properties is expected because damping mainly happens in the super-adiabatic regions near the surface (Goldreich & Kumar 1991). The studies of *CoRoT* and *Kepler* targets also suggested that $\Gamma(\nu_{\max})$ correlates mainly with T_{eff} , but only weakly depends on $\log g$ (Baudin et al. 2011; Appourchaux et al. 2014; Vrard et al. 2018).

To estimate $\Gamma(\nu_{\max})$, we used the MCMC samples from the fit of $\Gamma - \nu$ relation (Section 6.1) to draw the probability distribution of Γ at ν_{\max} . This method assumes that $\Gamma - \nu$ follows the power-law model (or the power-law with a dip). Figure 12 shows an estimation for Gemma (KIC 11026764), marked by a red star around 700 μHz .

In Figure 14, we show $\Gamma(\nu_{\max})$ for our subgiant sample, together with MS stars from Lund et al. (2017), and RGB and HeB stars from Vrard et al. (2018). Note that Vrard et al. (2018) calculated $\Gamma(\nu_{\max})$ for the giants differently to how it was done for subgiants and MS stars by averaging linewidths using three modes near ν_{\max} . Figure 14 shows that $\Gamma(\nu_{\max})$ mainly depends on T_{eff} , and weakly correlates with $\log g$. To parametrise this relation, we fitted $\Gamma(\nu_{\max})$ using

$$\log(\Gamma/\Gamma_0) = c_1 \log(T_{\text{eff}}/5777 \text{ K}) + c_2 \log(g/274 \text{ m} \cdot \text{s}^{-1}). \quad (26)$$

We optimised the likelihood function:

$$\ln L \propto [\ln \Gamma_i - \ln \Gamma(T_i, g_i; \theta)]^2 / (2\sigma_{\ln \Gamma_i}^2). \quad (27)$$

Some previous works (Belkacem et al. 2012; Samadi et al. 2015) pointed out that $\Gamma(\nu_{\max})$ depends on T_{eff} and $\log g$ differently in each evolutionary stage, which motivates us to fit them separately as well.

The fitted parameters are shown in Table 5. From the table, we conclude that $\Gamma(\nu_{\max})$ primarily depends on T_{eff} but with significantly different power-law indices (c_1) for red giants and non-red giants. This could be attributed to different dominant damping mechanisms, as some works suggested (e.g. Baudin et al. 2011). However it could also be an artefact while selecting modes to compute $\Gamma(\nu_{\max})$ for red giants (Belkacem et al. 2012). The power-law index for $\log g$ (c_2) in subgiants has a reversed sign compared to MS stars and red giants. This effect could be slightly spotted in Figure 14.

7 MODE AMPLITUDES

7.1 Amplitudes as a function of frequency

The amplitudes of radial modes follow a roughly Gaussian distribution centred on ν_{\max} , as we analysed in Section 4. The dipole mixed modes have an added dependence on mode inertia, but are still predictable using the stretch function: $A_1^2 = (1 - \zeta)A_0^2$, with A_0 being the radial mode amplitudes

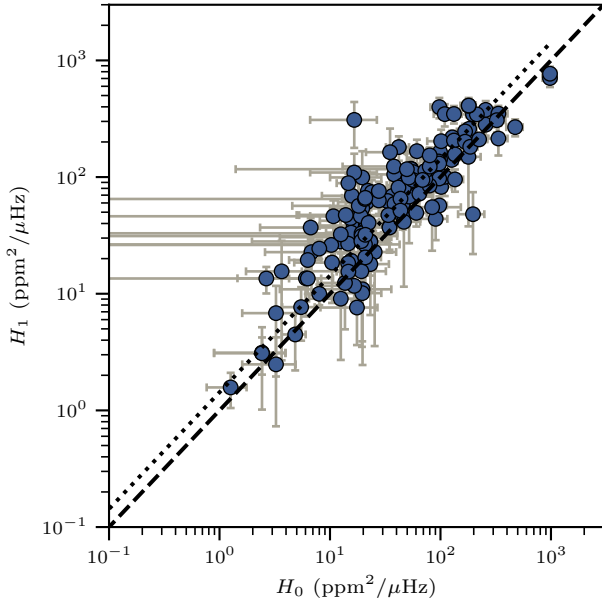


Figure 15. Height of dipole mixed modes H_1 vs. those of radial modes H_0 . The dashed line indicate the 1:1 relation, and the dotted line shows 1.5:1 relation. The factor of 1.5 shows the median value of our observed H_1/H_0 , which stems from a geometric effect.

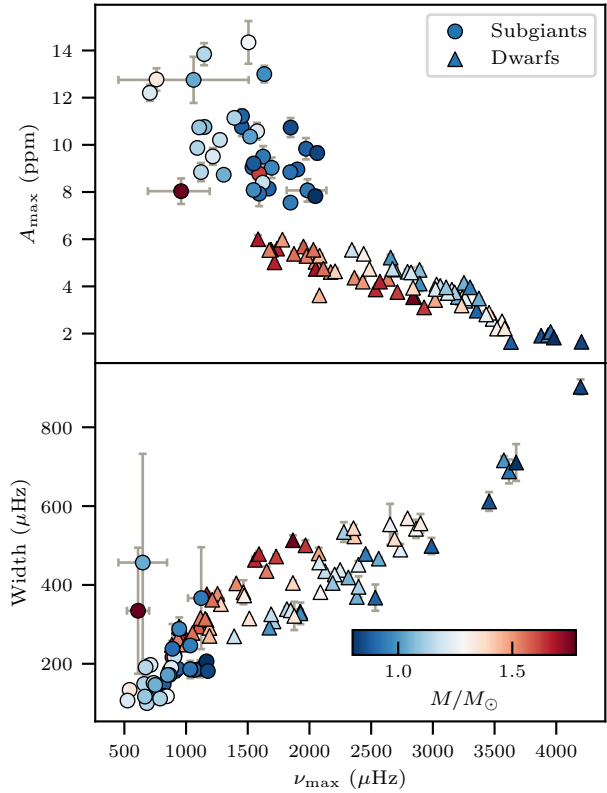


Figure 17. A_{\max} and width of the Gaussian envelope against ν_{\max} . The colour denotes stellar mass.

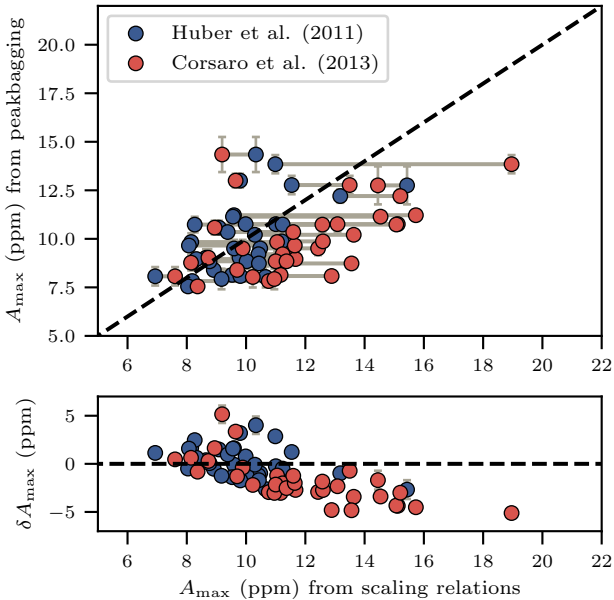


Figure 16. Top: A_{\max} estimated using the radial mode amplitudes vs. A_{\max} from the scaling relations. The dashed line indicates the 1:1 relation. Bottom: the absolute differences in the top panel.

(Benomar et al. 2014; Belkacem et al. 2015; Mosser et al. 2018). Considering $\Gamma_1 = (1 - \zeta)\Gamma_0$, we obtained $H_1 = H_0$, suggesting similar mode heights. In Figure 15, we show H_1 against H_0 . The points deviate from the 1:1 relation because the height of dipole modes are influenced by a geometric effect. Dividing H_1 by H_0 , we get the visibility factor V_1^2 with a median value equal to 1.5, similar to the one calculated using stellar atmosphere models (Ballot et al. 2011), which is also around 1.5.

7.2 Scaling relations for amplitudes

Kjeldsen & Bedding (1995) first proposed a scaling relation for the amplitudes of solar-like oscillations to scale from the Sun to other stars, relating both radial velocity and photometric amplitude to fundamental parameters L , M and T_{eff} . It received numerous application, e.g. for optimising target selections (Chaplin et al. 2011a; Schofield et al. 2019), and understanding how modes are excited with different treatment for convection and excitation processes (e.g. Goldreich & Keeley 1977; Balmforth 1992b; Samadi & Goupil 2001; Chaplin et al. 2005; Zhou et al. 2019). As we mentioned in Section 4, while estimating ν_{\max} we also measured the maximum photometric amplitude expressed by A_{\max} and the width of the Gaussian-like envelopes. To compare A_{\max} with scaling relations, we used two results from Huber et al.

(2011):

$$\frac{A_{\max}}{A_{\text{bol},\odot}} = c_K \left(\frac{L}{L_\odot} \right)^{0.838} \left(\frac{M}{M_\odot} \right)^{-1.32} \left(\frac{T_{\text{eff}}}{T_{\text{eff},\odot}} \right)^{-1}, \quad (28)$$

and Corsaro et al. (2013):

$$\frac{A_{\max}}{A_{\text{bol},\odot}} = 1.38 c_K \left(\frac{\nu_{\max}}{\nu_{\max,\odot}} \right)^{-2.314} \left(\frac{\Delta\nu}{\Delta\nu_\odot} \right)^{2.088} \left(\frac{T_{\text{eff}}}{T_{\text{eff},\odot}} \right)^{0.365}, \quad (29)$$

where $A_{\text{bol},\odot} = 3.6 \pm 0.11$ ppm and $c_K = (T_{\text{eff}}/5934 \text{ K})^{0.8}$ (Huber et al. 2011). There has been some discussions concerning the exponent of each term (e.g. Houdek et al. 1999; Houdek 2006; Samadi et al. 2007), and the above two papers set the exponents free and calibrated with observations (see also e.g. Stello et al. 2011). Figure 16 shows the comparison. In the regime of subgiants, Huber et al. (2011)’s relation seems to fit better, with a correlation coefficient of 0.55 against 0.49 from Corsaro et al. (2013). However, both relations overestimate the amplitudes, by factors of 9% and 24% respectively. The scatter of the data points could be caused by activity (Chaplin et al. 2011b) or an unaccounted metallicity effect (Yu et al. 2018). We also verified that the suppression effect of non-radial modes seen in red giants (Mosser et al. 2012a; Stello et al. 2016) does not affect the subgiants in our sample (García et al. 2014; Fuller et al. 2015).

In Figure 17 we plot both A_{\max} and the width against ν_{\max} . The values of A_{\max} increase and the widths decrease with decreasing ν_{\max} , indicating that the Gaussian envelope becomes higher and narrower as the star evolves. The points in Figure 17 are also colour-coded with mass, and we identify a weak correlation: at a given ν_{\max} , A_{\max} is smaller in higher-mass stars, with the width being larger. This phenomenon is also seen in the *Kepler* red giant sample (e.g. Yu et al. 2018). We also analysed the effect of metallicity on mode amplitude but due to the small size of our sample we were not able to draw any conclusions.

8 CONCLUSIONS

In this paper, we presented oscillation frequencies, linewidths and amplitudes for 36 subgiants observed by the 4 year *Kepler* mission. We derived those parameters with uncertainties from MCMC fitting, using an open-source software package SOLARLIKEPEAKBAGGING. Significance tests and visual inspections were applied to ensure a robust identification. Our main results are summarised as follows:

(i) With the long baseline of *Kepler* observations, the median value for the frequency uncertainties of the subgiants is $0.180 \mu\text{Hz}$. For modes with S/N=3, the typical uncertainty is $0.1 \mu\text{Hz}$, providing strong constraint on stellar models with these data.

(ii) The asymptotic parameters ϵ_p , $\Delta\nu$, ν_{\max} and $\delta\nu_{0l}$ were derived using the mode parameters. We identified a T_{eff} and $\log g$ dependence for ϵ_p . We also revisited the C–D diagram and the $\Delta\nu - \nu_{\max}$ diagram with a focus on subgiants. The subgiants deviate slightly from the general trend, but could be explained using simple scaling arguments or stellar models.

(iii) We presented two p–g diagrams, the $\gamma_1 - \Delta\nu$ diagram for less-evolved subgiants and the $\Delta\Pi_1 - \Delta\nu$ diagram for more-evolved subgiants. Both diagrams were populated with *Kepler* observations and can be used as a first simple estimation of stellar mass.

(iv) The linewidths of radial modes were analysed as functions of frequencies, and the linewidths of dipolar mixed modes agree well with asymptotic predictions. We verified the dependence of $\Gamma(\nu_{\max})$ on T_{eff} and also observed a weak $\log g$ effect.

(v) The amplitudes of dipolar mixed modes also agree with asymptotic predictions. The mass dependence of A_{\max} and the width is present both in subgiants and MS stars.

The unprecedented quality of asteroseismic data presented by this sample is valuable for the study of stellar physics. The mode frequencies are further used as modelling input in Paper II. The linewidths and amplitudes derived in this work can be used to study mode excitation and damping. In the observation data, one missing piece that remains unexplored in this work is the rotational splitting, which provides a golden opportunity to study the angular momentum transport in subgiants. We will continue to study this topic in this series of papers.

ACKNOWLEDGEMENTS

We thank Mikkel Lund and Jørgen Christensen-Dalsgaard for very helpful discussions. We also appreciate efforts from the referee to improve the quality of this paper, especially during a pandemic outbreak. The *Kepler* Discovery mission is funded by NASA’s Science Mission Directorate. We acknowledge the Joint Research Fund in Astronomy (U1631236) under cooperative agreement between the National Natural Science Foundation of China (NSFC) and Chinese Academy of Sciences (CAS), (NSFC 11273007 and 10933002), and the Fundamental Research Funds for the Central Universities. We also acknowledge funding from the Australian Research Council.

References

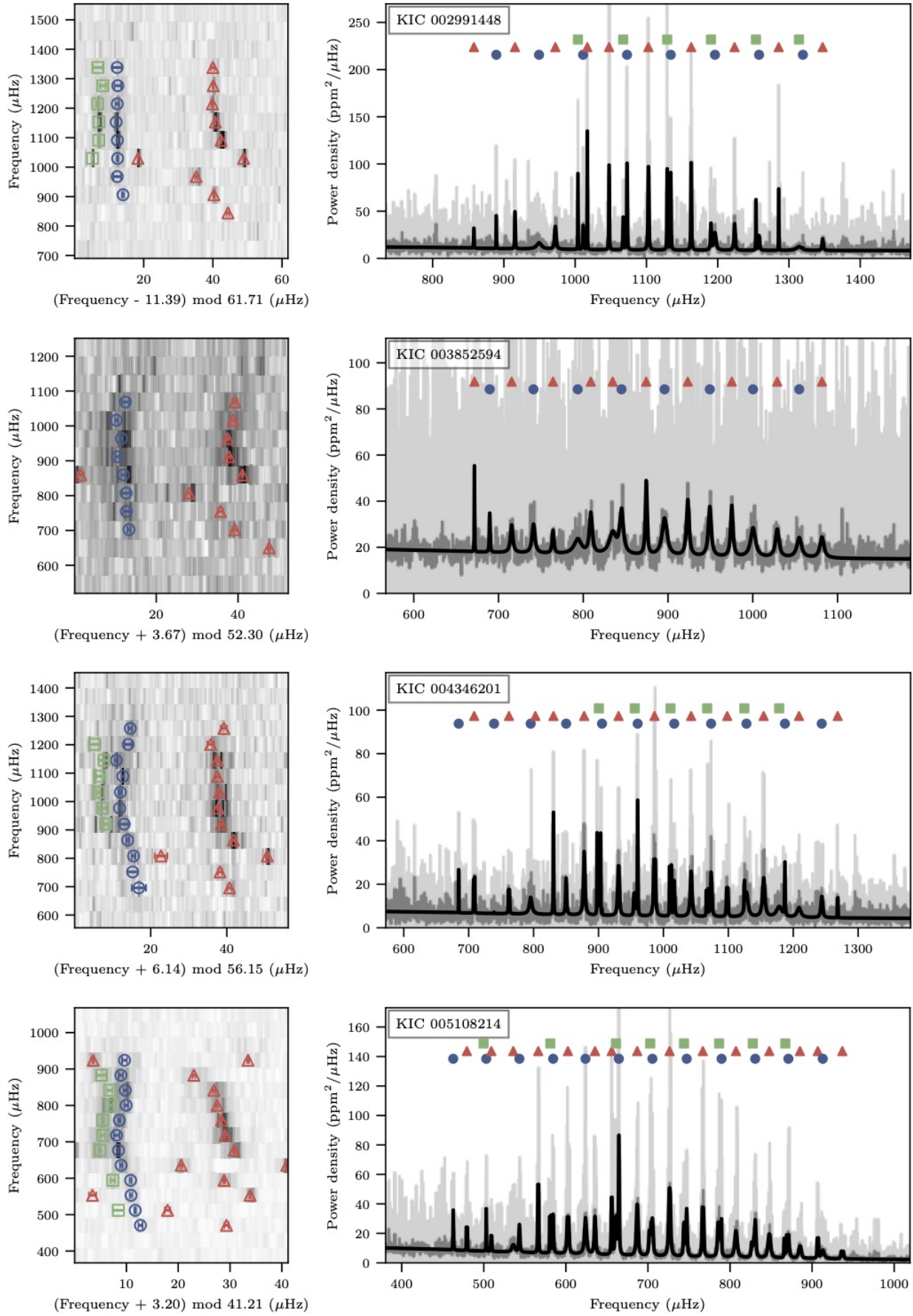
- Aarslev M. J., Houdek G., Handberg R., Christensen-Dalsgaard J., 2018, *MNRAS*, **478**, 69
- Aizenman M., Smeyers P., Weigert A., 1977, *A&A*, **58**, 41
- Anderson E. R., Duvall Thomas L. J., Jeffries S. M., 1990, *ApJ*, **364**, 699
- Appourchaux T., et al., 2012, *A&A*, **543**, A54
- Appourchaux T., et al., 2014, *A&A*, **566**, A20
- Appourchaux T., et al., 2016, *A&A*, **595**, C2
- Astropy Collaboration et al., 2013, *A&A*, **558**, A33
- Astropy Collaboration et al., 2018, preprint, p. [arXiv:1801.02634](https://arxiv.org/abs/1801.02634)
- Ballot J., Appourchaux T., Toutain T., Guittet M., 2008, *A&A*, **486**, 867
- Ballot J., Barban C., van’t Veer-Mennen C., 2011, *A&A*, **531**, A124
- Balmforth N. J., 1992a, *MNRAS*, **255**, 603
- Balmforth N. J., 1992b, *MNRAS*, **255**, 639
- Baudin F., et al., 2011, *A&A*, **529**, A84
- Bedding T. R., 2012, in Progress in Solar/Stellar Physics with Helio- and Asteroseismology. Proceedings of a Fujihara Seminar held at Hakone, Japan, 13–17 March, 2011. ASP Con-

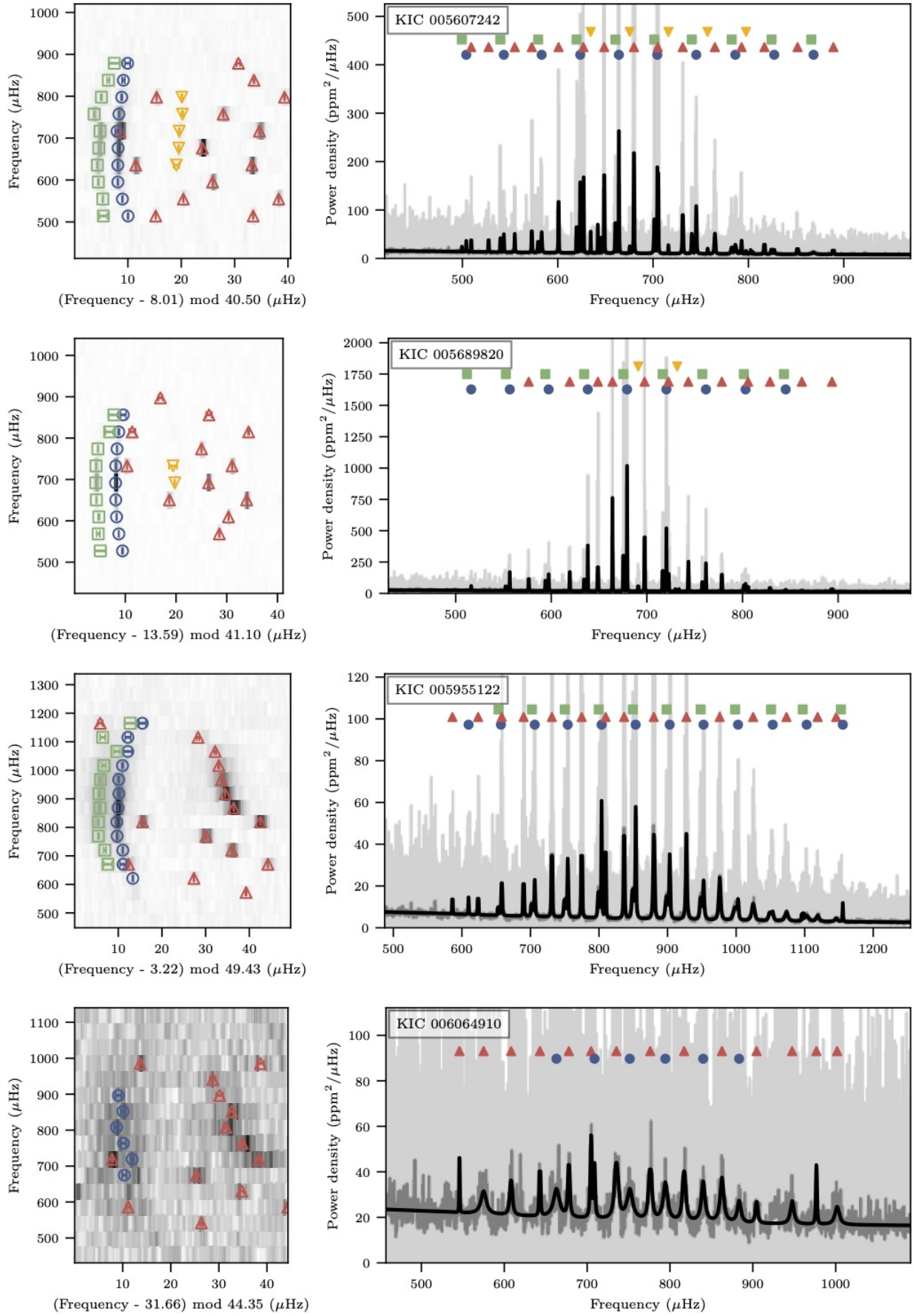
- ference Proceeding, Vol. 462. Edited by H. Shibahashi, M. Takata, and A.E. Lynas-Gray. San Francisco: Astronomical Society of the Pacific, 2012, p.195. p. 195
- Bedding T. R., 2014, in Pallé P. L., Esteban C., eds, Asteroseismology: 22nd Canary Islands Winter School of Astrophysics. Cambridge: Cambridge University Press, p. 60
- Bedding T. R., et al., 2001, *ApJ*, **549**, L105
- Bedding T. R., et al., 2006, *ApJ*, **647**, 558
- Bedding T. R., et al., 2007, *ApJ*, **663**, 1315
- Bedding T. R., et al., 2010, *ApJ*, **713**, L176
- Bedding T. R., et al., 2011, *Nature*, **471**, 608
- Belkacem K., Goupil M. J., Dupret M. A., Samadi R., Baudin F., Noels A., Mosser B., 2011, *A&A*, **530**, A142
- Belkacem K., Dupret M. A., Baudin F., Appourchaux T., Marques J. P., Samadi R., 2012, *A&A*, **540**, L7
- Belkacem K., et al., 2015, *A&A*, **579**, A31
- Belkacem K., Kupka F., Samadi R., Grimm-Strele H., 2019, *A&A*, **625**, A20
- Benomar O., Bedding T. R., Stello D., Deheuvels S., White T. R., Christensen-Dalsgaard J., 2012, *ApJ*, **745**, L33
- Benomar O., et al., 2013, *ApJ*, **767**, 158
- Benomar O., et al., 2014, *ApJ*, **781**, L29
- Bonanno A., Benatti S., Claudi R., Desidera S., Gratton R., Lecchia S., Paternò L., 2008, *ApJ*, **676**, 1248
- Brandão I. M., et al., 2011, *A&A*, **527**, A37
- Brown T. M., Gilliland R. L., Noyes R. W., Ramsey L. W., 1991, *ApJ*, **368**, 599
- Campante T. L., et al., 2011, *A&A*, **534**, A6
- Carrier F., et al., 2001, *A&A*, **378**, 142
- Carrier F., Eggenberger P., Bouchy F., 2005, *A&A*, **434**, 1085
- Carrier F., et al., 2007, *A&A*, **470**, 1059
- Chaplin W. J., Houdek G., Elsworth Y., Gough D. O., Isaak G. R., New R., 2005, *MNRAS*, **360**, 859
- Chaplin W. J., Houdek G., Karoff C., Elsworth Y., New R., 2009, *A&A*, **500**, L21
- Chaplin W. J., et al., 2011a, *ApJ*, **732**, 54
- Chaplin W. J., et al., 2011b, *ApJ*, **732**, L5
- Choi J., Dotter A., Conroy C., Cantiello M., Paxton B., Johnson B. D., 2016, *ApJ*, **823**, 102
- Christensen-Dalsgaard J., 1984, in Mangeney A., Praderie F., eds, Space Research in Stellar Activity and Variability. p. 11
- Christensen-Dalsgaard J., Dappen W., Lebreton Y., 1988, *Nature*, **336**, 634
- Christensen-Dalsgaard J., Bedding T. R., Kjeldsen H., 1995, *ApJ*, **443**, L29
- Corsaro E., De Ridder J., 2014, *A&A*, **571**, A71
- Corsaro E., Fröhlich H. E., Bonanno A., Huber D., Bedding T. R., Benomar O., De Ridder J., Stello D., 2013, *MNRAS*, **430**, 2313
- Davies G. R., et al., 2016, *MNRAS*, **456**, 2183
- Deheuvels S., Michel E., 2010, *Ap&SS*, **328**, 259
- Deheuvels S., et al., 2014, *A&A*, **564**, A27
- Deheuvels S., Brandão I., Silva Aguirre V., Ballot J., Michel E., Cunha M. S., Lebreton Y., Appourchaux T., 2016, *A&A*, **589**, A93
- Di Mauro M. P., Christensen-Dalsgaard J., Paternò L., 2003a, *Ap&SS*, **284**, 229
- Di Mauro M. P., Christensen-Dalsgaard J., Kjeldsen H., Bedding T. R., Paternò L., 2003b, *A&A*, **404**, 341
- Eggenberger P., et al., 2019, *A&A*, **621**, A66
- Fernandes J., Monteiro M. J. P. F. G., 2003, *A&A*, **399**, 243
- Foreman-Mackey D., Hogg D. W., Lang D., Goodman J., 2013, *Publications of the Astronomical Society of the Pacific*, **125**, 306
- Fuller J., Cantiello M., Stello D., Garcia R. A., Bildsten L., 2015, *Science*, **350**, 423
- Gabriel M., 1996, *Bulletin of the Astronomical Society of India*, **24**, 233
- Gai N., Tang Y., Yu P., Dou X., 2017, *ApJ*, **836**, 3
- García R. A., et al., 2011, *MNRAS*, **414**, L6
- García R. A., et al., 2014, *A&A*, **572**, A34
- Ge Z. S., Bi S. L., Li T. D., Liu K., Tian Z. J., Yang W. M., Liu Z. E., Yu J., 2015, *MNRAS*, **447**, 680
- Gilliland R. L., et al., 2010, *ApJ*, **713**, L160
- Gizon L., Solanki S. K., 2003, *ApJ*, **589**, 1009
- Goldreich P., Keeley D. A., 1977, *ApJ*, **212**, 243
- Goldreich P., Kumar P., 1991, *ApJ*, **374**, 366
- Goodman J., Weare J., 2010, *Communications in Applied Mathematics and Computational Science*, **5**, 65
- Gough D., 1980, Some theoretical remarks on solar oscillations. Springer, Berlin, Heidelberg, pp 273–299, doi:10.1007/3-540-09994-8_27
- Gough D. O., 1986, in Osaki Y., ed., Hydrodynamic and Magnetodynamic Problems in the Sun and Stars. p. 117
- Goupil M. J., Mosser B., Marques J. P., Ouazzani R. M., Belkacem K., Lebreton Y., Samadi R., 2013, *A&A*, **549**, A75
- Grigahcène A., Dupret M. A., Gabriel M., Garrido R., Scuflaire R., 2005, *A&A*, **434**, 1055
- Grundahl F., et al., 2017, *ApJ*, **836**, 142
- Guenther D. B., 2004, *ApJ*, **612**, 454
- Guenther D. B., Demarque P., 1996, *ApJ*, **456**, 798
- Handberg R., Campante T. L., 2011, *A&A*, **527**, A56
- Handberg R., Lund M. N., 2014, *MNRAS*, **445**, 2698
- Harvey J., 1985, in Rolfe E., Battick B., eds, ESA Special Publication Vol. 235, Future Missions in Solar, Heliospheric & Space Plasma Physics. p. 199
- Hekker S., Christensen-Dalsgaard J., 2017, *A&ARv*, **25**, 1
- Hon M., Stello D., Yu J., 2018, *MNRAS*, **476**, 3233
- Houdek G., 2006, in Proceedings of SOHO 18/GONG 2006/HELAS I, Beyond the spherical Sun. p. 28
- Houdek G., Balmforth N. J., Christensen-Dalsgaard J., Gough D. O., 1999, *A&A*, **351**, 582
- Houdek G., Lund M. N., Trampedach R., Christensen-Dalsgaard J., Handberg R., Appourchaux T., 2019, *MNRAS*, **487**, 595
- Huber D., Stello D., Bedding T. R., Chaplin W. J., Arentoft T., Quirion P. O., Kjeldsen H., 2009, *Communications in Asteroseismology*, **160**, 74
- Huber D., et al., 2010, *ApJ*, **723**, 1607
- Huber D., et al., 2011, *ApJ*, **743**, 143
- Kallinger T., et al., 2010, *A&A*, **509**, A77
- Kallinger T., et al., 2012, *A&A*, **541**, A51
- Kallinger T., et al., 2014, *A&A*, **570**, A41
- Kass R. E., Raftery A. E., 1995, *Journal of the American Statistical Association*, **90**, 773
- Kjeldsen H., Bedding T. R., 1995, *A&A*, **293**, 87
- Kjeldsen H., Bedding T. R., Viskum M., Frandsen S., 1995, *AJ*, **109**, 1313
- Kjeldsen H., et al., 2003, *AJ*, **126**, 1483
- Li Y., Bedding T. R., Li T., Bi S., Murphy S. J., Corsaro E., Chen L., Tian Z., 2018, *MNRAS*, **476**, 470
- Li T., Bedding T. R., Kjeldsen H., Stello D., Christensen-Dalsgaard J., Deng L., 2019, *MNRAS*, **483**, 780
- Libbrecht K. G., 1992, *ApJ*, **387**, 712
- Lomb N. R., 1976, *Ap&SS*, **39**, 447
- Lund M. N., et al., 2017, *ApJ*, **835**, 172
- Mathur S., et al., 2011, *ApJ*, **733**, 95
- Mathur S., et al., 2013, *A&A*, **549**, A12
- Mathur S., et al., 2017, *ApJS*, **229**, 30
- Mazumdar A., 2005, *A&A*, **441**, 1079
- Metcalfe T. S., et al., 2010, *ApJ*, **723**, 1583
- Mosser B., et al., 2011, *A&A*, **525**, L9
- Mosser B., et al., 2012a, *A&A*, **537**, A30
- Mosser B., et al., 2012b, *A&A*, **540**, A143
- Mosser B., Vrard M., Belkacem K., Deheuvels S., Goupil M. J., 2015, *A&A*, **584**, A50
- Mosser B., Gehan C., Belkacem K., Samadi R., Michel E., Goupil M. J., 2018, *A&A*, **618**, A109

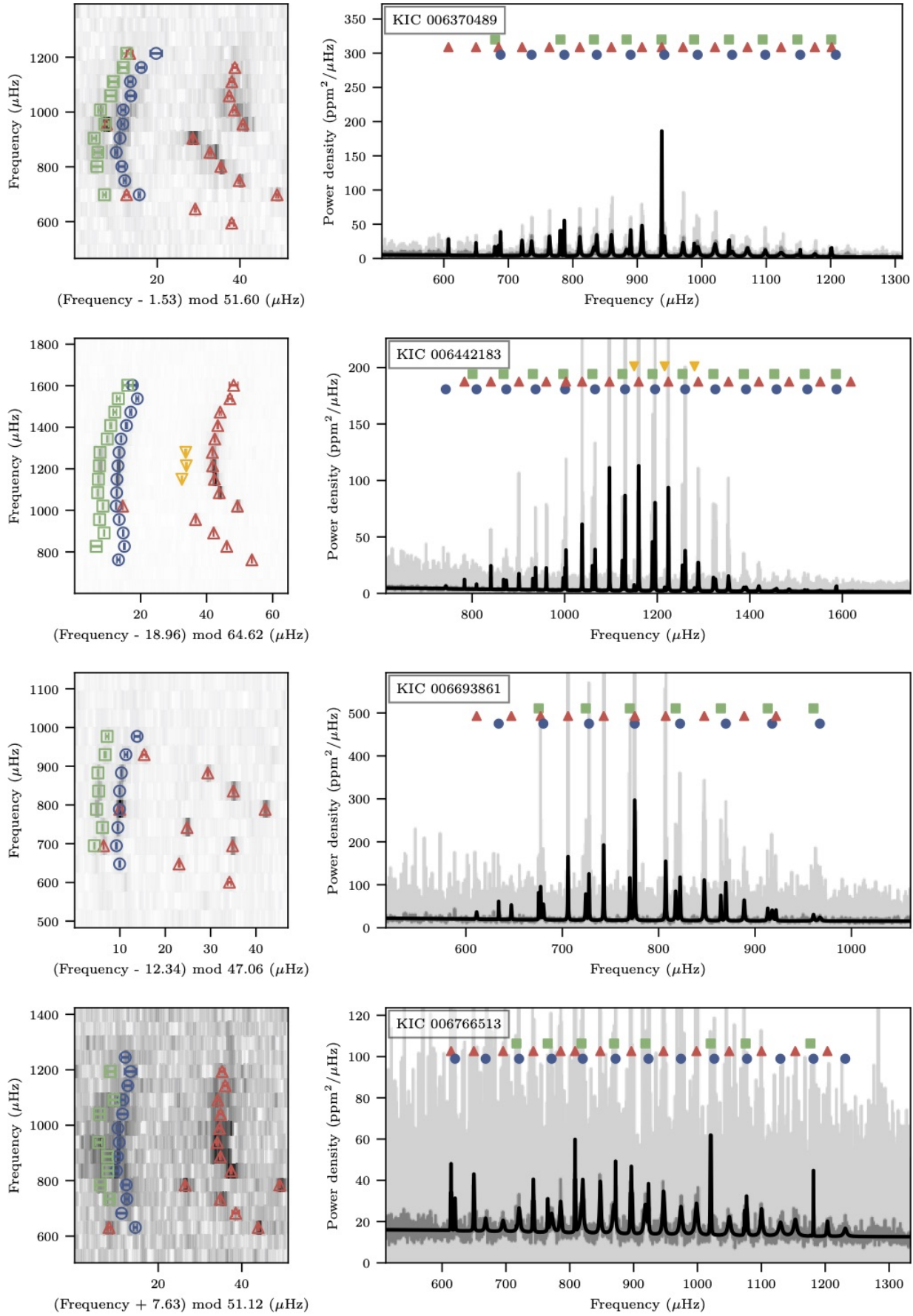
- Ong J. M. J., Basu S., 2019, [ApJ](#), **885**, 26
- Paxton B., et al., 2013, [ApJS](#), **208**, 4
- Pinheiro F. J. G., Fernandes J. M., 2010, [Ap&SS](#), **328**, 73
- Samadi R., Goupil M. J., 2001, [A&A](#), **370**, 136
- Samadi R., Georgobiani D., Trampedach R., Goupil M. J., Stein R. F., Nordlund Å., 2007, [A&A](#), **463**, 297
- Samadi R., Belkacem K., Sono T., 2015, in EAS Publications Series. pp 111–191 ([arXiv:1510.01151](#)), doi:10.1051/eas/1573003
- Scargle J. D., 1982, [ApJ](#), **263**, 835
- Schofield M., et al., 2019, [ApJS](#), **241**, 12
- Shibahashi H., 1979, [PASJ](#), **31**, 87
- Stello D., Bruntt H., Preston H., Buzasi D., 2008, [ApJ](#), **674**, L53
- Stello D., Chaplin W. J., Basu S., Elsworth Y., Bedding T. R., 2009, [MNRAS](#), **400**, L80
- Stello D., et al., 2011, [ApJ](#), **737**, L10
- Stello D., et al., 2013, [ApJ](#), **765**, L41
- Stello D., Cantiello M., Fuller J., Garcia R. A., Huber D., 2016, [Publ. Astron. Soc. Australia](#), **33**, e011
- Tassoul M., 1980, [ApJS](#), **43**, 469
- Tian Z., Bi S., Bedding T. R., Yang W., 2015, [A&A](#), **580**, A44
- Toutain T., Appourchaux T., 1994, [A&A](#), **289**, 649
- Vrard M., Mosser B., Samadi R., 2016, [A&A](#), **588**, A87
- Vrard M., Kallinger T., Mosser B., Barban C., Baudin F., Belkacem K., Cunha M. S., 2018, [A&A](#), **616**, A94
- White T. R., et al., 2011a, [ApJ](#), **742**, L3
- White T. R., Bedding T. R., Stello D., Christensen-Dalsgaard J., Huber D., Kjeldsen H., 2011b, [ApJ](#), **743**, 161
- White T. R., et al., 2012, [ApJ](#), **751**, L36
- Xiong D. R., Deng L., Zhang C., 2015, [MNRAS](#), **451**, 3354
- Yu J., Huber D., Bedding T. R., Stello D., Hon M., Murphy S. J., Khanna S., 2018, [ApJS](#), **236**, 42
- Zhou Y., Asplund M., Collet R., 2019, [ApJ](#), **880**, 13

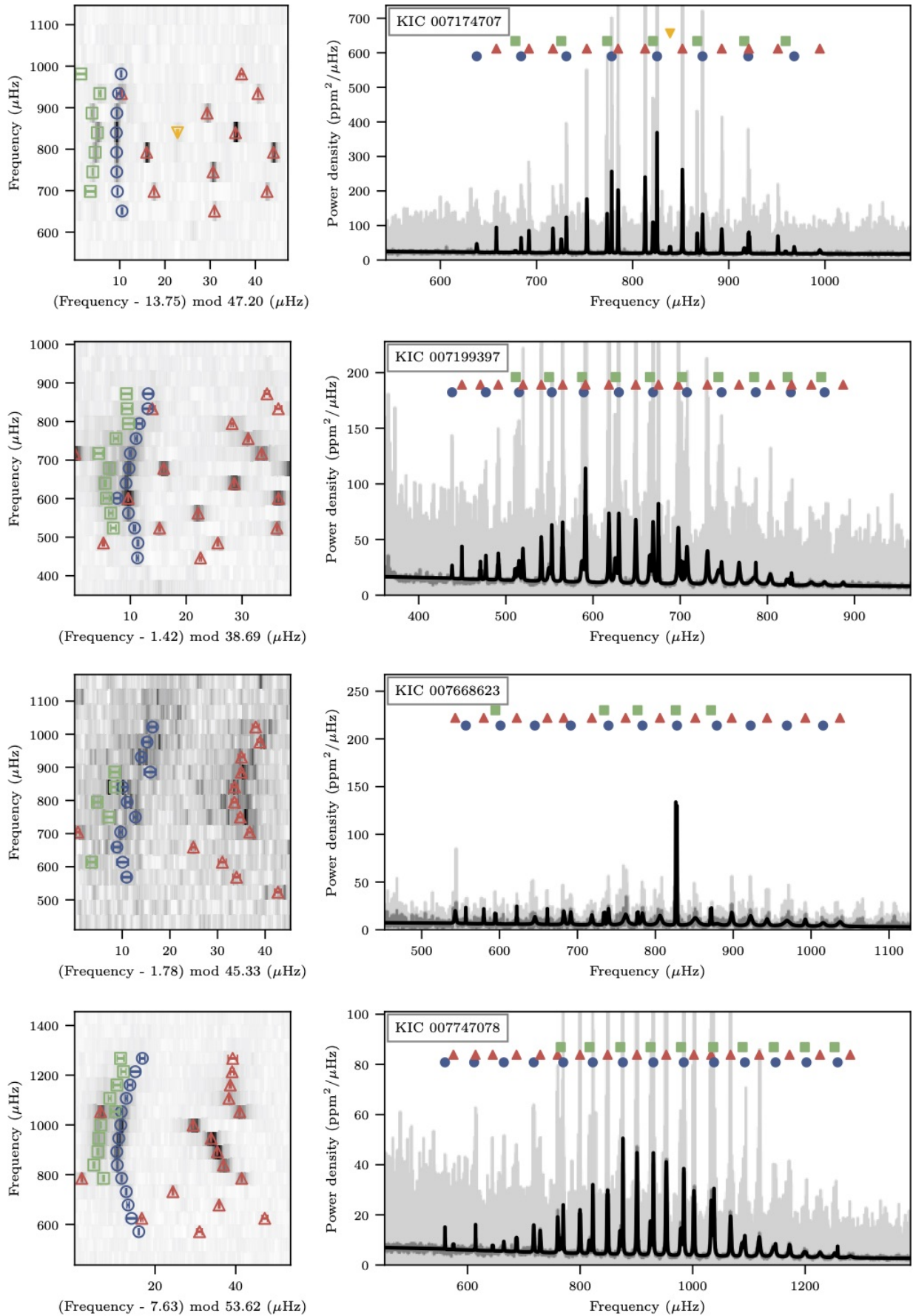
APPENDIX A: POWER SPECTRA OF 36 SUBGIANTS.

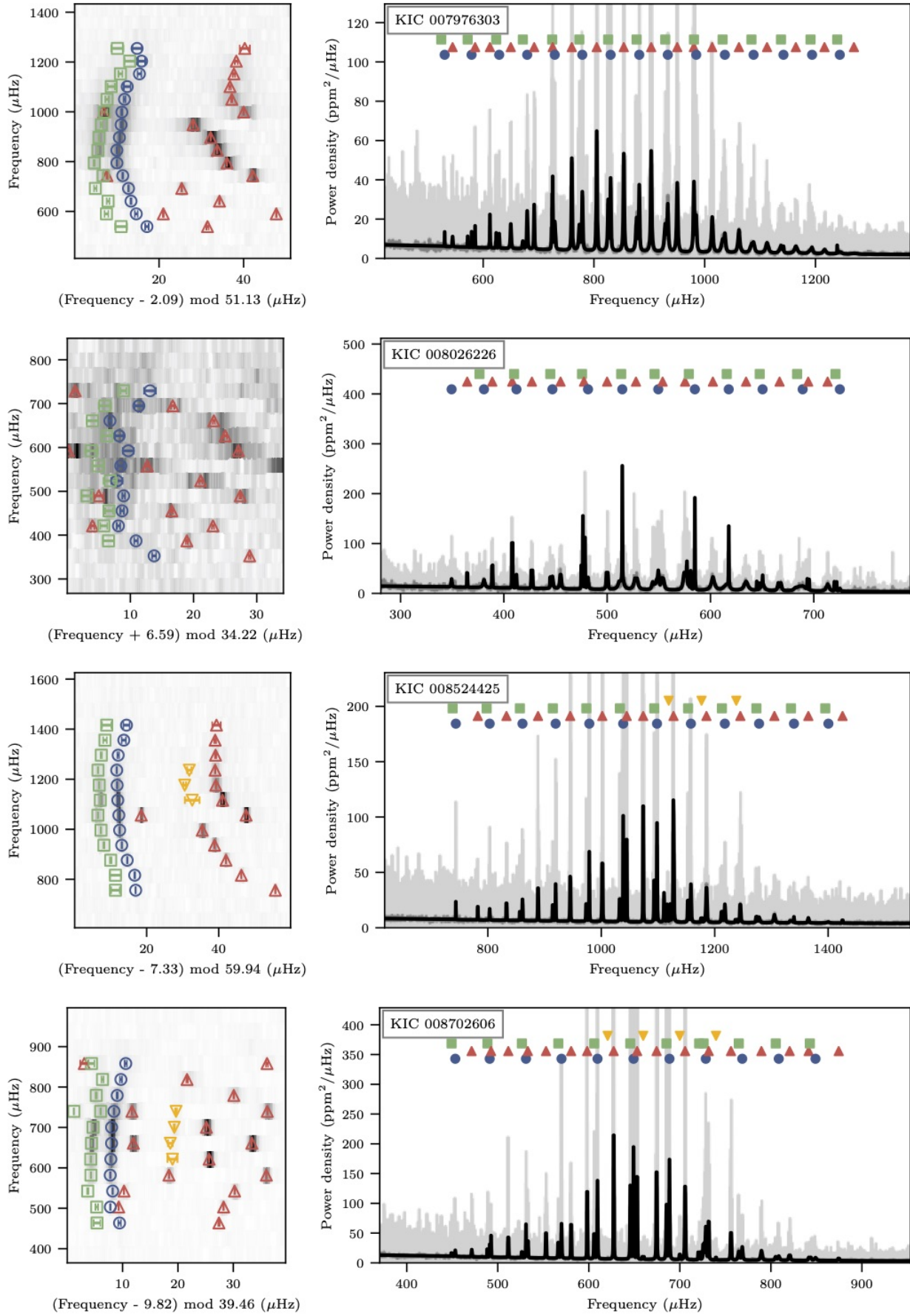
Left: échelle diagrams. The blue circles ($l = 0$), red upward triangles ($l = 1$), green squares ($l = 2$) and purple downward triangles ($l = 3$) mark the extracted frequencies. Right: power spectra. The fitted power spectra (black) are overlaid on the original power spectra (light grey) and the $1.0 \mu\text{Hz}$ smoothed spectra (grey).

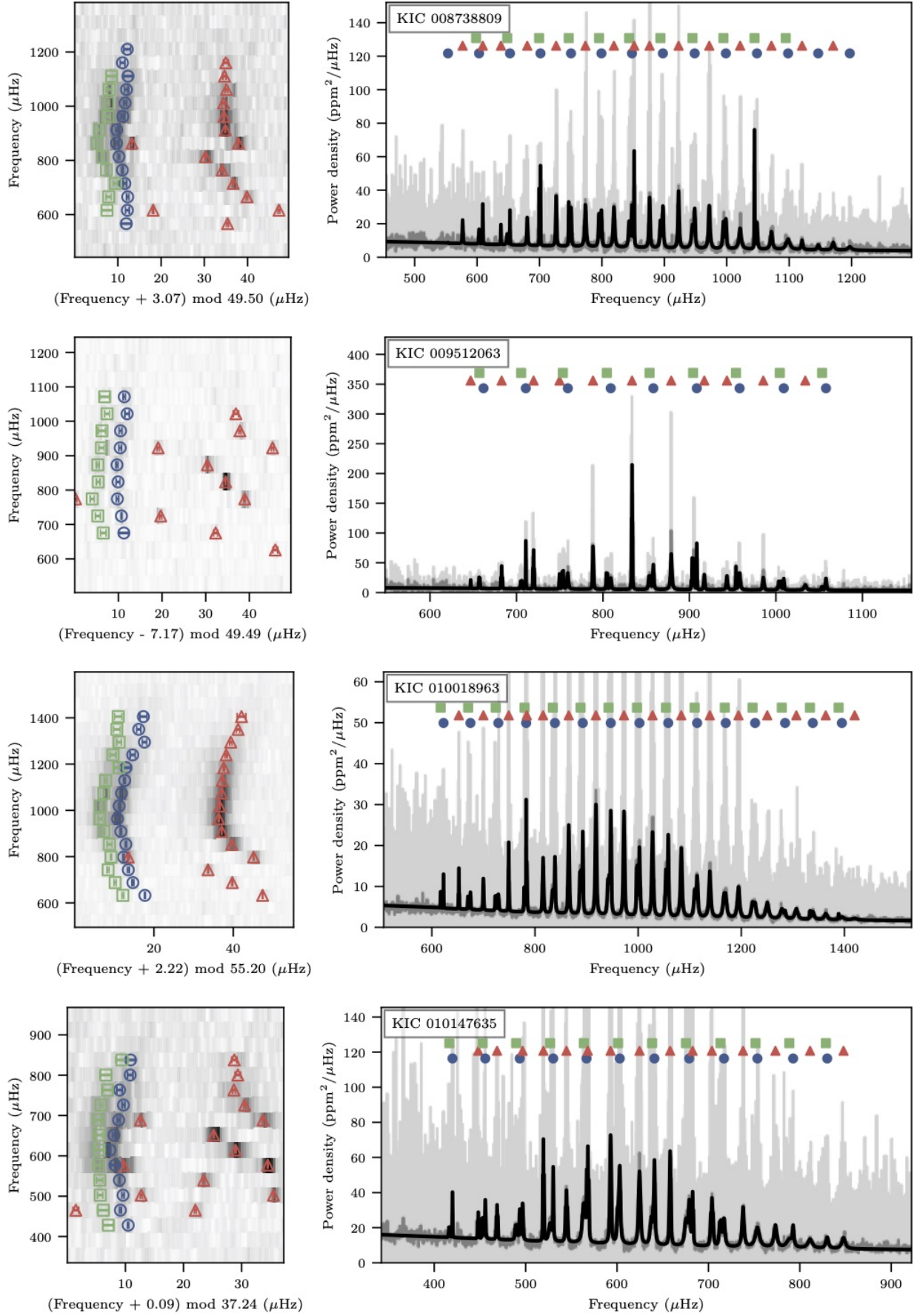


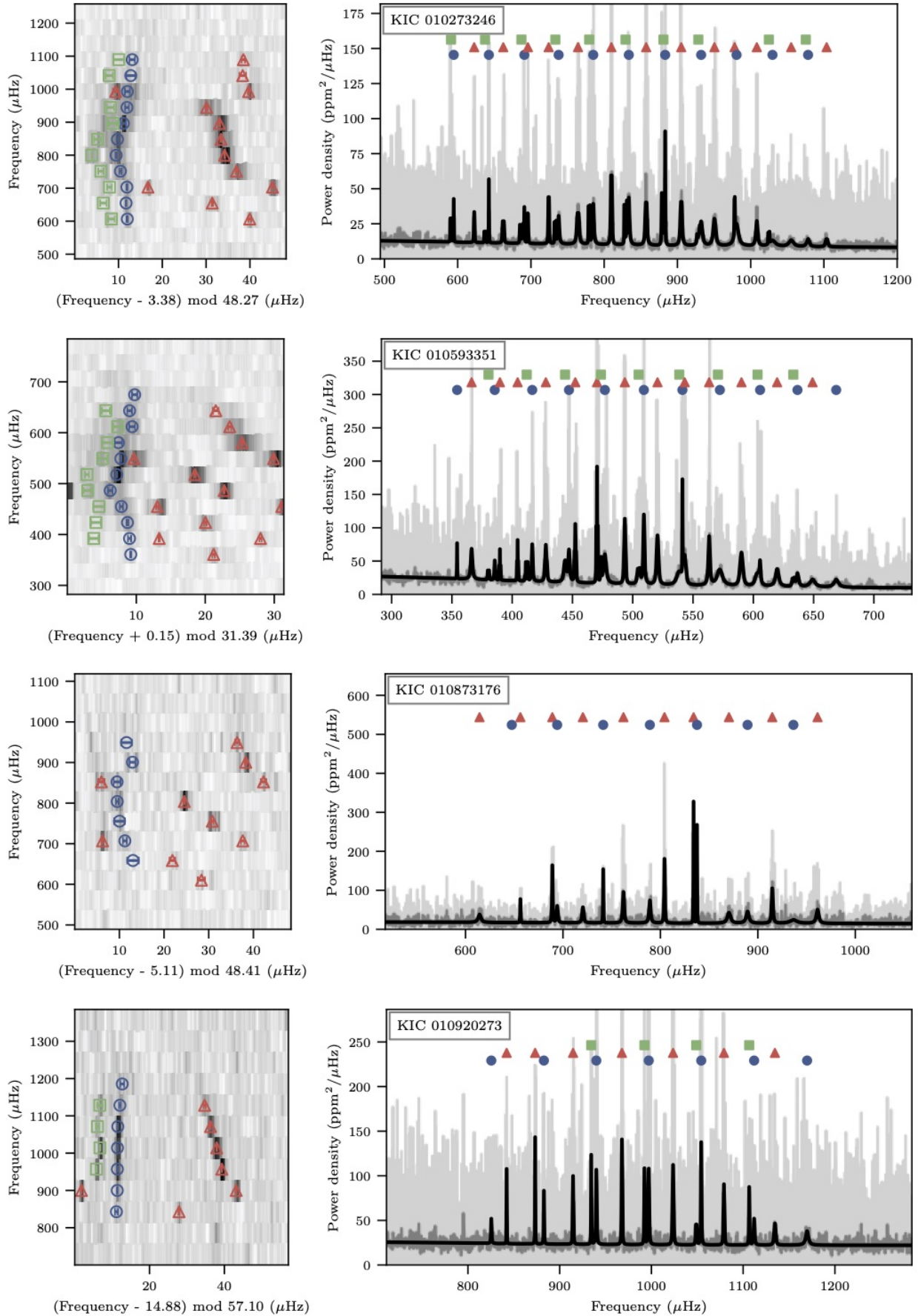


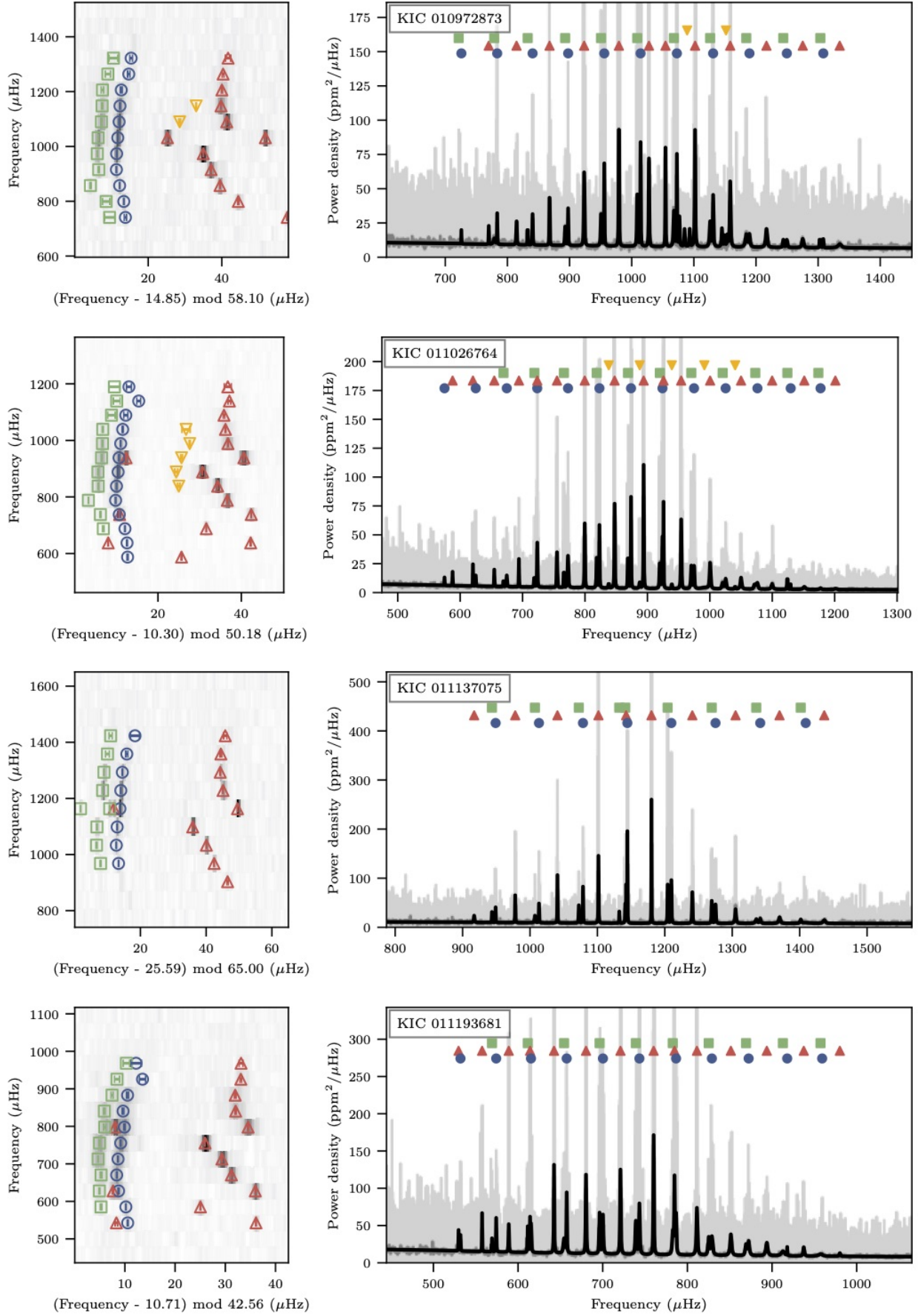












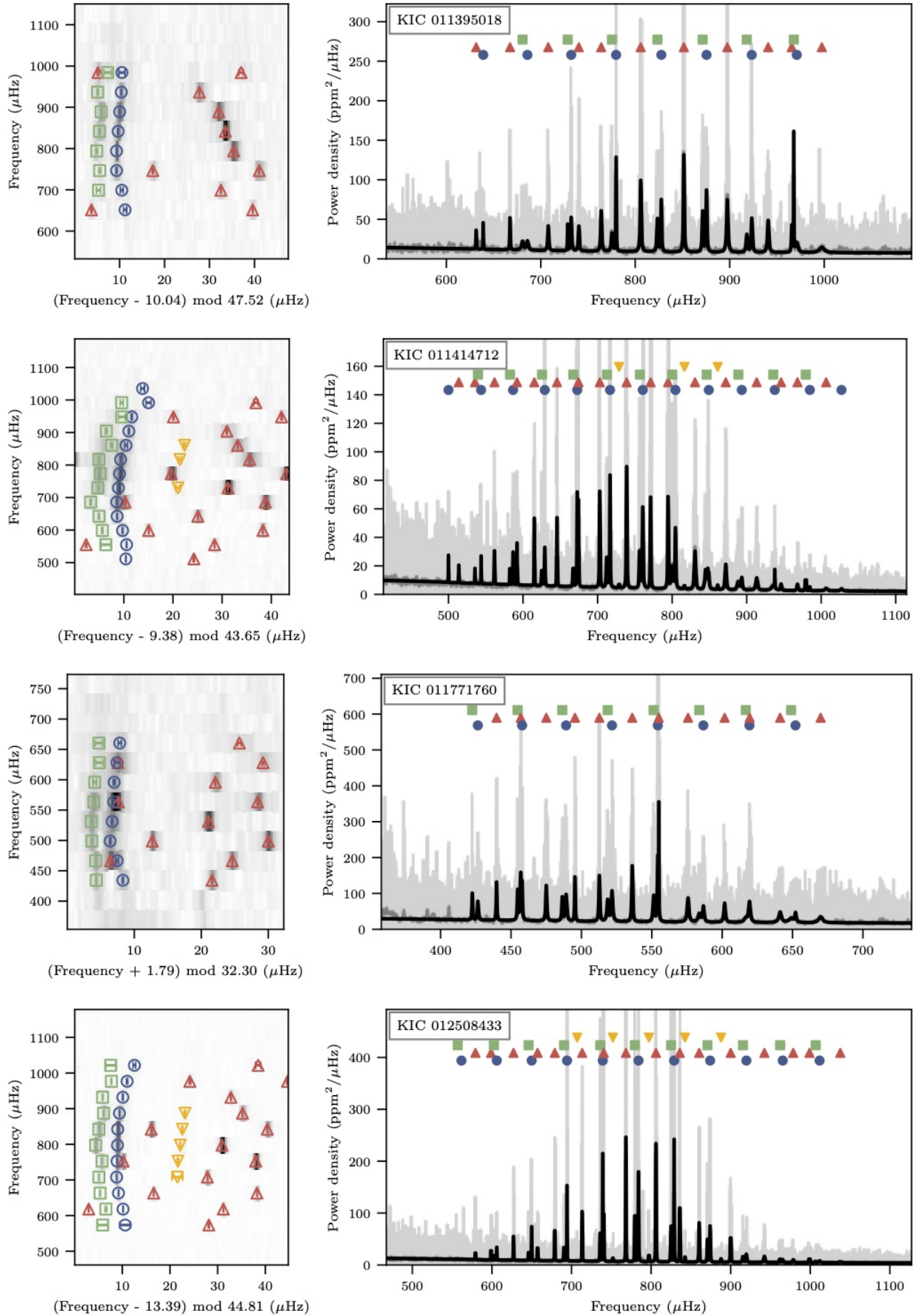


Table 2. Mode parameters obtained from the peakbagging. These are $m = 0$ modes.

KIC	l	ν_{nl} (μHz)	Γ_{nl} (μHz)	A_{nl} (ppm)	$\ln K$
2991448	0	889.34 ± 0.312	0.79 ± 0.96	4.04 ± 1.08	2.16 ± 0.75
2991448	0	949.46 ± 1.111	8.02 ± 2.37	9.16 ± 1.13	3.61 ± 0.98
2991448	0	1011.17 ± 0.202	1.15 ± 0.46	6.69 ± 0.87	20.49 ± 4.32
2991448	0	1072.78 ± 0.099	0.76 ± 0.24	10.45 ± 1.06	39.42 ± 2.54
2991448	0	1134.18 ± 0.113	0.89 ± 0.28	10.05 ± 0.98	47.86 ± 2.81
2991448	0	1195.89 ± 0.547	3.29 ± 1.72	9.45 ± 1.68	5.40 ± 2.13
2991448	0	1257.81 ± 0.969	3.53 ± 2.63	7.10 ± 2.09	2.68 ± 1.52
2991448	0	1319.52 ± 1.294	3.00 ± 3.56	3.60 ± 2.33	0.18 ± 1.20
2991448	1	857.88 ± 0.384	0.97 ± 0.79	4.16 ± 1.15	-0.21 ± 0.69
2991448	1	915.60 ± 0.153	0.81 ± 0.32	6.80 ± 0.90	19.19 ± 1.16
2991448	1	972.21 ± 0.315	2.29 ± 0.65	9.42 ± 0.88	26.94 ± 1.18
2991448	1	1017.00 ± 0.062	0.37 ± 0.08	7.71 ± 0.97	47.76 ± 4.28
2991448	1	1047.57 ± 0.098	0.73 ± 0.26	9.63 ± 1.01	50.36 ± 1.28
2991448	1	1102.77 ± 0.126	1.24 ± 0.30	12.93 ± 1.00	81.17 ± 1.46
2991448	1	1162.83 ± 0.110	0.94 ± 0.26	11.35 ± 1.01	71.85 ± 1.41
2991448	1	1223.72 ± 0.253	2.28 ± 1.05	9.14 ± 0.97	19.00 ± 1.09
2991448	1	1285.63 ± 0.137	0.85 ± 0.50	6.17 ± 0.92	15.99 ± 1.17
2991448	1	1347.43 ± 0.498	2.54 ± 1.57	5.88 ± 1.00	6.32 ± 0.88
2991448	2	1003.88 ± 0.060	0.36 ± 0.07	6.38 ± 0.87	41.16 ± 4.07
2991448	2	1067.44 ± 0.229	1.39 ± 0.80	6.86 ± 1.00	18.34 ± 2.37
2991448	2	1129.15 ± 0.103	0.71 ± 0.22	9.83 ± 1.02	47.01 ± 2.75
2991448	2	1190.73 ± 0.442	1.75 ± 1.28	7.45 ± 1.73	4.80 ± 2.07
2991448	2	1253.60 ± 0.908	3.29 ± 2.73	5.42 ± 2.61	0.52 ± 1.40
2991448	2	1314.25 ± 1.429	7.87 ± 3.61	7.41 ± 1.99	1.10 ± 1.51
3852594	0	689.59 ± 0.397	1.75 ± 1.45	5.01 ± 1.14	1.11 ± 0.75
3852594	0	740.92 ± 0.777	4.54 ± 1.60	9.02 ± 1.00	12.82 ± 0.97
3852594	0	793.75 ± 0.983	9.10 ± 1.82	10.43 ± 1.01	0.76 ± 1.02
3852594	0	845.10 ± 0.469	5.50 ± 1.28	12.31 ± 0.87	20.40 ± 1.09
3852594	0	895.93 ± 0.513	7.08 ± 1.31	13.39 ± 0.83	18.72 ± 1.07
3852594	0	949.32 ± 0.350	4.15 ± 1.07	11.85 ± 0.85	24.81 ± 1.15
3852594	0	1000.63 ± 0.437	6.97 ± 1.34	11.82 ± 0.83	17.36 ± 1.13
3852594	0	1054.72 ± 0.838	7.11 ± 1.87	9.59 ± 0.93	7.16 ± 0.93
3852594	1	671.63 ± 0.336	1.20 ± 0.96	4.53 ± 1.03	3.80 ± 0.80
3852594	1	715.57 ± 0.571	3.72 ± 1.31	7.95 ± 0.95	10.69 ± 0.97
3852594	1	764.36 ± 0.650	3.42 ± 1.91	6.33 ± 1.12	4.52 ± 0.78
3852594	1	808.82 ± 0.398	3.92 ± 1.10	10.06 ± 0.86	17.11 ± 1.08
3852594	1	834.80 ± 0.735	8.73 ± 0.99	11.98 ± 0.90	-1.77 ± 1.17
3852594	1	874.27 ± 0.195	2.26 ± 0.50	10.58 ± 0.72	45.03 ± 1.34
3852594	1	923.27 ± 0.301	3.75 ± 0.75	11.69 ± 0.73	35.44 ± 1.31
3852594	1	975.26 ± 0.276	3.31 ± 0.82	10.72 ± 0.78	27.57 ± 1.26
3852594	1	1028.80 ± 0.561	5.15 ± 1.21	9.79 ± 0.83	16.14 ± 0.97
3852594	1	1081.75 ± 0.729	5.68 ± 1.65	8.89 ± 0.91	7.43 ± 0.86
4346201	0	684.41 ± 1.900	0.69 ± 1.17	3.18 ± 1.16	3.38 ± 0.53
4346201	0	739.16 ± 1.301	2.06 ± 2.24	2.47 ± 1.37	1.25 ± 0.23
4346201	0	795.14 ± 0.482	4.71 ± 1.77	7.70 ± 1.21	9.77 ± 1.63
4346201	0	850.26 ± 0.404	1.99 ± 0.90	6.70 ± 0.95	12.61 ± 1.01
4346201	0	904.78 ± 1.131	1.38 ± 1.99	3.35 ± 1.97	0.46 ± 1.90
4346201	0	960.36 ± 0.240	1.10 ± 0.68	7.17 ± 1.39	2.56 ± 1.90
4346201	0	1016.86 ± 0.476	2.16 ± 1.47	6.19 ± 1.28	2.50 ± 2.07
4346201	0	1073.55 ± 0.358	2.35 ± 0.97	8.54 ± 1.12	6.10 ± 2.92
4346201	0	1128.51 ± 0.505	5.74 ± 1.82	10.16 ± 1.35	5.81 ± 1.97
4346201	0	1187.01 ± 0.949	3.95 ± 3.29	5.56 ± 2.24	1.16 ± 1.64
4346201	0	1243.84 ± 0.521	3.44 ± 1.77	6.98 ± 0.94	9.34 ± 0.90
4346201	1	708.74 ± 0.530	0.94 ± 0.68	5.01 ± 0.99	8.08 ± 0.91
4346201	1	762.14 ± 0.568	1.60 ± 1.23	5.36 ± 1.05	5.83 ± 0.74
4346201	1	804.71 ± 1.693	2.18 ± 2.36	2.24 ± 1.64	-0.30 ± 1.55
4346201	1	830.58 ± 0.382	0.93 ± 0.54	7.07 ± 1.03	18.46 ± 1.10
4346201	1	877.90 ± 0.371	2.63 ± 0.77	10.89 ± 0.95	31.27 ± 1.18

Continued on next page

KIC	l	ν_{nl} (μHz)	Γ_{nl} (μHz)	A_{nl} (ppm)	$\ln K$
4346201	1	930.92 \pm 0.303	2.07 \pm 0.73	10.03 \pm 0.95	27.27 \pm 1.17
4346201	1	986.31 \pm 0.285	1.99 \pm 0.69	11.44 \pm 0.95	36.92 \pm 1.33
4346201	1	1042.66 \pm 0.391	3.13 \pm 1.20	10.04 \pm 0.93	—
4346201	1	1098.33 \pm 0.544	1.96 \pm 1.06	7.02 \pm 0.86	14.88 \pm 0.99
4346201	1	1154.44 \pm 0.440	4.02 \pm 1.22	10.73 \pm 0.88	18.57 \pm 1.09
4346201	1	1209.31 \pm 0.887	6.56 \pm 2.54	6.90 \pm 0.99	1.40 \pm 0.86
4346201	1	1268.31 \pm 0.824	1.79 \pm 2.14	3.40 \pm 1.11	1.23 \pm 0.41
4346201	2	900.65 \pm 0.646	2.14 \pm 3.06	9.76 \pm 1.49	5.40 \pm 2.03
4346201	2	956.18 \pm 1.156	3.05 \pm 2.66	6.63 \pm 1.58	3.76 \pm 1.62
4346201	2	1011.02 \pm 0.498	1.47 \pm 1.32	7.63 \pm 1.14	7.30 \pm 2.04
4346201	2	1068.24 \pm 0.986	1.42 \pm 1.42	5.56 \pm 1.29	3.78 \pm 1.80
4346201	2	1123.67 \pm 1.433	1.75 \pm 2.17	4.13 \pm 2.16	-0.11 \pm 1.70
4346201	2	1179.74 \pm 1.471	7.80 \pm 1.91	8.43 \pm 1.74	2.43 \pm 1.74
5108214	0	463.00 \pm 0.397	1.51 \pm 1.15	4.62 \pm 1.00	5.51 \pm 0.73
5108214	0	503.02 \pm 0.152	0.60 \pm 0.34	4.49 \pm 0.81	6.42 \pm 2.54
5108214	0	543.41 \pm 0.238	1.34 \pm 0.48	6.06 \pm 0.74	19.51 \pm 2.14
5108214	0	584.53 \pm 0.189	1.25 \pm 0.51	6.80 \pm 0.94	3.49 \pm 2.81
5108214	0	623.92 \pm 0.240	2.96 \pm 0.68	10.36 \pm 0.69	—
5108214	0	664.59 \pm 0.111	0.96 \pm 0.27	10.51 \pm 1.01	7.94 \pm 4.34
5108214	0	705.22 \pm 0.536	2.25 \pm 0.91	8.65 \pm 1.82	8.32 \pm 2.66
5108214	0	747.17 \pm 0.210	1.61 \pm 0.50	8.41 \pm 0.89	18.71 \pm 3.09
5108214	0	789.65 \pm 0.379	0.80 \pm 0.64	3.89 \pm 1.49	0.14 \pm 2.49
5108214	0	830.55 \pm 0.358	1.78 \pm 0.68	8.38 \pm 1.24	20.72 \pm 3.15
5108214	0	871.18 \pm 0.428	2.57 \pm 0.93	7.03 \pm 1.44	3.04 \pm 2.62
5108214	0	913.01 \pm 0.467	4.17 \pm 1.00	6.01 \pm 0.52	23.28 \pm 2.57
5108214	1	479.27 \pm 0.402	0.59 \pm 0.52	3.81 \pm 0.84	5.50 \pm 0.94
5108214	1	509.08 \pm 0.533	1.03 \pm 0.76	3.69 \pm 0.92	3.81 \pm 1.66
5108214	1	535.07 \pm 0.721	3.52 \pm 1.86	5.69 \pm 0.97	8.71 \pm 1.84
5108214	1	566.37 \pm 0.089	0.56 \pm 0.19	8.42 \pm 0.78	62.66 \pm 1.59
5108214	1	602.59 \pm 0.183	1.53 \pm 0.41	9.83 \pm 0.68	57.31 \pm 1.41
5108214	1	635.51 \pm 0.212	1.63 \pm 0.43	8.76 \pm 0.65	47.35 \pm 1.37
5108214	1	655.89 \pm 0.122	0.81 \pm 0.31	8.33 \pm 0.80	1.83 \pm 4.92
5108214	1	686.90 \pm 0.166	1.78 \pm 0.39	10.95 \pm 0.67	72.04 \pm 1.44
5108214	1	726.37 \pm 0.151	1.83 \pm 0.34	13.00 \pm 0.71	96.52 \pm 1.47
5108214	1	766.90 \pm 0.132	1.26 \pm 0.33	10.38 \pm 0.66	92.53 \pm 1.51
5108214	1	807.25 \pm 0.222	2.93 \pm 0.67	9.75 \pm 0.55	—
5108214	1	847.85 \pm 0.236	2.82 \pm 0.60	9.35 \pm 0.52	—
5108214	1	885.18 \pm 0.281	2.45 \pm 0.63	6.55 \pm 0.46	34.52 \pm 1.25
5108214	1	906.98 \pm 0.147	0.85 \pm 0.31	5.36 \pm 0.52	31.17 \pm 2.62
5108214	1	937.04 \pm 0.182	2.30 \pm 1.15	4.67 \pm 0.46	11.57 \pm 1.14
5108214	2	498.86 \pm 1.049	1.02 \pm 1.33	1.39 \pm 0.93	-0.35 \pm 1.96
5108214	2	581.10 \pm 0.462	0.88 \pm 0.62	5.58 \pm 0.97	8.07 \pm 2.27
5108214	2	661.07 \pm 0.269	1.48 \pm 0.77	9.47 \pm 1.05	12.21 \pm 6.22
5108214	2	702.28 \pm 0.475	1.72 \pm 0.95	8.00 \pm 1.97	2.61 \pm 2.32
5108214	2	744.02 \pm 0.229	1.30 \pm 0.58	7.48 \pm 0.91	8.69 \pm 2.56
5108214	2	786.76 \pm 0.280	1.79 \pm 0.46	11.25 \pm 0.77	16.24 \pm 2.64
5108214	2	827.37 \pm 0.568	1.78 \pm 1.02	6.16 \pm 1.53	3.75 \pm 2.40
5108214	2	867.42 \pm 0.894	1.83 \pm 1.48	5.72 \pm 1.56	4.23 \pm 2.14
5607242	0	504.04 \pm 0.086	0.48 \pm 0.20	3.52 \pm 0.49	10.68 \pm 3.35
5607242	0	543.45 \pm 0.056	0.44 \pm 0.12	4.90 \pm 0.44	28.87 \pm 3.49
5607242	0	583.07 \pm 0.058	0.72 \pm 0.14	6.93 \pm 0.43	33.81 \pm 5.65
5607242	0	623.57 \pm 0.033	0.45 \pm 0.07	9.51 \pm 0.53	64.17 \pm 7.70
5607242	0	664.12 \pm 0.024	0.34 \pm 0.05	11.70 \pm 0.67	129.28 \pm 4.24
5607242	0	704.45 \pm 0.347	0.57 \pm 0.87	3.32 \pm 1.84	-2.33 \pm 5.65
5607242	0	745.27 \pm 0.040	0.63 \pm 0.09	9.85 \pm 0.47	128.69 \pm 6.81
5607242	0	786.33 \pm 0.123	1.56 \pm 0.27	6.77 \pm 0.41	8.16 \pm 5.52
5607242	0	827.16 \pm 0.235	1.56 \pm 0.81	4.10 \pm 0.67	8.81 \pm 4.14
5607242	0	868.23 \pm 0.493	3.25 \pm 1.37	4.34 \pm 0.66	1.21 \pm 2.97
5607242	1	509.18 \pm 0.062	0.25 \pm 0.09	3.90 \pm 0.44	20.81 \pm 2.89
5607242	1	527.44 \pm 0.064	0.32 \pm 0.11	4.34 \pm 0.42	32.00 \pm 1.73

Continued on next page

KIC	l	ν_{nl} (μHz)	Γ_{nl} (μHz)	A_{nl} (ppm)	$\ln K$
5607242	1	554.85 ± 0.063	0.54 ± 0.17	5.59 ± 0.46	60.97 ± 1.67
5607242	1	572.74 ± 0.053	0.34 ± 0.09	6.40 ± 0.43	105.04 ± 10.13
5607242	1	600.84 ± 0.030	0.31 ± 0.06	9.42 ± 0.53	285.83 ± 2.18
5607242	1	626.92 ± 0.028	0.24 ± 0.02	9.14 ± 0.49	256.00 ± 6.77
5607242	1	648.71 ± 0.027	0.29 ± 0.05	11.36 ± 0.59	445.24 ± 2.30
5607242	1	679.91 ± 0.025	0.31 ± 0.05	13.63 ± 0.68	280.07 ± 5.05
5607242	1	704.97 ± 0.067	0.32 ± 0.05	14.09 ± 0.88	23.94 ± 5.39
5607242	1	731.10 ± 0.041	0.52 ± 0.09	10.50 ± 0.48	356.76 ± 10.12
5607242	1	764.81 ± 0.062	0.79 ± 0.14	8.44 ± 0.39	103.11 ± 4.89
5607242	1	792.82 ± 0.069	0.49 ± 0.17	4.75 ± 0.39	58.17 ± 4.59
5607242	1	816.76 ± 0.101	0.72 ± 0.39	5.09 ± 0.42	27.14 ± 3.87
5607242	1	851.64 ± 0.148	0.63 ± 0.50	3.95 ± 0.42	21.17 ± 1.45
5607242	1	889.14 ± 0.338	0.86 ± 1.33	3.10 ± 0.54	4.88 ± 1.09
5607242	2	499.35 ± 0.731	0.52 ± 0.74	1.93 ± 0.94	0.24 ± 3.42
5607242	2	539.75 ± 0.051	0.25 ± 0.06	4.51 ± 0.42	43.30 ± 3.12
5607242	2	579.42 ± 0.086	0.43 ± 0.18	4.96 ± 0.44	40.86 ± 5.11
5607242	2	619.74 ± 0.039	0.30 ± 0.07	6.81 ± 0.43	149.24 ± 6.58
5607242	2	660.50 ± 0.048	0.41 ± 0.10	8.59 ± 0.46	264.40 ± 3.81
5607242	2	701.23 ± 0.043	0.56 ± 0.11	9.49 ± 0.47	129.57 ± 5.71
5607242	2	740.62 ± 0.058	0.54 ± 0.12	6.67 ± 0.41	145.80 ± 5.87
5607242	2	782.51 ± 0.128	0.90 ± 0.36	5.23 ± 0.44	31.20 ± 4.70
5607242	2	824.21 ± 0.217	1.01 ± 0.77	3.96 ± 0.66	3.27 ± 3.98
5607242	2	864.69 ± 0.992	1.04 ± 1.43	1.21 ± 0.81	-0.57 ± 1.35
5607242	3	635.31 ± 0.526	0.28 ± 0.05	9.16 ± 0.75	111.54 ± 9.99
5607242	3	675.52 ± 0.091	0.38 ± 0.15	3.16 ± 0.42	10.87 ± 4.50
5607242	3	716.12 ± 0.128	0.28 ± 0.12	3.05 ± 0.39	15.79 ± 2.56
5607242	3	757.19 ± 0.178	0.36 ± 0.18	2.53 ± 0.44	5.00 ± 3.83
5607242	3	797.58 ± 0.141	0.67 ± 0.14	5.46 ± 0.43	18.49 ± 4.19
5689820	0	516.24 ± 0.138	0.55 ± 0.33	4.64 ± 0.98	5.58 ± 1.12
5689820	0	556.61 ± 0.036	0.22 ± 0.05	6.67 ± 0.79	2.96 ± 4.99
5689820	0	597.29 ± 0.054	0.36 ± 0.10	8.54 ± 0.94	6.67 ± 3.25
5689820	0	638.20 ± 0.026	0.22 ± 0.03	10.83 ± 0.93	38.94 ± 4.64
5689820	0	679.26 ± 0.016	0.20 ± 0.01	17.68 ± 1.19	80.50 ± 6.14
5689820	0	720.38 ± 0.023	0.24 ± 0.02	13.29 ± 1.00	21.20 ± 7.99
5689820	0	761.75 ± 0.035	0.27 ± 0.05	9.11 ± 0.83	41.91 ± 4.26
5689820	0	803.23 ± 0.149	0.72 ± 0.33	6.81 ± 1.90	-0.52 ± 4.18
5689820	0	845.36 ± 0.529	1.68 ± 1.36	4.38 ± 1.47	0.50 ± 1.56
5689820	1	576.41 ± 0.056	0.27 ± 0.07	7.76 ± 0.77	50.11 ± 1.62
5689820	1	619.32 ± 0.042	0.26 ± 0.06	9.42 ± 0.86	88.66 ± 1.88
5689820	1	648.78 ± 0.022	0.26 ± 0.02	11.97 ± 0.89	172.65 ± 2.65
5689820	1	664.01 ± 0.026	0.21 ± 0.02	15.36 ± 1.09	345.39 ± 2.52
5689820	1	697.60 ± 0.024	0.22 ± 0.01	16.25 ± 1.08	115.26 ± 5.00
5689820	1	722.62 ± 0.020	0.23 ± 0.01	9.76 ± 0.76	124.05 ± 7.32
5689820	1	743.32 ± 0.045	0.28 ± 0.06	12.41 ± 0.96	193.88 ± 1.98
5689820	1	778.39 ± 0.047	0.31 ± 0.08	10.23 ± 0.83	126.07 ± 1.82
5689820	1	805.82 ± 0.624	0.39 ± 0.16	5.43 ± 0.93	11.46 ± 4.25
5689820	1	828.78 ± 0.126	0.54 ± 0.32	5.39 ± 0.69	12.32 ± 1.62
5689820	1	862.48 ± 0.567	1.80 ± 1.31	4.98 ± 1.00	4.41 ± 0.74
5689820	1	893.86 ± 0.420	1.29 ± 0.88	5.83 ± 0.82	6.55 ± 1.05
5689820	2	511.19 ± 1.115	0.84 ± 1.27	1.19 ± 0.81	-1.13 ± 1.48
5689820	2	552.53 ± 0.321	0.40 ± 0.26	5.31 ± 0.83	7.28 ± 3.14
5689820	2	593.81 ± 0.159	0.39 ± 0.16	6.10 ± 0.92	18.21 ± 2.96
5689820	2	634.39 ± 0.064	0.31 ± 0.09	8.84 ± 0.79	81.23 ± 3.81
5689820	2	675.38 ± 0.030	0.23 ± 0.02	14.61 ± 1.08	346.43 ± 4.67
5689820	2	716.51 ± 0.030	0.24 ± 0.03	11.15 ± 0.92	156.51 ± 11.24
5689820	2	757.98 ± 0.069	0.39 ± 0.13	8.42 ± 0.73	78.13 ± 3.57
5689820	2	799.84 ± 0.849	0.74 ± 0.47	6.57 ± 1.30	9.60 ± 4.71
5689820	2	842.40 ± 1.064	1.14 ± 1.40	3.07 ± 1.75	0.32 ± 1.08
5689820	3	690.94 ± 0.066	0.31 ± 0.10	5.96 ± 0.68	24.76 ± 4.64
5689820	3	731.47 ± 0.785	0.70 ± 0.92	4.59 ± 1.09	2.70 ± 8.64

Continued on next page

KIC	l	ν_{nl} (μHz)	Γ_{nl} (μHz)	A_{nl} (ppm)	$\ln K$
5955122	0	609.68 ± 0.125	0.83 ± 0.35	3.04 ± 0.37	18.24 ± 1.49
5955122	0	657.01 ± 0.732	1.32 ± 0.99	2.28 ± 1.52	-0.41 ± 3.25
5955122	0	706.28 ± 0.096	1.37 ± 0.23	6.11 ± 0.36	14.14 ± 3.57
5955122	0	754.44 ± 0.075	1.29 ± 0.18	7.44 ± 0.34	32.31 ± 4.26
5955122	0	803.80 ± 0.050	0.92 ± 0.12	8.84 ± 0.38	47.80 ± 6.48
5955122	0	853.52 ± 0.058	1.13 ± 0.14	9.68 ± 0.39	40.47 ± 4.34
5955122	0	903.11 ± 0.080	1.54 ± 0.19	8.48 ± 0.36	21.30 ± 4.38
5955122	0	952.53 ± 0.113	2.06 ± 0.25	7.74 ± 0.36	49.43 ± 4.23
5955122	0	1002.84 ± 0.173	1.65 ± 0.47	4.68 ± 0.69	3.86 ± 3.35
5955122	0	1053.78 ± 0.985	2.69 ± 1.88	2.02 ± 1.46	-1.00 ± 2.80
5955122	0	1102.72 ± 0.636	6.54 ± 1.46	5.17 ± 0.54	25.68 ± 2.71
5955122	0	1154.91 ± 0.811	2.98 ± 1.83	2.71 ± 0.82	2.97 ± 2.70
5955122	1	586.26 ± 0.144	0.51 ± 0.30	2.73 ± 0.35	13.11 ± 1.66
5955122	1	623.69 ± 0.107	0.63 ± 0.23	3.98 ± 0.31	43.18 ± 1.54
5955122	1	658.21 ± 0.188	0.94 ± 0.32	5.66 ± 0.87	0.44 ± 3.29
5955122	1	690.06 ± 0.072	0.73 ± 0.15	6.01 ± 0.28	153.03 ± 2.07
5955122	1	731.22 ± 0.057	0.78 ± 0.11	8.69 ± 0.32	369.42 ± 2.15
5955122	1	774.76 ± 0.055	0.83 ± 0.11	9.02 ± 0.31	388.14 ± 2.21
5955122	1	809.66 ± 0.047	0.59 ± 0.11	7.60 ± 0.33	261.62 ± 6.51
5955122	1	836.63 ± 0.054	0.93 ± 0.12	10.11 ± 0.33	507.46 ± 2.15
5955122	1	879.92 ± 0.062	1.37 ± 0.15	11.76 ± 0.33	—
5955122	1	927.43 ± 0.069	1.85 ± 0.17	10.98 ± 0.30	—
5955122	1	976.04 ± 0.091	2.39 ± 0.25	9.73 ± 0.26	333.30 ± 1.93
5955122	1	1024.88 ± 0.164	3.59 ± 0.50	7.47 ± 0.24	147.44 ± 1.65
5955122	1	1073.40 ± 0.250	4.92 ± 0.73	5.91 ± 0.25	—
5955122	1	1118.98 ± 0.299	4.03 ± 1.07	4.48 ± 0.29	33.59 ± 1.33
5955122	1	1145.92 ± 0.557	4.17 ± 1.68	3.28 ± 0.49	2.12 ± 3.88
5955122	2	653.87 ± 0.962	1.03 ± 0.68	3.01 ± 0.71	4.28 ± 3.08
5955122	2	702.25 ± 0.269	0.98 ± 0.36	4.58 ± 0.39	33.63 ± 3.17
5955122	2	750.13 ± 0.148	1.13 ± 0.37	5.66 ± 0.36	57.63 ± 3.63
5955122	2	799.59 ± 0.118	1.22 ± 0.29	6.98 ± 0.33	104.76 ± 6.02
5955122	2	849.33 ± 0.169	1.91 ± 0.45	8.04 ± 0.38	107.93 ± 3.70
5955122	2	898.59 ± 0.191	2.49 ± 0.54	7.60 ± 0.39	78.91 ± 3.56
5955122	2	948.37 ± 0.161	1.97 ± 0.45	6.69 ± 0.40	51.60 ± 3.55
5955122	2	998.69 ± 0.426	3.80 ± 0.91	7.27 ± 0.54	23.27 ± 3.25
5955122	2	1050.64 ± 0.722	3.46 ± 1.01	6.15 ± 0.65	10.71 ± 2.72
5955122	2	1097.26 ± 0.605	1.95 ± 1.50	2.68 ± 0.73	2.54 ± 2.27
5955122	2	1151.99 ± 1.346	2.10 ± 2.37	1.76 ± 1.11	-0.05 ± 2.55
6064910	0	663.44 ± 0.441	7.60 ± 0.90	12.90 ± 0.96	2.07 ± 1.33
6064910	0	709.03 ± 0.320	1.97 ± 0.95	7.80 ± 1.33	5.58 ± 2.57
6064910	0	751.59 ± 0.552	7.43 ± 1.08	13.19 ± 0.90	6.80 ± 1.01
6064910	0	794.41 ± 0.496	6.43 ± 1.37	12.96 ± 0.94	—
6064910	0	840.14 ± 0.473	5.50 ± 1.18	12.01 ± 0.87	16.31 ± 0.99
6064910	0	883.46 ± 0.622	5.28 ± 1.68	8.70 ± 1.04	3.26 ± 1.00
6064910	1	545.91 ± 0.335	0.88 ± 0.63	5.40 ± 0.99	7.31 ± 0.99
6064910	1	575.54 ± 0.462	6.37 ± 1.51	10.97 ± 1.09	4.34 ± 1.16
6064910	1	608.54 ± 0.475	2.85 ± 1.52	9.06 ± 1.18	11.82 ± 0.93
6064910	1	642.67 ± 0.395	1.33 ± 0.74	7.19 ± 0.91	10.21 ± 1.12
6064910	1	677.94 ± 0.267	2.09 ± 0.69	9.86 ± 0.84	22.31 ± 1.17
6064910	1	704.86 ± 0.214	1.82 ± 0.68	10.82 ± 1.11	18.88 ± 2.50
6064910	1	735.26 ± 0.366	4.34 ± 1.05	14.23 ± 0.83	30.76 ± 1.32
6064910	1	776.20 ± 0.312	3.07 ± 0.92	12.70 ± 0.82	31.19 ± 1.32
6064910	1	817.15 ± 0.364	3.92 ± 1.12	12.48 ± 0.86	23.17 ± 1.18
6064910	1	862.70 ± 0.433	5.28 ± 1.32	12.53 ± 0.92	12.77 ± 1.08
6064910	1	904.86 ± 0.743	3.06 ± 1.47	7.01 ± 0.99	7.23 ± 0.85
6064910	1	947.52 ± 0.614	4.88 ± 1.71	9.04 ± 1.01	5.72 ± 0.84
6064910	1	976.69 ± 0.191	1.37 ± 0.60	7.70 ± 0.82	15.27 ± 1.25
6064910	1	1001.45 ± 0.730	5.57 ± 1.81	8.69 ± 1.05	3.66 ± 0.87
6370489	0	687.93 ± 0.216	0.72 ± 0.51	4.54 ± 1.09	3.21 ± 2.55
6370489	0	735.98 ± 0.325	2.41 ± 0.87	8.48 ± 0.86	21.91 ± 1.07

Continued on next page

KIC	l	ν_{nl} (μHz)	Γ_{nl} (μHz)	A_{nl} (ppm)	$\ln K$
6370489	0	786.74 ± 0.765	2.70 ± 2.75	5.73 ± 2.53	0.93 ± 1.37
6370489	0	837.21 ± 0.367	1.81 ± 0.92	8.41 ± 1.69	2.36 ± 2.25
6370489	0	889.73 ± 0.206	1.34 ± 0.46	8.45 ± 0.99	19.60 ± 2.39
6370489	0	941.95 ± 0.385	2.13 ± 0.85	9.11 ± 1.35	5.00 ± 2.25
6370489	0	993.71 ± 0.581	4.82 ± 1.31	10.36 ± 1.14	3.45 ± 2.18
6370489	0	1046.82 ± 0.886	5.49 ± 2.36	7.57 ± 1.48	6.22 ± 1.77
6370489	0	1098.46 ± 0.604	4.28 ± 1.50	7.42 ± 0.97	5.47 ± 1.66
6370489	0	1152.83 ± 0.835	1.77 ± 2.90	2.37 ± 1.55	0.31 ± 1.40
6370489	0	1206.00 ± 1.478	6.08 ± 3.24	3.13 ± 1.75	0.53 ± 1.27
6370489	1	607.06 ± 0.555	1.31 ± 1.28	3.79 ± 0.99	4.67 ± 0.59
6370489	1	649.91 ± 0.201	0.48 ± 0.35	3.34 ± 0.81	6.39 ± 1.01
6370489	1	685.04 ± 0.549	1.09 ± 0.98	3.90 ± 1.15	2.96 ± 2.37
6370489	1	721.36 ± 0.280	1.37 ± 0.70	6.55 ± 0.84	13.85 ± 0.99
6370489	1	763.68 ± 0.267	1.60 ± 0.58	8.53 ± 0.86	33.94 ± 1.15
6370489	1	810.87 ± 0.275	2.25 ± 0.64	9.85 ± 0.85	39.61 ± 1.26
6370489	1	859.87 ± 0.274	2.27 ± 0.71	11.01 ± 0.88	40.98 ± 1.31
6370489	1	907.32 ± 0.225	2.11 ± 0.51	12.33 ± 0.95	59.23 ± 1.32
6370489	1	938.18 ± 0.427	1.45 ± 1.17	9.37 ± 3.70	0.43 ± 2.47
6370489	1	971.02 ± 0.327	3.05 ± 0.77	9.68 ± 0.74	35.46 ± 1.24
6370489	1	1020.56 ± 0.390	4.41 ± 0.94	11.04 ± 0.73	28.91 ± 1.22
6370489	1	1070.93 ± 0.461	5.43 ± 1.25	10.16 ± 0.68	18.99 ± 1.12
6370489	1	1123.06 ± 0.659	7.06 ± 1.45	8.48 ± 0.64	—
6370489	1	1175.54 ± 0.612	5.03 ± 1.75	5.88 ± 0.62	8.36 ± 0.87
6370489	1	1201.19 ± 0.769	5.81 ± 2.20	4.81 ± 0.65	3.75 ± 0.85
6370489	2	679.59 ± 0.386	0.87 ± 0.65	4.56 ± 0.83	6.79 ± 2.35
6370489	2	782.70 ± 1.401	5.45 ± 3.25	6.83 ± 2.46	0.81 ± 1.42
6370489	2	833.00 ± 0.893	3.61 ± 1.71	8.72 ± 1.69	3.65 ± 1.93
6370489	2	883.50 ± 0.524	3.39 ± 1.63	7.59 ± 0.91	14.47 ± 2.09
6370489	2	937.24 ± 0.897	1.43 ± 1.18	5.83 ± 3.84	0.20 ± 2.47
6370489	2	988.43 ± 0.617	1.02 ± 1.66	5.13 ± 1.62	3.28 ± 2.12
6370489	2	1041.68 ± 1.174	3.41 ± 2.62	4.36 ± 2.15	0.35 ± 1.51
6370489	2	1094.54 ± 1.013	2.07 ± 2.31	2.94 ± 1.64	-0.14 ± 1.39
6370489	2	1148.45 ± 0.962	6.94 ± 2.69	5.95 ± 1.11	2.37 ± 1.68
6370489	2	1200.13 ± 1.013	3.63 ± 3.00	3.83 ± 1.26	1.70 ± 1.65
6442183	0	743.40 ± 0.457	2.21 ± 1.04	2.66 ± 0.42	9.13 ± 1.10
6442183	0	809.59 ± 0.186	0.60 ± 0.30	1.65 ± 0.33	4.95 ± 1.18
6442183	0	873.84 ± 0.099	0.89 ± 0.18	3.30 ± 0.25	58.23 ± 2.98
6442183	0	937.23 ± 0.048	0.52 ± 0.10	3.96 ± 0.26	132.89 ± 3.27
6442183	0	1000.94 ± 0.064	0.91 ± 0.16	5.15 ± 0.29	62.08 ± 4.98
6442183	0	1065.71 ± 0.044	0.72 ± 0.10	6.35 ± 0.30	301.02 ± 3.92
6442183	0	1130.44 ± 0.033	0.56 ± 0.07	8.82 ± 0.43	500.58 ± 4.40
6442183	0	1195.36 ± 0.035	0.62 ± 0.08	8.75 ± 0.40	517.79 ± 4.47
6442183	0	1260.30 ± 0.046	0.84 ± 0.10	6.93 ± 0.29	346.31 ± 4.18
6442183	0	1325.57 ± 0.108	2.13 ± 0.27	5.96 ± 0.24	72.14 ± 3.72
6442183	0	1391.80 ± 0.227	2.53 ± 0.57	3.60 ± 0.33	17.95 ± 2.92
6442183	0	1457.73 ± 0.264	2.31 ± 0.84	2.59 ± 0.38	8.62 ± 2.78
6442183	0	1524.24 ± 0.387	2.41 ± 1.29	1.99 ± 0.38	7.29 ± 2.13
6442183	0	1588.74 ± 1.177	3.72 ± 2.62	1.41 ± 0.65	0.74 ± 1.39
6442183	1	783.56 ± 0.119	0.68 ± 0.38	2.11 ± 0.32	12.60 ± 1.50
6442183	1	840.56 ± 0.042	0.36 ± 0.06	3.11 ± 0.26	78.15 ± 1.55
6442183	1	901.22 ± 0.062	0.73 ± 0.15	3.98 ± 0.26	109.72 ± 1.70
6442183	1	960.35 ± 0.057	0.76 ± 0.12	4.83 ± 0.26	216.84 ± 1.85
6442183	1	1002.88 ± 0.038	0.41 ± 0.05	4.47 ± 0.31	61.95 ± 5.02
6442183	1	1037.66 ± 0.035	0.52 ± 0.07	6.98 ± 0.35	542.82 ± 1.81
6442183	1	1096.79 ± 0.030	0.50 ± 0.06	9.41 ± 0.47	930.06 ± 1.94
6442183	1	1159.94 ± 0.034	0.66 ± 0.07	10.94 ± 0.47	1499.66 ± 7.18
6442183	1	1224.04 ± 0.037	0.75 ± 0.08	10.39 ± 0.42	1105.40 ± 4.82
6442183	1	1288.57 ± 0.063	1.48 ± 0.15	7.78 ± 0.26	527.44 ± 3.84
6442183	1	1353.94 ± 0.085	1.94 ± 0.19	6.44 ± 0.21	367.93 ± 1.82
6442183	1	1419.48 ± 0.151	2.87 ± 0.36	4.62 ± 0.18	137.11 ± 1.65

Continued on next page

KIC	<i>l</i>	ν_{nl} (μHz)	Γ_{nl} (μHz)	A_{nl} (ppm)	$\ln K$
6442183	1	1484.87 \pm 0.306	4.66 \pm 0.77	3.69 \pm 0.20	45.65 \pm 1.42
6442183	1	1552.23 \pm 0.638	6.67 \pm 1.53	2.96 \pm 0.24	16.93 \pm 0.98
6442183	1	1617.38 \pm 1.309	8.17 \pm 2.51	2.06 \pm 0.33	2.78 \pm 0.94
6442183	2	800.88 \pm 1.629	0.96 \pm 1.28	0.32 \pm 0.28	-1.01 \pm 1.61
6442183	2	868.07 \pm 0.102	0.45 \pm 0.20	1.83 \pm 0.28	9.76 \pm 2.88
6442183	2	931.29 \pm 0.063	0.51 \pm 0.13	2.64 \pm 0.25	42.93 \pm 3.20
6442183	2	996.95 \pm 0.078	0.79 \pm 0.15	3.66 \pm 0.25	76.45 \pm 5.01
6442183	2	1059.98 \pm 0.055	0.77 \pm 0.12	5.13 \pm 0.26	264.17 \pm 3.67
6442183	2	1124.81 \pm 0.053	0.85 \pm 0.11	6.07 \pm 0.27	391.64 \pm 3.96
6442183	2	1189.77 \pm 0.046	0.81 \pm 0.10	7.60 \pm 0.32	493.76 \pm 4.12
6442183	2	1254.56 \pm 0.063	1.16 \pm 0.13	6.49 \pm 0.25	332.97 \pm 3.98
6442183	2	1321.38 \pm 0.073	0.98 \pm 0.20	4.23 \pm 0.26	70.50 \pm 3.63
6442183	2	1387.10 \pm 0.254	3.37 \pm 0.63	4.17 \pm 0.31	17.88 \pm 3.02
6442183	2	1453.04 \pm 0.484	4.24 \pm 1.16	3.11 \pm 0.37	6.97 \pm 2.57
6442183	2	1518.67 \pm 0.511	2.97 \pm 1.67	2.03 \pm 0.40	5.47 \pm 2.07
6442183	2	1584.58 \pm 1.477	4.91 \pm 3.37	1.39 \pm 0.73	0.22 \pm 1.41
6442183	3	1150.08 \pm 0.095	0.67 \pm 0.21	2.22 \pm 0.22	30.08 \pm 3.58
6442183	3	1216.05 \pm 0.161	0.94 \pm 0.35	1.99 \pm 0.24	16.64 \pm 3.35
6442183	3	1280.53 \pm 0.189	1.32 \pm 0.37	2.34 \pm 0.22	26.65 \pm 3.31
6693861	0	634.03 \pm 0.136	0.58 \pm 0.41	4.25 \pm 0.88	6.78 \pm 1.09
6693861	0	680.38 \pm 0.129	0.92 \pm 0.28	7.32 \pm 0.77	16.30 \pm 3.88
6693861	0	727.75 \pm 0.057	0.54 \pm 0.15	9.20 \pm 0.78	44.87 \pm 2.92
6693861	0	775.14 \pm 0.119	0.62 \pm 0.21	15.78 \pm 6.36	0.10 \pm 3.73
6693861	0	822.25 \pm 0.067	0.70 \pm 0.16	10.33 \pm 0.74	73.33 \pm 3.22
6693861	0	869.69 \pm 0.068	0.74 \pm 0.17	10.33 \pm 0.74	74.21 \pm 3.14
6693861	0	917.86 \pm 0.333	2.41 \pm 1.04	8.51 \pm 1.32	7.67 \pm 3.29
6693861	0	967.09 \pm 0.662	4.00 \pm 2.34	6.46 \pm 1.39	5.16 \pm 1.70
6693861	1	611.08 \pm 0.369	1.16 \pm 0.71	4.47 \pm 1.05	5.14 \pm 0.76
6693861	1	647.19 \pm 0.139	0.61 \pm 0.25	5.43 \pm 0.77	15.87 \pm 1.31
6693861	1	677.55 \pm 0.073	0.56 \pm 0.17	7.84 \pm 0.77	6.91 \pm 3.69
6693861	1	705.99 \pm 0.052	0.52 \pm 0.12	10.81 \pm 0.80	115.62 \pm 1.63
6693861	1	742.99 \pm 0.052	0.55 \pm 0.11	11.92 \pm 0.82	152.31 \pm 1.70
6693861	1	775.60 \pm 0.453	0.78 \pm 0.61	6.43 \pm 6.54	-0.13 \pm 3.81
6693861	1	807.29 \pm 0.063	0.79 \pm 0.14	13.06 \pm 0.78	136.18 \pm 1.66
6693861	1	847.32 \pm 0.081	1.12 \pm 0.20	12.94 \pm 0.72	131.57 \pm 1.61
6693861	1	888.74 \pm 0.110	1.32 \pm 0.40	9.58 \pm 0.74	44.37 \pm 1.38
6693861	1	921.67 \pm 0.468	1.30 \pm 1.15	5.27 \pm 1.48	2.88 \pm 3.16
6693861	2	675.54 \pm 0.089	0.42 \pm 0.23	4.59 \pm 0.83	6.81 \pm 3.66
6693861	2	724.34 \pm 0.090	0.78 \pm 0.25	8.01 \pm 0.77	41.29 \pm 2.71
6693861	2	770.10 \pm 0.068	0.64 \pm 0.16	9.40 \pm 0.74	72.15 \pm 4.11
6693861	2	817.63 \pm 0.089	0.94 \pm 0.21	9.85 \pm 0.73	69.39 \pm 3.07
6693861	2	864.53 \pm 0.079	0.68 \pm 0.26	7.34 \pm 0.73	45.33 \pm 2.87
6693861	2	913.16 \pm 0.172	1.06 \pm 0.38	6.37 \pm 0.82	12.16 \pm 2.81
6693861	2	960.64 \pm 0.332	2.07 \pm 1.29	6.12 \pm 1.17	6.63 \pm 1.98
6766513	0	620.48 \pm 0.477	1.52 \pm 1.39	4.17 \pm 1.12	3.30 \pm 1.89
6766513	0	667.98 \pm 1.136	3.78 \pm 2.18	5.22 \pm 1.22	2.96 \pm 0.54
6766513	0	720.76 \pm 0.535	4.05 \pm 1.72	7.91 \pm 1.20	4.11 \pm 1.72
6766513	0	771.84 \pm 0.791	5.26 \pm 1.98	8.02 \pm 1.44	4.13 \pm 1.77
6766513	0	820.43 \pm 0.597	2.87 \pm 1.87	7.48 \pm 2.70	1.45 \pm 3.74
6766513	0	871.65 \pm 0.717	2.77 \pm 2.18	6.49 \pm 3.26	0.77 \pm 1.92
6766513	0	923.21 \pm 0.377	1.61 \pm 1.20	5.76 \pm 1.70	1.64 \pm 2.30
6766513	0	974.05 \pm 0.408	4.54 \pm 1.04	9.80 \pm 0.74	20.40 \pm 1.10
6766513	0	1026.00 \pm 1.228	6.06 \pm 3.16	6.99 \pm 3.55	0.24 \pm 1.38
6766513	0	1077.43 \pm 0.565	2.78 \pm 1.76	6.11 \pm 1.81	1.08 \pm 2.16
6766513	0	1129.97 \pm 0.836	6.47 \pm 1.91	8.07 \pm 0.89	6.26 \pm 0.96
6766513	0	1180.27 \pm 1.486	3.46 \pm 2.54	4.28 \pm 1.75	1.14 \pm 1.13
6766513	0	1231.99 \pm 0.855	4.91 \pm 2.28	5.61 \pm 1.16	2.09 \pm 0.76
6766513	1	614.23 \pm 0.356	0.89 \pm 0.58	6.10 \pm 0.74	14.77 \pm 1.86
6766513	1	649.80 \pm 0.175	1.01 \pm 0.58	6.76 \pm 0.81	19.87 \pm 1.22
6766513	1	695.62 \pm 0.867	4.35 \pm 2.66	5.79 \pm 1.25	1.76 \pm 0.65

Continued on next page

KIC	l	ν_{nl} (μHz)	Γ_{nl} (μHz)	A_{nl} (ppm)	$\ln K$
6766513	1	742.90 ± 0.203	1.22 ± 0.66	7.49 ± 0.70	21.11 ± 1.28
6766513	1	785.66 ± 0.190	1.56 ± 0.74	8.04 ± 0.72	21.99 ± 1.21
6766513	1	808.27 ± 0.089	0.47 ± 0.32	6.68 ± 0.72	23.63 ± 3.34
6766513	1	847.80 ± 0.199	2.10 ± 0.63	9.60 ± 0.71	36.46 ± 1.28
6766513	1	896.33 ± 0.179	1.36 ± 0.58	10.05 ± 0.64	49.43 ± 1.69
6766513	1	946.77 ± 0.259	2.77 ± 0.77	9.94 ± 0.72	33.23 ± 1.27
6766513	1	998.40 ± 0.412	4.72 ± 1.13	10.77 ± 0.75	22.17 ± 1.19
6766513	1	1049.81 ± 0.600	5.33 ± 1.71	8.55 ± 0.85	8.39 ± 0.90
6766513	1	1100.24 ± 0.408	3.69 ± 1.15	8.64 ± 0.76	14.78 ± 1.04
6766513	1	1152.93 ± 0.603	6.09 ± 1.74	8.36 ± 0.86	5.50 ± 0.94
6766513	1	1203.76 ± 0.675	3.00 ± 2.27	5.08 ± 1.09	1.44 ± 0.77
6766513	2	716.50 ± 1.041	1.46 ± 2.04	3.25 ± 1.64	0.15 ± 1.38
6766513	2	766.47 ± 1.185	1.36 ± 1.85	4.34 ± 1.76	1.24 ± 1.67
6766513	2	816.70 ± 1.344	5.32 ± 3.08	8.43 ± 2.74	1.33 ± 3.63
6766513	2	868.37 ± 1.116	4.06 ± 2.12	9.13 ± 2.81	1.52 ± 1.75
6766513	2	918.44 ± 0.737	3.92 ± 1.52	10.03 ± 1.29	8.42 ± 2.13
6766513	2	1022.05 ± 1.226	4.25 ± 3.20	7.13 ± 2.90	0.73 ± 1.45
6766513	2	1073.66 ± 1.204	1.32 ± 1.87	5.26 ± 1.71	2.28 ± 1.72
6766513	2	1176.63 ± 0.996	1.86 ± 2.17	3.22 ± 1.76	0.10 ± 1.05
7174707	0	637.85 ± 0.135	0.84 ± 0.31	5.34 ± 0.67	17.04 ± 1.48
7174707	0	684.01 ± 0.063	0.33 ± 0.10	4.48 ± 0.57	16.06 ± 3.64
7174707	0	731.06 ± 0.043	0.48 ± 0.10	8.75 ± 0.59	72.10 ± 6.26
7174707	0	778.23 ± 0.026	0.30 ± 0.05	10.10 ± 0.65	98.26 ± 7.31
7174707	0	825.38 ± 0.024	0.31 ± 0.05	12.63 ± 0.75	113.14 ± 15.11
7174707	0	872.69 ± 0.044	0.56 ± 0.10	9.86 ± 0.56	113.79 ± 4.52
7174707	0	920.39 ± 0.451	1.16 ± 1.11	4.07 ± 2.84	-0.35 ± 3.79
7174707	0	968.04 ± 0.112	0.83 ± 0.34	5.07 ± 0.65	18.40 ± 3.16
7174707	1	658.28 ± 0.047	0.30 ± 0.07	5.39 ± 0.55	34.99 ± 2.08
7174707	1	692.11 ± 0.042	0.28 ± 0.05	6.80 ± 0.55	71.76 ± 3.14
7174707	1	717.11 ± 0.055	0.38 ± 0.11	7.01 ± 0.56	67.42 ± 5.04
7174707	1	752.36 ± 0.035	0.37 ± 0.08	10.91 ± 0.66	198.95 ± 2.05
7174707	1	784.87 ± 0.020	0.25 ± 0.01	11.62 ± 0.64	406.96 ± 7.91
7174707	1	812.91 ± 0.030	0.32 ± 0.06	12.50 ± 0.69	333.56 ± 8.88
7174707	1	851.72 ± 0.029	0.35 ± 0.06	13.77 ± 0.75	356.61 ± 2.17
7174707	1	892.63 ± 0.052	0.51 ± 0.15	9.02 ± 0.55	109.93 ± 1.89
7174707	1	920.93 ± 0.102	0.49 ± 0.28	8.82 ± 1.60	2.16 ± 3.64
7174707	1	951.10 ± 0.068	0.51 ± 0.17	6.58 ± 0.54	60.08 ± 2.95
7174707	1	994.74 ± 0.373	2.15 ± 1.16	5.88 ± 0.81	9.98 ± 0.98
7174707	2	678.08 ± 1.043	1.63 ± 1.81	2.74 ± 1.33	0.05 ± 4.19
7174707	2	725.76 ± 0.081	0.47 ± 0.18	6.20 ± 0.57	37.70 ± 5.19
7174707	2	773.49 ± 0.047	0.51 ± 0.11	9.43 ± 0.58	157.24 ± 6.85
7174707	2	821.18 ± 0.046	0.46 ± 0.12	10.27 ± 0.60	200.51 ± 6.22
7174707	2	867.20 ± 0.047	0.27 ± 0.05	7.19 ± 0.51	90.95 ± 4.15
7174707	2	916.18 ± 0.222	1.16 ± 0.54	6.09 ± 0.72	14.64 ± 4.34
7174707	2	960.47 ± 1.148	1.20 ± 1.64	2.66 ± 1.24	0.48 ± 3.63
7174707	3	838.90 ± 0.183	0.72 ± 0.37	5.29 ± 0.60	14.31 ± 1.67
7199397	0	438.28 ± 0.176	0.65 ± 0.28	3.26 ± 0.55	7.83 ± 1.20
7199397	0	477.04 ± 0.110	0.71 ± 0.19	4.67 ± 0.45	29.90 ± 2.61
7199397	0	515.09 ± 0.167	1.64 ± 0.51	6.28 ± 0.68	22.01 ± 4.74
7199397	0	552.70 ± 0.065	0.83 ± 0.19	7.75 ± 0.65	11.72 ± 5.57
7199397	0	590.19 ± 0.594	1.19 ± 0.83	3.99 ± 1.87	-0.86 ± 4.37
7199397	0	629.65 ± 0.058	0.88 ± 0.17	9.22 ± 0.54	32.82 ± 6.49
7199397	0	668.89 ± 0.064	1.20 ± 0.17	10.12 ± 0.47	19.72 ± 6.61
7199397	0	707.78 ± 0.144	2.16 ± 0.32	10.63 ± 0.60	51.61 ± 6.32
7199397	0	747.50 ± 0.198	1.53 ± 0.42	6.13 ± 0.91	3.47 ± 3.23
7199397	0	786.64 ± 0.533	2.75 ± 2.30	4.63 ± 2.44	1.04 ± 2.05
7199397	0	826.33 ± 0.900	2.96 ± 2.06	3.53 ± 2.25	-0.11 ± 2.53
7199397	0	865.76 ± 0.777	4.92 ± 2.24	4.35 ± 0.93	3.59 ± 1.73
7199397	1	449.52 ± 0.175	0.35 ± 0.16	3.21 ± 0.51	5.28 ± 1.49
7199397	1	470.81 ± 0.164	0.42 ± 0.31	3.36 ± 0.52	7.21 ± 2.67

Continued on next page

KIC	l	ν_{nl} (μHz)	Γ_{nl} (μHz)	A_{nl} (ppm)	$\ln K$
7199397	1	491.35 \pm 0.111	0.74 \pm 0.27	6.20 \pm 0.43	53.88 \pm 1.50
7199397	1	519.64 \pm 0.127	0.64 \pm 0.21	6.68 \pm 0.44	53.55 \pm 3.81
7199397	1	540.64 \pm 0.118	0.68 \pm 0.18	7.86 \pm 0.40	150.06 \pm 5.90
7199397	1	565.18 \pm 0.057	0.64 \pm 0.14	9.25 \pm 0.40	201.37 \pm 2.00
7199397	1	591.36 \pm 0.074	0.56 \pm 0.11	12.12 \pm 0.93	4.50 \pm 4.56
7199397	1	618.24 \pm 0.063	0.88 \pm 0.17	11.06 \pm 0.42	230.42 \pm 7.92
7199397	1	649.04 \pm 0.063	0.97 \pm 0.17	11.23 \pm 0.40	277.17 \pm 1.89
7199397	1	675.09 \pm 0.036	0.44 \pm 0.10	9.06 \pm 0.42	230.13 \pm 6.07
7199397	1	697.85 \pm 0.074	1.42 \pm 0.24	11.81 \pm 0.44	83.30 \pm 8.35
7199397	1	731.32 \pm 0.099	2.06 \pm 0.31	10.43 \pm 0.37	—
7199397	1	767.62 \pm 0.142	2.58 \pm 0.40	8.84 \pm 0.37	83.46 \pm 1.54
7199397	1	803.42 \pm 0.215	2.81 \pm 0.75	7.25 \pm 0.41	44.90 \pm 1.45
7199397	1	827.94 \pm 0.512	1.08 \pm 1.00	3.78 \pm 1.39	1.09 \pm 2.56
7199397	1	850.55 \pm 0.604	5.25 \pm 1.45	5.10 \pm 0.54	3.57 \pm 0.92
7199397	1	887.10 \pm 0.468	2.96 \pm 1.74	3.80 \pm 0.59	4.54 \pm 0.89
7199397	2	511.38 \pm 0.472	0.83 \pm 0.56	4.54 \pm 0.77	6.32 \pm 4.22
7199397	2	549.54 \pm 0.378	1.51 \pm 0.56	6.46 \pm 0.77	32.11 \pm 4.68
7199397	2	587.63 \pm 0.555	1.54 \pm 0.47	8.51 \pm 1.11	20.13 \pm 4.61
7199397	2	625.94 \pm 0.162	1.51 \pm 0.49	8.96 \pm 0.58	69.27 \pm 5.30
7199397	2	665.35 \pm 0.118	1.31 \pm 0.37	8.95 \pm 0.49	58.33 \pm 5.75
7199397	2	702.21 \pm 0.718	0.53 \pm 1.09	4.94 \pm 1.12	11.24 \pm 5.37
7199397	2	744.02 \pm 0.421	4.08 \pm 0.88	9.31 \pm 0.76	13.62 \pm 2.95
7199397	2	784.10 \pm 1.068	6.63 \pm 1.51	7.88 \pm 1.80	0.80 \pm 1.94
7199397	2	823.27 \pm 0.836	1.97 \pm 1.41	4.75 \pm 1.30	2.57 \pm 2.63
7199397	2	861.76 \pm 0.893	1.86 \pm 2.10	1.85 \pm 1.21	-0.31 \pm 1.41
7668623	0	556.77 \pm 0.872	1.81 \pm 1.76	3.11 \pm 1.38	1.25 \pm 1.14
7668623	0	600.34 \pm 1.190	1.92 \pm 2.16	1.43 \pm 1.18	-0.14 \pm 0.51
7668623	0	645.21 \pm 0.764	3.64 \pm 1.80	5.91 \pm 1.03	5.13 \pm 0.72
7668623	0	691.37 \pm 0.396	2.15 \pm 1.07	6.34 \pm 0.96	12.66 \pm 1.75
7668623	0	739.75 \pm 0.462	2.01 \pm 1.29	6.62 \pm 1.17	9.09 \pm 1.73
7668623	0	783.38 \pm 0.520	3.26 \pm 1.28	7.67 \pm 1.00	11.64 \pm 1.73
7668623	0	828.27 \pm 0.968	3.81 \pm 2.41	6.37 \pm 3.25	0.52 \pm 1.40
7668623	0	877.76 \pm 1.231	6.30 \pm 2.60	5.58 \pm 1.55	2.88 \pm 1.55
7668623	0	922.34 \pm 0.547	5.46 \pm 1.62	9.24 \pm 0.80	8.31 \pm 0.89
7668623	0	969.18 \pm 0.779	8.34 \pm 1.43	9.43 \pm 0.78	—
7668623	0	1015.42 \pm 0.781	6.09 \pm 2.03	6.20 \pm 0.82	—
7668623	1	543.01 \pm 0.675	2.06 \pm 1.39	6.29 \pm 1.05	11.26 \pm 0.90
7668623	1	579.48 \pm 0.774	1.54 \pm 1.51	3.63 \pm 1.22	2.84 \pm 0.37
7668623	1	621.91 \pm 0.833	1.89 \pm 1.80	3.40 \pm 1.38	2.19 \pm 0.38
7668623	1	661.26 \pm 0.404	0.53 \pm 0.83	2.55 \pm 1.10	0.95 \pm 0.46
7668623	1	682.46 \pm 0.442	1.88 \pm 1.11	6.43 \pm 0.96	14.21 \pm 1.81
7668623	1	718.42 \pm 0.525	2.40 \pm 1.18	6.37 \pm 0.88	10.87 \pm 0.82
7668623	1	761.72 \pm 0.633	5.76 \pm 1.50	10.17 \pm 0.89	6.32 \pm 0.98
7668623	1	805.96 \pm 0.621	5.44 \pm 1.42	9.49 \pm 0.81	9.57 \pm 0.88
7668623	1	851.26 \pm 0.691	7.58 \pm 1.39	10.70 \pm 0.86	—
7668623	1	898.02 \pm 0.421	3.51 \pm 1.15	8.57 \pm 0.78	14.77 \pm 0.98
7668623	1	943.47 \pm 0.692	4.71 \pm 1.69	6.92 \pm 0.77	6.42 \pm 0.78
7668623	1	992.52 \pm 0.572	3.31 \pm 1.83	5.74 \pm 0.83	6.08 \pm 0.75
7668623	1	1037.21 \pm 0.721	6.10 \pm 1.42	7.21 \pm 0.71	4.85 \pm 0.89
7668623	2	594.60 \pm 0.874	1.47 \pm 1.62	3.66 \pm 1.23	2.35 \pm 0.41
7668623	2	733.87 \pm 1.101	2.85 \pm 2.51	4.77 \pm 1.59	2.29 \pm 1.42
7668623	2	777.37 \pm 0.844	1.79 \pm 1.76	4.19 \pm 1.35	1.95 \pm 1.44
7668623	2	826.03 \pm 1.021	2.49 \pm 2.58	6.89 \pm 2.89	0.96 \pm 1.46
7668623	2	870.66 \pm 0.935	3.91 \pm 2.79	4.65 \pm 1.69	1.34 \pm 1.63
7747078	0	559.83 \pm 0.101	0.46 \pm 0.21	2.12 \pm 0.36	9.11 \pm 1.48
7747078	0	611.49 \pm 1.256	2.19 \pm 2.00	1.46 \pm 0.81	0.35 \pm 1.68
7747078	0	664.40 \pm 0.307	1.51 \pm 0.92	2.60 \pm 0.45	8.60 \pm 1.05
7747078	0	717.56 \pm 0.109	1.42 \pm 0.28	4.77 \pm 0.30	54.12 \pm 1.40
7747078	0	770.02 \pm 0.065	0.91 \pm 0.17	5.22 \pm 0.30	37.53 \pm 5.71
7747078	0	822.56 \pm 0.058	0.97 \pm 0.15	6.32 \pm 0.31	79.67 \pm 3.90

Continued on next page

KIC	l	ν_{nl} (μHz)	Γ_{nl} (μHz)	A_{nl} (ppm)	$\ln K$
7747078	0	876.06 ± 0.047	0.85 ± 0.11	7.78 ± 0.34	67.48 ± 4.62
7747078	0	930.20 ± 0.054	1.11 ± 0.13	8.40 ± 0.32	69.38 ± 4.87
7747078	0	984.28 ± 0.064	1.30 ± 0.15	8.39 ± 0.31	51.69 ± 4.75
7747078	0	1038.20 ± 0.262	1.78 ± 0.31	6.69 ± 0.97	6.42 ± 4.85
7747078	0	1092.89 ± 0.256	2.10 ± 0.43	4.70 ± 0.57	4.47 ± 3.71
7747078	0	1147.35 ± 0.624	2.90 ± 2.23	3.42 ± 1.48	1.43 ± 2.76
7747078	0	1202.24 ± 1.209	2.16 ± 2.22	1.26 ± 0.99	-0.68 ± 2.02
7747078	0	1257.63 ± 0.635	2.21 ± 1.83	1.89 ± 0.79	0.76 ± 1.85
7747078	1	574.96 ± 0.667	0.79 ± 0.86	1.44 ± 0.65	1.64 ± 0.49
7747078	1	614.08 ± 0.275	0.68 ± 0.47	2.36 ± 0.44	1.92 ± 1.70
7747078	1	644.67 ± 0.714	0.89 ± 0.92	1.60 ± 0.60	1.80 ± 0.50
7747078	1	686.96 ± 0.138	0.71 ± 0.28	3.56 ± 0.29	33.11 ± 1.51
7747078	1	729.14 ± 0.114	0.86 ± 0.28	4.44 ± 0.28	68.65 ± 1.51
7747078	1	760.11 ± 0.095	0.96 ± 0.22	5.61 ± 0.30	46.48 ± 5.94
7747078	1	799.80 ± 0.068	0.94 ± 0.19	7.07 ± 0.28	236.50 ± 2.04
7747078	1	848.92 ± 0.051	0.79 ± 0.12	8.60 ± 0.29	400.94 ± 2.26
7747078	1	901.02 ± 0.057	1.12 ± 0.14	10.55 ± 0.32	605.65 ± 2.10
7747078	1	953.12 ± 0.059	1.13 ± 0.14	10.44 ± 0.32	593.11 ± 2.19
7747078	1	1002.26 ± 0.067	1.12 ± 0.15	9.19 ± 0.28	496.21 ± 2.19
7747078	1	1032.93 ± 0.124	1.51 ± 0.30	7.97 ± 0.74	5.17 ± 4.87
7747078	1	1067.46 ± 0.090	1.94 ± 0.27	8.05 ± 0.25	295.52 ± 1.87
7747078	1	1118.39 ± 0.161	3.59 ± 0.51	7.11 ± 0.24	135.94 ± 1.62
7747078	1	1172.31 ± 0.213	3.91 ± 0.62	5.59 ± 0.25	68.02 ± 1.54
7747078	1	1226.38 ± 0.455	6.07 ± 1.31	4.48 ± 0.30	21.61 ± 1.17
7747078	1	1280.28 ± 1.159	6.78 ± 1.66	3.01 ± 0.36	3.96 ± 0.95
7747078	2	765.57 ± 0.165	0.99 ± 0.34	4.38 ± 0.35	42.36 ± 5.05
7747078	2	816.80 ± 0.198	1.69 ± 0.82	4.84 ± 0.36	73.89 ± 3.32
7747078	2	871.44 ± 0.159	1.61 ± 0.48	6.24 ± 0.31	131.10 ± 3.57
7747078	2	925.23 ± 0.115	1.42 ± 0.28	7.17 ± 0.29	157.22 ± 3.82
7747078	2	979.34 ± 0.131	1.44 ± 0.34	6.89 ± 0.30	127.12 ± 3.78
7747078	2	1036.29 ± 1.030	1.11 ± 0.64	5.43 ± 1.31	4.75 ± 4.77
7747078	2	1088.80 ± 0.326	2.21 ± 0.68	5.96 ± 0.48	22.89 ± 3.35
7747078	2	1143.22 ± 0.905	5.36 ± 1.84	5.75 ± 1.09	2.69 ± 2.45
7747078	2	1199.07 ± 0.628	4.17 ± 1.48	4.58 ± 0.51	9.43 ± 2.03
7747078	2	1252.72 ± 0.853	4.66 ± 2.04	3.66 ± 0.56	6.70 ± 1.91
7976303	0	530.56 ± 0.405	0.86 ± 0.84	1.57 ± 0.58	1.85 ± 0.61
7976303	0	579.02 ± 0.334	0.87 ± 0.69	1.73 ± 0.51	2.33 ± 2.49
7976303	0	628.94 ± 0.134	1.03 ± 0.31	3.23 ± 0.32	24.99 ± 2.31
7976303	0	679.50 ± 0.080	1.38 ± 0.20	6.36 ± 0.29	184.68 ± 3.69
7976303	0	729.27 ± 0.115	1.91 ± 0.27	6.61 ± 0.32	42.81 ± 5.44
7976303	0	779.01 ± 0.079	1.63 ± 0.19	8.52 ± 0.32	123.68 ± 7.21
7976303	0	830.13 ± 0.074	1.45 ± 0.17	9.06 ± 0.34	95.69 ± 4.86
7976303	0	881.86 ± 0.069	1.38 ± 0.16	8.54 ± 0.34	95.91 ± 5.94
7976303	0	933.41 ± 0.120	2.18 ± 0.30	8.92 ± 0.46	42.56 ± 5.07
7976303	0	984.68 ± 0.128	2.10 ± 0.27	7.58 ± 0.38	29.42 ± 4.91
7976303	0	1036.46 ± 0.219	2.91 ± 0.61	5.94 ± 0.67	10.47 ± 3.15
7976303	0	1088.36 ± 0.796	3.98 ± 1.31	4.81 ± 1.49	2.38 ± 2.64
7976303	0	1142.11 ± 0.453	1.57 ± 1.35	2.25 ± 0.80	3.22 ± 2.58
7976303	0	1193.72 ± 0.856	3.91 ± 2.13	3.53 ± 1.26	4.01 ± 2.40
7976303	0	1244.63 ± 1.092	6.66 ± 2.53	3.16 ± 1.11	0.98 ± 1.63
7976303	1	544.78 ± 0.253	1.00 ± 0.40	2.86 ± 0.37	15.37 ± 1.22
7976303	1	585.49 ± 0.083	0.39 ± 0.13	2.42 ± 0.30	15.66 ± 2.26
7976303	1	612.24 ± 0.064	0.52 ± 0.16	3.82 ± 0.29	60.02 ± 1.43
7976303	1	649.93 ± 0.104	1.36 ± 0.26	5.46 ± 0.28	111.35 ± 1.61
7976303	1	692.11 ± 0.066	0.98 ± 0.16	6.27 ± 0.28	190.99 ± 1.77
7976303	1	725.57 ± 0.125	0.64 ± 0.34	4.44 ± 0.85	5.13 ± 5.12
7976303	1	760.03 ± 0.056	1.26 ± 0.14	10.04 ± 0.33	483.21 ± 1.86
7976303	1	805.09 ± 0.053	1.20 ± 0.17	11.36 ± 0.34	633.08 ± 2.11
7976303	1	853.91 ± 0.062	1.69 ± 0.15	11.73 ± 0.33	576.17 ± 1.98
7976303	1	903.44 ± 0.064	1.91 ± 0.15	12.50 ± 0.32	626.73 ± 2.01

Continued on next page

KIC	l	ν_{nl} (μHz)	Γ_{nl} (μHz)	A_{nl} (ppm)	$\ln K$
7976303	1	950.42 \pm 0.075	2.16 \pm 0.17	11.16 \pm 0.28	538.76 \pm 1.97
7976303	1	980.42 \pm 0.238	2.03 \pm 0.34	10.15 \pm 2.48	-0.49 \pm 4.29
7976303	1	1013.50 \pm 0.099	2.98 \pm 0.25	9.25 \pm 0.24	—
7976303	1	1061.83 \pm 0.122	3.59 \pm 0.32	8.19 \pm 0.22	—
7976303	1	1112.56 \pm 0.213	5.45 \pm 0.56	6.73 \pm 0.21	93.86 \pm 1.58
7976303	1	1164.57 \pm 0.266	6.02 \pm 0.75	5.91 \pm 0.22	57.15 \pm 1.56
7976303	1	1216.32 \pm 0.358	5.55 \pm 0.88	4.35 \pm 0.23	33.44 \pm 1.40
7976303	1	1269.42 \pm 1.201	8.26 \pm 1.82	2.60 \pm 0.33	1.39 \pm 1.03
7976303	2	522.71 \pm 1.412	0.99 \pm 1.35	0.33 \pm 0.28	-0.83 \pm 0.76
7976303	2	572.20 \pm 0.444	0.59 \pm 0.64	1.47 \pm 0.63	1.05 \pm 2.62
7976303	2	623.34 \pm 0.325	0.93 \pm 0.58	2.63 \pm 0.37	10.64 \pm 2.37
7976303	2	671.84 \pm 0.308	1.23 \pm 0.59	3.01 \pm 0.35	17.31 \pm 2.90
7976303	2	724.61 \pm 0.078	0.66 \pm 0.18	6.58 \pm 0.57	6.78 \pm 5.10
7976303	2	773.67 \pm 0.133	2.24 \pm 0.40	6.87 \pm 0.34	104.03 \pm 3.49
7976303	2	825.68 \pm 0.090	1.68 \pm 0.24	8.32 \pm 0.34	132.33 \pm 3.71
7976303	2	877.05 \pm 0.126	2.57 \pm 0.36	8.58 \pm 0.32	121.28 \pm 3.69
7976303	2	928.79 \pm 0.218	3.16 \pm 0.53	8.50 \pm 0.49	56.71 \pm 3.70
7976303	2	981.06 \pm 0.616	1.44 \pm 1.12	3.28 \pm 3.63	-0.66 \pm 4.27
7976303	2	1032.32 \pm 0.418	4.88 \pm 0.86	6.97 \pm 0.64	12.24 \pm 3.17
7976303	2	1084.65 \pm 0.866	4.90 \pm 1.20	5.66 \pm 1.28	2.90 \pm 2.71
7976303	2	1137.65 \pm 0.469	5.46 \pm 0.90	5.78 \pm 0.45	22.39 \pm 2.99
7976303	2	1189.67 \pm 1.231	6.05 \pm 2.12	3.94 \pm 1.30	1.39 \pm 2.19
7976303	2	1240.06 \pm 1.460	4.86 \pm 3.79	1.99 \pm 1.26	0.32 \pm 1.59
8026226	0	349.23 \pm 0.327	1.31 \pm 0.95	5.05 \pm 1.05	5.22 \pm 0.77
8026226	0	380.81 \pm 0.289	2.06 \pm 0.82	7.15 \pm 0.86	10.35 \pm 3.78
8026226	0	412.20 \pm 0.275	0.77 \pm 0.67	3.96 \pm 1.63	-0.17 \pm 2.38
8026226	0	447.00 \pm 0.288	1.60 \pm 0.79	7.29 \pm 1.34	2.84 \pm 3.40
8026226	0	481.44 \pm 0.223	1.29 \pm 0.69	6.21 \pm 1.13	3.43 \pm 4.24
8026226	0	515.26 \pm 0.913	3.81 \pm 2.20	8.29 \pm 3.75	0.94 \pm 2.25
8026226	0	549.39 \pm 0.474	2.48 \pm 1.78	8.69 \pm 3.61	1.36 \pm 3.12
8026226	0	584.02 \pm 0.894	3.34 \pm 2.10	7.51 \pm 3.28	1.23 \pm 3.30
8026226	0	617.54 \pm 0.647	2.70 \pm 2.11	6.62 \pm 3.21	1.37 \pm 2.03
8026226	0	650.42 \pm 0.277	3.60 \pm 0.86	9.10 \pm 0.78	4.05 \pm 2.86
8026226	0	688.92 \pm 0.639	5.09 \pm 2.19	9.03 \pm 2.74	3.38 \pm 3.61
8026226	0	724.46 \pm 0.952	2.75 \pm 1.69	3.39 \pm 1.52	1.07 \pm 3.15
8026226	1	364.57 \pm 0.153	0.39 \pm 0.21	4.14 \pm 0.77	7.48 \pm 1.39
8026226	1	388.85 \pm 0.159	0.26 \pm 0.13	5.36 \pm 0.73	21.69 \pm 2.29
8026226	1	408.07 \pm 0.281	0.87 \pm 0.61	6.10 \pm 1.64	0.56 \pm 2.31
8026226	1	427.12 \pm 0.155	0.68 \pm 0.33	6.39 \pm 0.72	25.28 \pm 1.42
8026226	1	454.89 \pm 0.162	1.09 \pm 0.36	8.50 \pm 0.75	57.93 \pm 2.74
8026226	1	478.37 \pm 0.764	0.69 \pm 0.58	8.50 \pm 1.81	2.98 \pm 3.73
8026226	1	499.95 \pm 0.117	0.93 \pm 0.39	8.25 \pm 0.67	34.68 \pm 1.52
8026226	1	527.95 \pm 0.253	2.62 \pm 0.64	11.66 \pm 0.64	40.98 \pm 1.46
8026226	1	553.66 \pm 0.295	2.05 \pm 0.66	10.03 \pm 1.14	11.60 \pm 2.78
8026226	1	575.39 \pm 0.265	2.43 \pm 0.77	13.30 \pm 1.22	12.79 \pm 3.64
8026226	1	602.31 \pm 0.229	3.59 \pm 0.63	12.18 \pm 0.59	—
8026226	1	634.39 \pm 0.284	4.32 \pm 0.82	11.17 \pm 0.57	24.61 \pm 1.31
8026226	1	666.88 \pm 0.154	1.65 \pm 0.38	8.37 \pm 0.49	38.13 \pm 1.98
8026226	1	694.60 \pm 0.276	0.52 \pm 0.65	4.86 \pm 1.05	12.39 \pm 3.21
8026226	1	713.49 \pm 0.282	3.19 \pm 0.70	8.25 \pm 0.53	32.88 \pm 4.95
8026226	2	376.39 \pm 0.892	1.12 \pm 1.40	1.74 \pm 1.19	-0.60 \pm 3.11
8026226	2	409.59 \pm 0.557	0.83 \pm 0.74	4.17 \pm 2.76	0.50 \pm 2.32
8026226	2	445.10 \pm 0.616	0.87 \pm 1.05	4.11 \pm 1.90	0.64 \pm 3.09
8026226	2	476.65 \pm 0.859	0.67 \pm 0.68	6.49 \pm 2.46	0.66 \pm 3.90
8026226	2	512.74 \pm 1.051	3.06 \pm 1.61	9.27 \pm 3.27	1.32 \pm 1.95
8026226	2	546.62 \pm 0.892	2.39 \pm 1.31	9.26 \pm 2.71	2.05 \pm 3.00
8026226	2	580.78 \pm 1.011	2.49 \pm 2.38	8.54 \pm 3.76	1.29 \pm 3.23
8026226	2	614.97 \pm 0.870	4.44 \pm 1.81	8.85 \pm 2.94	0.76 \pm 1.80
8026226	2	647.71 \pm 0.900	0.41 \pm 1.10	3.67 \pm 1.37	1.63 \pm 2.58
8026226	2	685.22 \pm 0.996	3.58 \pm 2.09	6.61 \pm 2.75	0.49 \pm 4.15

Continued on next page

KIC	l	ν_{nl} (μHz)	Γ_{nl} (μHz)	A_{nl} (ppm)	$\ln K$
8026226	2	721.02 ± 0.444	0.80 ± 1.33	4.74 ± 1.12	5.48 ± 3.33
8524425	0	743.64 ± 0.045	0.27 ± 0.06	2.45 ± 0.32	5.32 ± 3.35
8524425	0	803.26 ± 0.119	0.89 ± 0.33	3.34 ± 0.39	9.08 ± 3.14
8524425	0	861.16 ± 0.069	0.78 ± 0.15	4.83 ± 0.32	18.25 ± 3.33
8524425	0	919.57 ± 0.046	0.60 ± 0.11	5.69 ± 0.33	37.73 ± 4.78
8524425	0	978.93 ± 0.038	0.58 ± 0.08	7.50 ± 0.37	74.75 ± 5.16
8524425	0	1038.66 ± 0.033	0.58 ± 0.07	9.40 ± 0.43	155.54 ± 8.29
8524425	0	1098.30 ± 0.037	0.69 ± 0.08	9.82 ± 0.41	92.37 ± 5.02
8524425	0	1158.07 ± 0.061	1.15 ± 0.15	7.99 ± 0.33	27.47 ± 4.76
8524425	0	1217.91 ± 0.090	1.47 ± 0.21	6.13 ± 0.30	24.62 ± 3.98
8524425	0	1278.27 ± 0.238	2.79 ± 0.73	4.57 ± 0.41	4.17 ± 3.39
8524425	0	1339.69 ± 0.592	1.32 ± 1.90	2.54 ± 0.79	7.75 ± 2.33
8524425	0	1399.76 ± 0.874	4.70 ± 2.59	2.60 ± 0.64	2.87 ± 1.18
8524425	1	782.34 ± 0.066	0.33 ± 0.08	3.12 ± 0.31	30.16 ± 2.10
8524425	1	832.87 ± 0.055	0.41 ± 0.09	3.91 ± 0.31	55.23 ± 1.90
8524425	1	888.54 ± 0.043	0.49 ± 0.10	6.21 ± 0.33	194.10 ± 2.28
8524425	1	945.31 ± 0.046	0.63 ± 0.10	7.71 ± 0.35	335.32 ± 2.11
8524425	1	1001.85 ± 0.044	0.68 ± 0.10	9.50 ± 0.37	498.26 ± 2.25
8524425	1	1044.85 ± 0.025	0.34 ± 0.03	8.07 ± 0.39	497.67 ± 6.83
8524425	1	1073.96 ± 0.028	0.40 ± 0.05	10.54 ± 0.45	779.25 ± 2.51
8524425	1	1127.36 ± 0.037	0.70 ± 0.09	12.03 ± 0.44	796.60 ± 2.29
8524425	1	1185.44 ± 0.067	1.28 ± 0.16	9.42 ± 0.32	241.09 ± 8.16
8524425	1	1245.21 ± 0.082	1.19 ± 0.21	6.65 ± 0.29	125.12 ± 4.97
8524425	1	1305.26 ± 0.190	2.87 ± 0.48	5.72 ± 0.28	72.14 ± 1.58
8524425	1	1365.14 ± 0.246	2.18 ± 0.70	3.69 ± 0.33	26.93 ± 1.29
8524425	1	1425.29 ± 1.186	2.95 ± 2.94	1.58 ± 0.72	-0.74 ± 0.27
8524425	2	738.34 ± 1.184	1.13 ± 1.40	1.19 ± 0.71	-0.32 ± 2.81
8524425	2	798.65 ± 1.523	1.64 ± 2.33	0.81 ± 0.57	-0.89 ± 1.82
8524425	2	856.55 ± 0.211	0.65 ± 0.30	3.19 ± 0.35	19.49 ± 3.09
8524425	2	914.54 ± 0.111	0.48 ± 0.14	4.37 ± 0.30	75.25 ± 3.80
8524425	2	973.73 ± 0.079	0.65 ± 0.19	5.55 ± 0.31	152.38 ± 3.91
8524425	2	1032.84 ± 0.076	0.74 ± 0.17	6.80 ± 0.31	277.83 ± 6.88
8524425	2	1093.45 ± 0.045	0.51 ± 0.10	7.87 ± 0.34	337.41 ± 4.24
8524425	2	1153.09 ± 0.057	0.72 ± 0.24	6.81 ± 0.32	163.28 ± 3.94
8524425	2	1212.72 ± 0.110	1.18 ± 0.41	5.55 ± 0.32	79.71 ± 3.63
8524425	2	1273.62 ± 0.188	1.35 ± 0.60	3.89 ± 0.39	15.70 ± 2.91
8524425	2	1334.23 ± 0.501	3.03 ± 1.81	3.63 ± 0.71	3.32 ± 2.29
8524425	2	1394.33 ± 1.317	2.12 ± 2.67	1.19 ± 0.73	-0.19 ± 1.25
8524425	3	1118.96 ± 2.031	0.82 ± 0.05	10.37 ± 0.04	482.42 ± 7.75
8524425	3	1177.12 ± 0.388	0.94 ± 0.60	2.69 ± 0.35	10.22 ± 3.56
8524425	3	1237.72 ± 0.607	1.44 ± 1.05	2.78 ± 0.41	9.17 ± 3.15
8702606	0	453.22 ± 0.240	0.90 ± 0.57	2.92 ± 0.59	5.19 ± 1.37
8702606	0	491.10 ± 0.062	0.37 ± 0.20	2.83 ± 0.47	1.41 ± 4.80
8702606	0	530.99 ± 0.040	0.43 ± 0.09	5.59 ± 0.40	7.71 ± 5.85
8702606	0	569.99 ± 0.041	0.55 ± 0.09	7.08 ± 0.40	42.48 ± 4.61
8702606	0	609.55 ± 0.030	0.45 ± 0.06	9.68 ± 0.51	114.19 ± 7.88
8702606	0	649.15 ± 0.028	0.46 ± 0.06	11.45 ± 0.55	73.22 ± 9.07
8702606	0	688.61 ± 0.030	0.53 ± 0.07	11.79 ± 0.54	61.49 ± 4.94
8702606	0	728.49 ± 0.060	1.02 ± 0.14	9.35 ± 0.42	15.40 ± 10.16
8702606	0	768.52 ± 0.076	1.15 ± 0.17	6.34 ± 0.31	18.96 ± 6.48
8702606	0	808.71 ± 0.185	2.04 ± 0.52	4.50 ± 0.43	2.94 ± 3.32
8702606	0	848.98 ± 0.199	2.41 ± 0.47	4.30 ± 0.30	10.31 ± 3.65
8702606	1	471.28 ± 0.125	0.45 ± 0.20	3.10 ± 0.42	12.02 ± 1.80
8702606	1	492.63 ± 0.039	0.27 ± 0.07	4.46 ± 0.41	5.30 ± 5.16
8702606	1	511.55 ± 0.041	0.30 ± 0.06	5.27 ± 0.37	95.40 ± 2.01
8702606	1	533.04 ± 0.033	0.30 ± 0.05	4.68 ± 0.37	44.97 ± 5.46
8702606	1	552.99 ± 0.037	0.38 ± 0.09	6.43 ± 0.38	168.57 ± 2.15
8702606	1	580.59 ± 0.029	0.29 ± 0.05	6.95 ± 0.38	244.91 ± 2.52
8702606	1	598.19 ± 0.019	0.24 ± 0.02	8.75 ± 0.44	160.23 ± 9.88
8702606	1	627.31 ± 0.022	0.30 ± 0.04	12.92 ± 0.63	550.73 ± 4.44

Continued on next page

KIC	l	ν_{nl} (μHz)	Γ_{nl} (μHz)	A_{nl} (ppm)	$\ln K$
8702606	1	653.08 \pm 0.014	0.24 \pm 0.01	9.85 \pm 0.47	451.53 \pm 7.74
8702606	1	674.49 \pm 0.026	0.40 \pm 0.05	12.54 \pm 0.57	747.48 \pm 2.44
8702606	1	705.73 \pm 0.030	0.45 \pm 0.06	12.01 \pm 0.53	274.88 \pm 13.33
8702606	1	731.73 \pm 0.029	0.35 \pm 0.06	8.06 \pm 0.42	162.59 \pm 11.89
8702606	1	756.19 \pm 0.041	0.56 \pm 0.08	8.23 \pm 0.35	194.19 \pm 13.60
8702606	1	789.60 \pm 0.084	1.44 \pm 0.24	6.67 \pm 0.27	151.73 \pm 1.75
8702606	1	820.64 \pm 0.133	1.22 \pm 0.29	5.11 \pm 0.25	97.22 \pm 1.70
8702606	1	841.67 \pm 0.732	1.18 \pm 0.83	2.20 \pm 1.40	-0.51 \pm 3.58
8702606	1	874.54 \pm 0.171	1.33 \pm 0.62	3.07 \pm 0.29	19.92 \pm 1.27
8702606	2	449.17 \pm 0.597	0.79 \pm 0.88	2.12 \pm 0.88	1.02 \pm 1.51
8702606	2	488.74 \pm 0.241	0.31 \pm 0.35	2.24 \pm 0.60	2.87 \pm 4.66
8702606	2	526.45 \pm 0.118	0.41 \pm 0.20	2.83 \pm 0.40	9.66 \pm 5.99
8702606	2	566.51 \pm 0.055	0.41 \pm 0.12	5.47 \pm 0.37	113.24 \pm 3.78
8702606	2	605.94 \pm 0.043	0.35 \pm 0.08	6.96 \pm 0.37	241.99 \pm 6.95
8702606	2	645.53 \pm 0.040	0.47 \pm 0.08	9.71 \pm 0.49	315.90 \pm 7.53
8702606	2	685.25 \pm 0.034	0.47 \pm 0.08	10.12 \pm 0.47	318.64 \pm 4.23
8702606	2	721.26 \pm 0.035	0.34 \pm 0.05	3.98 \pm 0.27	48.16 \pm 8.91
8702606	2	726.08 \pm 0.075	0.55 \pm 0.18	6.79 \pm 0.42	54.08 \pm 9.42
8702606	2	764.75 \pm 0.117	1.12 \pm 0.26	6.07 \pm 0.32	82.91 \pm 5.93
8702606	2	805.36 \pm 0.190	1.44 \pm 0.56	3.99 \pm 0.47	11.97 \pm 2.88
8702606	2	843.08 \pm 0.519	1.25 \pm 0.52	4.06 \pm 0.95	0.80 \pm 3.74
8702606	3	620.94 \pm 0.903	0.64 \pm 1.01	0.78 \pm 0.54	-1.11 \pm 3.46
8702606	3	659.83 \pm 0.418	0.65 \pm 0.52	2.08 \pm 0.43	3.03 \pm 8.41
8702606	3	699.95 \pm 0.084	0.48 \pm 0.18	3.44 \pm 0.30	44.19 \pm 4.23
8702606	3	739.75 \pm 0.147	0.34 \pm 0.18	1.89 \pm 0.30	4.73 \pm 9.30
8738809	0	553.47 \pm 1.185	2.55 \pm 2.48	2.32 \pm 1.31	-0.16 \pm 0.19
8738809	0	603.28 \pm 0.456	1.61 \pm 1.10	3.53 \pm 0.86	4.22 \pm 1.68
8738809	0	652.81 \pm 0.273	0.85 \pm 0.67	3.12 \pm 0.79	3.25 \pm 2.52
8738809	0	701.58 \pm 0.396	1.98 \pm 1.29	5.12 \pm 1.35	2.64 \pm 1.77
8738809	0	750.54 \pm 0.157	1.54 \pm 0.47	7.18 \pm 0.65	17.31 \pm 2.56
8738809	0	799.23 \pm 0.197	1.62 \pm 0.45	6.99 \pm 0.69	14.26 \pm 2.64
8738809	0	848.18 \pm 0.222	2.35 \pm 0.63	9.34 \pm 0.87	21.32 \pm 4.01
8738809	0	897.73 \pm 0.250	1.93 \pm 0.52	8.39 \pm 0.89	13.88 \pm 2.77
8738809	0	948.54 \pm 0.395	1.79 \pm 0.74	7.53 \pm 1.52	6.42 \pm 2.51
8738809	0	998.65 \pm 0.275	2.02 \pm 0.61	7.08 \pm 0.84	9.73 \pm 2.72
8738809	0	1048.31 \pm 0.491	2.77 \pm 1.78	6.69 \pm 2.06	3.40 \pm 2.26
8738809	0	1098.09 \pm 1.022	5.09 \pm 2.84	6.29 \pm 2.37	1.45 \pm 1.80
8738809	0	1147.15 \pm 0.545	3.64 \pm 1.31	4.04 \pm 0.57	8.50 \pm 1.07
8738809	0	1197.55 \pm 0.798	5.68 \pm 2.27	4.44 \pm 0.70	0.30 \pm 0.92
8738809	1	576.86 \pm 0.233	1.16 \pm 0.59	4.46 \pm 0.68	10.49 \pm 1.14
8738809	1	609.13 \pm 0.141	0.63 \pm 0.30	4.01 \pm 0.64	11.31 \pm 1.55
8738809	1	638.15 \pm 0.232	0.66 \pm 0.38	3.14 \pm 0.65	5.09 \pm 2.37
8738809	1	680.35 \pm 0.214	1.45 \pm 0.38	6.00 \pm 0.56	31.96 \pm 1.18
8738809	1	726.63 \pm 0.141	1.42 \pm 0.31	8.04 \pm 0.57	67.94 \pm 1.39
8738809	1	773.64 \pm 0.188	2.53 \pm 0.42	10.01 \pm 0.54	77.06 \pm 1.44
8738809	1	819.23 \pm 0.188	2.53 \pm 0.44	9.86 \pm 0.53	73.85 \pm 1.45
8738809	1	851.73 \pm 0.084	0.56 \pm 0.18	6.32 \pm 0.73	21.70 \pm 3.60
8738809	1	876.35 \pm 0.145	1.91 \pm 0.33	9.46 \pm 0.53	90.98 \pm 1.47
8738809	1	922.84 \pm 0.137	2.03 \pm 0.33	10.55 \pm 0.54	118.60 \pm 1.49
8738809	1	972.05 \pm 0.182	2.83 \pm 0.42	10.43 \pm 0.50	85.78 \pm 1.46
8738809	1	1021.46 \pm 0.283	4.32 \pm 0.82	9.12 \pm 0.50	—
8738809	1	1071.58 \pm 0.298	3.88 \pm 0.70	7.93 \pm 0.47	—
8738809	1	1120.69 \pm 0.405	3.33 \pm 1.51	4.83 \pm 0.60	8.23 \pm 0.90
8738809	1	1170.25 \pm 0.605	4.97 \pm 1.97	5.34 \pm 0.61	6.98 \pm 0.87
8738809	2	597.88 \pm 1.274	0.98 \pm 1.28	0.51 \pm 0.46	-0.77 \pm 2.10
8738809	2	648.43 \pm 0.611	2.17 \pm 1.23	4.12 \pm 0.85	4.85 \pm 2.57
8738809	2	699.34 \pm 0.536	1.39 \pm 1.09	4.03 \pm 1.50	1.07 \pm 1.70
8738809	2	746.86 \pm 0.157	1.00 \pm 0.55	5.28 \pm 0.73	13.84 \pm 2.35
8738809	2	795.41 \pm 0.236	1.89 \pm 0.49	7.49 \pm 0.67	14.99 \pm 2.64
8738809	2	843.71 \pm 0.333	2.31 \pm 0.75	7.04 \pm 0.89	10.41 \pm 3.67

Continued on next page

KIC	l	ν_{nl} (μHz)	Γ_{nl} (μHz)	A_{nl} (ppm)	$\ln K$
8738809	2	893.83 ± 0.363	2.35 ± 0.85	7.22 ± 1.00	10.30 ± 2.53
8738809	2	945.09 ± 0.661	3.46 ± 0.90	8.76 ± 1.44	6.70 ± 2.60
8738809	2	994.76 ± 0.287	2.54 ± 0.70	7.83 ± 0.81	9.83 ± 2.72
8738809	2	1044.55 ± 0.682	3.94 ± 2.62	6.65 ± 2.32	2.96 ± 2.15
8738809	2	1094.64 ± 1.144	5.61 ± 3.06	5.14 ± 2.90	-0.11 ± 1.54
9512063	0	661.81 ± 1.095	1.67 ± 2.02	2.65 ± 1.49	0.39 ± 0.92
9512063	0	710.80 ± 0.119	0.53 ± 0.29	6.62 ± 1.14	6.05 ± 4.67
9512063	0	759.37 ± 0.259	1.63 ± 0.79	8.09 ± 1.13	8.12 ± 3.32
9512063	0	809.02 ± 0.431	1.56 ± 0.75	6.40 ± 1.12	3.47 ± 2.60
9512063	0	858.24 ± 0.224	1.26 ± 0.45	8.74 ± 1.10	4.40 ± 3.38
9512063	0	908.46 ± 0.305	1.14 ± 0.91	6.31 ± 1.72	0.66 ± 3.61
9512063	0	958.00 ± 0.334	2.18 ± 0.84	8.96 ± 1.20	2.98 ± 2.38
9512063	0	1008.98 ± 0.518	1.57 ± 1.48	4.81 ± 1.45	2.14 ± 1.72
9512063	0	1057.91 ± 0.256	1.45 ± 0.64	6.35 ± 0.91	3.04 ± 2.62
9512063	1	647.01 ± 0.541	0.65 ± 0.87	2.75 ± 1.30	1.63 ± 0.43
9512063	1	682.65 ± 0.490	1.18 ± 1.04	5.98 ± 1.06	7.13 ± 0.86
9512063	1	719.59 ± 0.251	0.61 ± 0.33	8.10 ± 1.04	40.55 ± 2.70
9512063	1	749.85 ± 0.265	0.63 ± 0.44	4.74 ± 1.08	3.24 ± 2.80
9512063	1	788.50 ± 0.159	0.67 ± 0.26	10.79 ± 1.22	63.18 ± 1.31
9512063	1	833.62 ± 0.082	0.46 ± 0.16	15.03 ± 1.68	103.10 ± 1.58
9512063	1	878.95 ± 0.212	1.69 ± 0.46	12.57 ± 1.06	57.71 ± 1.33
9512063	1	917.16 ± 0.256	1.14 ± 0.65	7.14 ± 0.92	24.57 ± 3.33
9512063	1	943.36 ± 0.298	1.94 ± 1.12	7.43 ± 0.93	4.47 ± 0.92
9512063	1	985.34 ± 0.238	1.21 ± 0.51	7.34 ± 0.84	28.65 ± 1.09
9512063	1	1033.89 ± 0.606	3.39 ± 1.52	6.41 ± 0.82	7.22 ± 0.81
9512063	2	657.24 ± 0.642	1.29 ± 1.44	4.85 ± 1.21	2.99 ± 0.90
9512063	2	705.73 ± 0.569	1.11 ± 0.97	4.56 ± 1.06	4.24 ± 2.99
9512063	2	753.81 ± 0.452	1.30 ± 1.02	6.76 ± 1.24	6.43 ± 2.83
9512063	2	804.58 ± 0.395	0.82 ± 0.59	6.09 ± 1.09	7.68 ± 2.04
9512063	2	853.85 ± 0.313	1.27 ± 0.63	8.90 ± 1.03	13.65 ± 2.28
9512063	2	904.51 ± 0.600	0.91 ± 0.89	9.80 ± 1.36	8.16 ± 3.35
9512063	2	953.67 ± 0.841	1.53 ± 1.85	5.36 ± 1.59	3.17 ± 1.75
9512063	2	1004.53 ± 0.547	1.93 ± 1.67	6.91 ± 1.21	3.90 ± 1.78
9512063	2	1053.72 ± 1.123	1.50 ± 1.86	2.79 ± 1.32	0.70 ± 1.42
10018963	0	622.73 ± 0.087	0.43 ± 0.16	1.99 ± 0.29	9.99 ± 2.85
10018963	0	674.93 ± 0.241	1.08 ± 0.35	2.51 ± 0.33	4.00 ± 3.58
10018963	0	728.91 ± 0.256	2.00 ± 0.47	3.48 ± 0.32	5.62 ± 3.83
10018963	0	782.93 ± 0.080	0.54 ± 0.24	3.63 ± 0.63	4.17 ± 4.90
10018963	0	838.75 ± 0.163	1.50 ± 0.36	5.44 ± 0.68	5.85 ± 3.90
10018963	0	892.65 ± 0.101	1.34 ± 0.20	6.21 ± 0.40	20.26 ± 4.66
10018963	0	946.99 ± 0.138	1.64 ± 0.25	7.77 ± 0.65	22.36 ± 4.41
10018963	0	1002.61 ± 0.112	2.42 ± 0.26	7.93 ± 0.29	37.68 ± 4.83
10018963	0	1058.40 ± 0.095	1.84 ± 0.23	7.37 ± 0.33	9.22 ± 4.36
10018963	0	1114.42 ± 0.179	3.19 ± 0.43	6.86 ± 0.38	3.74 ± 4.34
10018963	0	1170.14 ± 1.106	4.44 ± 1.83	4.35 ± 2.72	-0.93 ± 3.24
10018963	0	1227.00 ± 0.625	4.08 ± 1.20	4.23 ± 1.22	-0.16 ± 3.83
10018963	0	1285.05 ± 0.567	3.42 ± 1.84	2.68 ± 0.73	4.16 ± 2.47
10018963	0	1338.82 ± 0.507	5.68 ± 1.48	4.01 ± 0.47	12.91 ± 2.43
10018963	0	1394.98 ± 0.882	8.09 ± 2.26	3.03 ± 0.38	4.58 ± 1.75
10018963	1	652.38 ± 0.071	0.47 ± 0.15	2.97 ± 0.27	32.91 ± 1.75
10018963	1	699.95 ± 0.138	0.91 ± 0.26	3.80 ± 0.26	65.51 ± 1.36
10018963	1	749.06 ± 0.067	0.66 ± 0.17	4.92 ± 0.25	161.16 ± 2.05
10018963	1	784.16 ± 0.162	1.04 ± 0.32	5.05 ± 0.52	5.82 ± 4.96
10018963	1	815.75 ± 0.104	1.33 ± 0.27	6.30 ± 0.24	220.40 ± 2.02
10018963	1	865.42 ± 0.089	1.56 ± 0.21	8.56 ± 0.26	398.10 ± 2.13
10018963	1	918.11 ± 0.078	2.02 ± 0.24	10.29 ± 0.27	—
10018963	1	972.55 ± 0.083	1.93 ± 0.21	10.07 ± 0.26	518.66 ± 2.14
10018963	1	1027.95 ± 0.092	2.41 ± 0.28	9.85 ± 0.25	448.83 ± 2.03
10018963	1	1083.64 ± 0.103	3.11 ± 0.27	9.36 ± 0.22	—
10018963	1	1139.04 ± 0.126	3.83 ± 0.33	8.35 ± 0.21	—

Continued on next page

KIC	l	ν_{nl} (μHz)	Γ_{nl} (μHz)	A_{nl} (ppm)	$\ln K$
10018963	1	1194.62 \pm 0.158	4.40 \pm 0.43	7.48 \pm 0.20	194.09 \pm 1.75
10018963	1	1250.42 \pm 0.260	6.40 \pm 0.67	6.33 \pm 0.20	93.86 \pm 1.58
10018963	1	1306.76 \pm 0.307	6.11 \pm 0.77	5.00 \pm 0.20	58.37 \pm 1.58
10018963	1	1363.84 \pm 0.419	6.54 \pm 1.34	3.91 \pm 0.24	21.42 \pm 1.27
10018963	1	1419.42 \pm 1.110	9.59 \pm 1.93	2.69 \pm 0.29	0.99 \pm 1.01
10018963	2	617.15 \pm 0.217	0.64 \pm 0.37	2.10 \pm 0.33	6.54 \pm 3.08
10018963	2	670.51 \pm 0.289	0.94 \pm 0.49	2.57 \pm 0.33	12.45 \pm 2.30
10018963	2	723.92 \pm 0.262	0.78 \pm 0.46	2.62 \pm 0.34	9.99 \pm 2.70
10018963	2	779.80 \pm 0.137	0.70 \pm 0.41	3.50 \pm 0.34	10.56 \pm 4.78
10018963	2	834.71 \pm 0.629	2.22 \pm 0.66	5.69 \pm 0.63	35.51 \pm 3.21
10018963	2	888.41 \pm 0.262	1.47 \pm 0.29	7.13 \pm 0.36	84.37 \pm 3.86
10018963	2	942.91 \pm 0.532	2.03 \pm 0.45	7.04 \pm 0.68	61.59 \pm 3.80
10018963	2	997.85 \pm 0.112	1.29 \pm 0.36	6.44 \pm 0.32	76.04 \pm 3.77
10018963	2	1054.02 \pm 0.169	2.67 \pm 0.42	6.80 \pm 0.34	64.95 \pm 3.64
10018963	2	1109.70 \pm 0.247	2.79 \pm 0.64	5.54 \pm 0.45	29.23 \pm 3.22
10018963	2	1167.43 \pm 1.160	3.96 \pm 1.11	7.00 \pm 1.83	5.18 \pm 2.92
10018963	2	1222.33 \pm 0.754	4.25 \pm 1.07	5.49 \pm 0.81	30.68 \pm 3.40
10018963	2	1278.64 \pm 0.609	6.78 \pm 1.76	5.06 \pm 0.53	15.84 \pm 2.83
10018963	2	1333.33 \pm 0.830	2.80 \pm 2.82	1.91 \pm 0.75	1.51 \pm 2.03
10018963	2	1389.11 \pm 0.920	1.84 \pm 2.47	1.24 \pm 0.52	0.42 \pm 1.51
10147635	0	419.98 \pm 0.127	0.54 \pm 0.28	3.71 \pm 0.64	7.16 \pm 1.37
10147635	0	455.88 \pm 0.170	0.91 \pm 0.35	4.95 \pm 0.89	0.98 \pm 3.44
10147635	0	493.60 \pm 0.202	1.22 \pm 0.61	5.23 \pm 0.88	6.62 \pm 3.33
10147635	0	530.18 \pm 0.072	0.69 \pm 0.25	6.62 \pm 0.82	8.65 \pm 4.33
10147635	0	566.39 \pm 0.658	1.62 \pm 1.38	4.77 \pm 2.74	-0.65 \pm 4.22
10147635	0	603.02 \pm 0.168	1.76 \pm 0.36	10.20 \pm 1.40	7.30 \pm 5.22
10147635	0	641.01 \pm 0.207	1.34 \pm 0.40	8.59 \pm 1.28	21.33 \pm 3.51
10147635	0	679.05 \pm 0.265	2.31 \pm 0.80	8.67 \pm 1.69	2.89 \pm 4.50
10147635	0	717.07 \pm 0.234	2.36 \pm 0.61	7.56 \pm 0.81	5.03 \pm 5.09
10147635	0	753.75 \pm 0.463	5.28 \pm 0.94	9.64 \pm 0.81	15.06 \pm 2.34
10147635	0	792.62 \pm 0.464	2.12 \pm 1.27	5.33 \pm 1.81	2.08 \pm 2.02
10147635	0	830.09 \pm 0.777	3.40 \pm 1.75	4.89 \pm 1.58	1.42 \pm 1.49
10147635	1	448.17 \pm 0.512	0.83 \pm 0.86	4.14 \pm 0.75	5.39 \pm 2.75
10147635	1	468.82 \pm 0.162	0.68 \pm 0.33	5.64 \pm 0.53	28.31 \pm 1.34
10147635	1	496.68 \pm 0.166	0.87 \pm 0.41	6.16 \pm 0.67	13.42 \pm 3.04
10147635	1	519.46 \pm 0.071	0.54 \pm 0.30	8.04 \pm 0.57	90.53 \pm 7.22
10147635	1	544.70 \pm 0.129	1.00 \pm 0.36	8.52 \pm 0.49	79.38 \pm 1.52
10147635	1	568.07 \pm 0.126	0.73 \pm 0.20	10.09 \pm 1.04	6.88 \pm 3.77
10147635	1	592.91 \pm 0.075	1.08 \pm 0.23	12.04 \pm 0.54	112.03 \pm 12.87
10147635	1	624.64 \pm 0.098	1.52 \pm 0.33	12.11 \pm 0.49	161.18 \pm 1.60
10147635	1	658.09 \pm 0.077	0.84 \pm 0.20	11.06 \pm 0.48	179.88 \pm 1.87
10147635	1	682.69 \pm 0.146	0.67 \pm 0.32	6.68 \pm 0.66	20.87 \pm 3.76
10147635	1	703.81 \pm 0.135	1.54 \pm 0.55	9.74 \pm 0.49	108.11 \pm 8.11
10147635	1	737.91 \pm 0.163	2.53 \pm 0.44	9.23 \pm 0.45	—
10147635	1	773.32 \pm 0.242	3.31 \pm 0.76	8.33 \pm 0.47	—
10147635	1	811.12 \pm 0.501	5.38 \pm 1.40	6.71 \pm 0.57	—
10147635	1	847.71 \pm 0.441	4.24 \pm 1.03	6.58 \pm 0.52	9.87 \pm 1.01
10147635	2	415.37 \pm 0.918	1.71 \pm 1.89	2.53 \pm 1.30	0.48 \pm 1.67
10147635	2	453.11 \pm 0.994	1.10 \pm 1.32	3.91 \pm 1.30	2.43 \pm 2.82
10147635	2	489.62 \pm 0.464	1.72 \pm 1.17	5.14 \pm 0.87	6.70 \pm 3.20
10147635	2	527.03 \pm 0.563	2.95 \pm 1.22	7.26 \pm 0.98	17.05 \pm 4.03
10147635	2	563.80 \pm 0.524	2.61 \pm 0.78	11.16 \pm 1.31	7.72 \pm 4.46
10147635	2	599.94 \pm 0.791	1.35 \pm 0.62	7.57 \pm 1.56	13.80 \pm 4.56
10147635	2	637.84 \pm 0.606	2.15 \pm 0.72	8.88 \pm 1.21	18.72 \pm 2.74
10147635	2	675.58 \pm 0.633	2.38 \pm 0.81	8.71 \pm 1.49	8.98 \pm 3.91
10147635	2	713.20 \pm 0.229	1.46 \pm 0.88	7.34 \pm 0.86	13.35 \pm 4.57
10147635	2	750.66 \pm 0.804	1.51 \pm 1.69	2.51 \pm 1.59	-0.69 \pm 1.84
10147635	2	789.76 \pm 1.020	4.89 \pm 1.51	6.72 \pm 1.60	1.56 \pm 1.89
10147635	2	827.56 \pm 1.088	2.37 \pm 2.04	3.17 \pm 1.95	-0.05 \pm 1.38
10273246	0	594.61 \pm 0.148	0.61 \pm 0.35	4.23 \pm 1.43	0.23 \pm 3.69

Continued on next page

KIC	l	ν_{nl} (μHz)	Γ_{nl} (μHz)	A_{nl} (ppm)	$\ln K$
10273246	0	642.61 ± 0.078	0.54 ± 0.23	4.96 ± 0.60	9.08 ± 2.71
10273246	0	691.05 ± 0.131	0.89 ± 0.42	5.24 ± 0.84	4.45 ± 4.21
10273246	0	737.86 ± 0.247	2.02 ± 0.51	7.82 ± 0.93	5.04 ± 4.92
10273246	0	785.08 ± 0.141	2.06 ± 0.29	9.74 ± 0.48	48.58 ± 4.40
10273246	0	833.70 ± 0.207	2.06 ± 0.43	10.10 ± 1.08	15.42 ± 3.41
10273246	0	883.37 ± 0.588	1.06 ± 0.58	6.36 ± 2.08	8.90 ± 3.49
10273246	0	932.40 ± 0.426	3.60 ± 0.84	9.57 ± 1.14	18.71 ± 3.64
10273246	0	980.75 ± 0.552	5.93 ± 1.17	11.98 ± 1.42	1.85 ± 2.98
10273246	0	1029.62 ± 1.000	8.23 ± 1.98	7.64 ± 1.01	4.22 ± 2.04
10273246	0	1078.47 ± 0.620	4.82 ± 2.11	5.71 ± 0.94	3.75 ± 1.61
10273246	1	622.75 ± 0.312	0.76 ± 0.28	5.52 ± 0.53	28.53 ± 1.25
10273246	1	662.24 ± 0.157	1.07 ± 0.30	6.68 ± 0.49	43.18 ± 1.47
10273246	1	695.84 ± 0.156	0.85 ± 0.37	5.57 ± 0.59	15.60 ± 5.00
10273246	1	724.24 ± 0.088	0.85 ± 0.27	7.80 ± 0.53	57.61 ± 12.85
10273246	1	764.30 ± 0.175	2.20 ± 0.45	10.75 ± 0.49	99.06 ± 1.58
10273246	1	809.86 ± 0.074	1.08 ± 0.21	11.52 ± 0.51	184.92 ± 1.88
10273246	1	857.34 ± 0.181	1.63 ± 0.29	11.12 ± 0.47	167.57 ± 1.66
10273246	1	905.23 ± 0.122	1.80 ± 0.32	11.43 ± 0.47	141.38 ± 1.65
10273246	1	950.58 ± 0.194	3.22 ± 0.54	10.58 ± 0.47	73.51 ± 1.53
10273246	1	978.11 ± 0.648	0.93 ± 0.86	5.88 ± 2.02	3.79 ± 2.84
10273246	1	1008.38 ± 0.184	2.77 ± 0.52	8.77 ± 0.48	55.48 ± 1.61
10273246	1	1055.15 ± 0.772	7.14 ± 1.88	7.12 ± 0.64	5.24 ± 0.84
10273246	1	1103.74 ± 0.388	2.99 ± 1.90	5.45 ± 0.72	8.51 ± 0.93
10273246	2	590.98 ± 0.755	0.56 ± 0.55	5.69 ± 0.93	15.27 ± 2.80
10273246	2	637.67 ± 0.729	1.44 ± 1.70	3.76 ± 0.87	3.69 ± 2.11
10273246	2	687.12 ± 0.561	1.89 ± 2.18	6.23 ± 1.10	7.37 ± 3.78
10273246	2	733.65 ± 0.593	0.74 ± 0.77	5.28 ± 1.06	10.70 ± 4.52
10273246	2	779.54 ± 0.052	0.42 ± 0.10	6.41 ± 0.47	47.51 ± 3.66
10273246	2	829.83 ± 0.798	1.53 ± 0.87	7.81 ± 1.29	15.01 ± 2.88
10273246	2	880.86 ± 0.914	2.01 ± 1.07	10.15 ± 1.40	32.99 ± 3.15
10273246	2	928.03 ± 0.813	1.38 ± 0.71	6.01 ± 1.42	7.03 ± 2.65
10273246	2	1024.94 ± 0.825	0.90 ± 1.32	3.60 ± 1.14	1.40 ± 1.87
10273246	2	1074.20 ± 1.187	1.77 ± 2.40	2.29 ± 1.33	-0.18 ± 1.35
10593351	0	354.32 ± 0.089	0.32 ± 0.23	4.13 ± 0.90	6.89 ± 1.05
10593351	0	385.50 ± 0.228	1.07 ± 0.68	5.54 ± 1.07	7.20 ± 2.55
10593351	0	416.60 ± 0.126	1.06 ± 0.37	8.84 ± 0.92	21.61 ± 2.50
10593351	0	447.14 ± 0.229	1.48 ± 0.66	9.38 ± 2.24	2.39 ± 3.89
10593351	0	476.93 ± 0.343	2.98 ± 0.89	12.80 ± 1.63	5.66 ± 4.41
10593351	0	509.24 ± 0.086	1.20 ± 0.25	13.54 ± 0.87	45.72 ± 7.36
10593351	0	541.22 ± 0.091	0.48 ± 0.33	8.00 ± 1.82	4.80 ± 3.56
10593351	0	572.47 ± 0.519	4.71 ± 1.29	13.33 ± 2.14	6.15 ± 3.63
10593351	0	605.49 ± 0.430	1.43 ± 1.08	6.83 ± 2.51	2.55 ± 2.35
10593351	0	636.54 ± 0.344	2.68 ± 1.13	8.36 ± 1.31	10.42 ± 2.08
10593351	0	668.71 ± 0.380	4.62 ± 1.10	8.97 ± 0.70	—
10593351	1	366.31 ± 0.188	1.41 ± 0.55	10.23 ± 0.87	29.42 ± 1.17
10593351	1	389.83 ± 0.087	0.32 ± 0.20	5.30 ± 0.80	9.69 ± 2.23
10593351	1	404.57 ± 0.155	0.62 ± 0.41	6.33 ± 0.82	11.75 ± 1.23
10593351	1	427.90 ± 0.165	0.89 ± 0.27	10.64 ± 0.72	58.09 ± 1.38
10593351	1	452.37 ± 0.175	0.61 ± 0.25	10.84 ± 0.80	52.17 ± 3.25
10593351	1	470.51 ± 0.146	0.52 ± 0.30	11.54 ± 0.89	16.41 ± 4.22
10593351	1	493.40 ± 0.080	0.80 ± 0.21	12.86 ± 0.74	111.06 ± 1.55
10593351	1	520.54 ± 0.109	1.27 ± 0.28	13.93 ± 0.70	105.17 ± 1.48
10593351	1	543.18 ± 0.275	1.57 ± 0.78	11.67 ± 1.64	5.26 ± 3.47
10593351	1	563.37 ± 0.119	1.36 ± 0.32	12.62 ± 0.76	39.07 ± 10.37
10593351	1	590.17 ± 0.134	1.87 ± 0.41	13.83 ± 0.63	82.34 ± 1.47
10593351	1	619.73 ± 0.223	3.06 ± 0.66	11.31 ± 0.65	—
10593351	1	649.13 ± 0.417	4.69 ± 0.98	9.30 ± 0.67	8.75 ± 1.00
10593351	2	380.32 ± 0.674	1.07 ± 1.09	3.68 ± 1.56	0.97 ± 2.94
10593351	2	412.17 ± 0.719	2.35 ± 1.91	5.89 ± 1.55	3.62 ± 1.85
10593351	2	444.43 ± 0.843	2.80 ± 1.59	10.01 ± 2.14	3.48 ± 3.54

Continued on next page

KIC	l	ν_{nl} (μHz)	Γ_{nl} (μHz)	A_{nl} (ppm)	$\ln K$
10593351	2	473.85 \pm 0.587	1.00 \pm 1.28	6.57 \pm 2.48	2.04 \pm 3.78
10593351	2	504.99 \pm 0.285	1.84 \pm 1.10	8.87 \pm 1.11	22.26 \pm 2.53
10593351	2	538.40 \pm 0.597	3.42 \pm 1.36	11.70 \pm 1.76	6.67 \pm 3.50
10593351	2	569.52 \pm 0.815	2.65 \pm 2.37	5.58 \pm 3.81	-0.29 \pm 3.44
10593351	2	602.95 \pm 0.615	3.02 \pm 1.19	10.21 \pm 2.02	2.28 \pm 2.03
10593351	2	633.15 \pm 0.580	1.73 \pm 1.54	5.36 \pm 1.79	1.68 \pm 1.73
10873176	0	646.22 \pm 1.323	1.39 \pm 1.82	1.51 \pm 1.26	-0.47 \pm 0.69
10873176	0	694.07 \pm 0.442	1.87 \pm 1.23	9.35 \pm 1.85	6.96 \pm 1.78
10873176	0	740.59 \pm 1.221	2.76 \pm 2.38	9.63 \pm 2.20	3.36 \pm 0.77
10873176	0	789.14 \pm 0.322	2.19 \pm 0.94	13.26 \pm 1.55	9.95 \pm 0.99
10873176	0	837.26 \pm 0.747	2.88 \pm 2.11	9.92 \pm 4.58	1.01 \pm 1.22
10873176	0	889.23 \pm 0.658	4.34 \pm 2.41	12.73 \pm 1.80	1.62 \pm 0.84
10873176	0	936.32 \pm 1.203	7.21 \pm 1.44	11.25 \pm 1.82	-4.85 \pm 1.01
10873176	1	614.66 \pm 0.801	4.35 \pm 2.19	10.36 \pm 1.91	0.86 \pm 0.71
10873176	1	656.42 \pm 0.639	1.26 \pm 0.99	6.15 \pm 1.78	3.22 \pm 0.52
10873176	1	689.08 \pm 0.175	0.92 \pm 0.49	12.53 \pm 1.77	13.86 \pm 2.08
10873176	1	720.47 \pm 0.406	2.11 \pm 1.04	10.52 \pm 1.53	10.65 \pm 0.90
10873176	1	762.07 \pm 0.260	1.65 \pm 0.57	14.19 \pm 1.52	25.55 \pm 1.09
10873176	1	804.19 \pm 0.134	0.76 \pm 0.30	14.60 \pm 1.74	38.04 \pm 1.18
10873176	1	834.45 \pm 0.699	2.46 \pm 1.77	11.34 \pm 3.81	0.83 \pm 1.22
10873176	1	870.23 \pm 0.635	4.16 \pm 1.53	12.62 \pm 1.52	7.68 \pm 0.81
10873176	1	914.73 \pm 0.231	1.54 \pm 0.63	14.11 \pm 1.53	19.81 \pm 1.11
10873176	1	961.26 \pm 0.509	3.68 \pm 1.59	13.13 \pm 1.55	5.41 \pm 0.84
10920273	0	825.73 \pm 0.411	1.62 \pm 1.80	5.91 \pm 1.37	1.70 \pm 0.75
10920273	0	882.84 \pm 0.103	0.59 \pm 0.23	6.57 \pm 0.86	17.58 \pm 2.80
10920273	0	939.96 \pm 0.090	0.90 \pm 0.27	10.48 \pm 0.88	37.46 \pm 4.20
10920273	0	997.10 \pm 0.095	0.93 \pm 0.23	10.79 \pm 0.84	7.76 \pm 3.73
10920273	0	1054.31 \pm 0.076	0.69 \pm 0.16	10.77 \pm 0.86	26.09 \pm 8.69
10920273	0	1111.92 \pm 0.244	1.43 \pm 0.75	7.45 \pm 1.26	4.81 \pm 3.09
10920273	0	1169.66 \pm 0.534	3.85 \pm 1.30	9.20 \pm 1.07	12.29 \pm 1.10
10920273	1	842.17 \pm 0.158	0.40 \pm 0.25	6.37 \pm 0.87	13.23 \pm 1.41
10920273	1	873.25 \pm 0.085	0.43 \pm 0.15	7.89 \pm 0.84	37.29 \pm 2.79
10920273	1	914.62 \pm 0.136	0.59 \pm 0.24	9.39 \pm 0.83	33.45 \pm 1.40
10920273	1	967.89 \pm 0.089	0.56 \pm 0.19	10.88 \pm 0.85	72.90 \pm 1.59
10920273	1	1023.60 \pm 0.105	0.74 \pm 0.27	12.53 \pm 0.83	78.60 \pm 1.63
10920273	1	1079.07 \pm 0.112	0.66 \pm 0.25	10.34 \pm 0.81	57.60 \pm 1.41
10920273	1	1134.68 \pm 0.281	1.47 \pm 0.73	8.21 \pm 0.96	16.05 \pm 1.13
10920273	2	934.41 \pm 0.091	0.47 \pm 0.15	7.41 \pm 0.82	28.34 \pm 2.96
10920273	2	992.46 \pm 0.087	0.49 \pm 0.15	9.03 \pm 0.85	46.37 \pm 2.92
10920273	2	1048.93 \pm 0.366	1.00 \pm 0.64	6.38 \pm 0.99	8.88 \pm 2.67
10920273	2	1106.73 \pm 0.720	0.92 \pm 0.57	7.59 \pm 1.20	9.56 \pm 2.50
10972873	0	725.81 \pm 0.302	0.83 \pm 1.50	2.47 \pm 0.73	2.03 \pm 1.01
10972873	0	783.51 \pm 0.079	0.61 \pm 0.20	4.41 \pm 0.49	8.56 \pm 4.47
10972873	0	840.45 \pm 0.083	0.84 \pm 0.22	5.38 \pm 0.41	30.32 \pm 12.43
10972873	0	897.69 \pm 0.068	0.77 \pm 0.20	5.58 \pm 0.43	8.42 \pm 3.56
10972873	0	955.85 \pm 0.051	0.75 \pm 0.12	8.30 \pm 0.43	33.11 \pm 4.68
10972873	0	1014.27 \pm 0.046	0.69 \pm 0.11	8.99 \pm 0.46	64.78 \pm 4.90
10972873	0	1072.72 \pm 0.050	0.72 \pm 0.11	8.63 \pm 0.44	40.93 \pm 4.38
10972873	0	1131.09 \pm 0.076	1.21 \pm 0.19	8.35 \pm 0.42	22.62 \pm 3.93
10972873	0	1189.57 \pm 0.229	2.18 \pm 0.55	5.60 \pm 0.59	3.14 \pm 3.32
10972873	0	1249.65 \pm 0.311	2.11 \pm 0.65	4.15 \pm 0.48	6.05 \pm 2.83
10972873	0	1308.48 \pm 0.371	1.53 \pm 1.79	2.85 \pm 0.85	1.52 \pm 1.70
10972873	1	769.89 \pm 0.152	0.52 \pm 0.22	3.28 \pm 0.45	10.42 \pm 3.34
10972873	1	814.64 \pm 0.110	0.90 \pm 0.22	5.58 \pm 0.40	59.29 \pm 1.47
10972873	1	867.76 \pm 0.056	0.58 \pm 0.13	6.84 \pm 0.41	143.28 \pm 1.97
10972873	1	923.43 \pm 0.063	0.95 \pm 0.15	9.93 \pm 0.43	269.08 \pm 1.98
10972873	1	979.41 \pm 0.043	0.61 \pm 0.10	11.72 \pm 0.51	445.63 \pm 2.21
10972873	1	1027.77 \pm 0.050	0.78 \pm 0.13	9.99 \pm 0.45	302.17 \pm 2.09
10972873	1	1054.40 \pm 0.046	0.66 \pm 0.12	8.73 \pm 0.44	221.15 \pm 2.07
10972873	1	1101.97 \pm 0.056	1.00 \pm 0.13	10.80 \pm 0.44	327.20 \pm 2.09

Continued on next page

KIC	l	ν_{nl} (μHz)	Γ_{nl} (μHz)	A_{nl} (ppm)	$\ln K$
10972873	1	1158.53 ± 0.082	1.42 ± 0.22	9.51 ± 0.38	204.46 ± 1.87
10972873	1	1216.89 ± 0.166	2.58 ± 0.52	7.48 ± 0.39	71.75 ± 1.60
10972873	1	1275.32 ± 0.243	2.34 ± 0.68	5.39 ± 0.42	30.82 ± 1.29
10972873	1	1334.71 ± 0.711	5.91 ± 2.35	5.20 ± 0.59	6.46 ± 0.87
10972873	2	721.67 ± 1.395	2.30 ± 2.76	1.72 ± 1.08	-0.13 ± 1.13
10972873	2	778.62 ± 0.979	3.77 ± 2.40	4.74 ± 0.86	10.29 ± 3.78
10972873	2	832.54 ± 0.177	0.54 ± 0.24	3.59 ± 0.41	16.37 ± 2.91
10972873	2	892.93 ± 0.145	1.15 ± 0.40	5.32 ± 0.46	43.45 ± 3.06
10972873	2	950.61 ± 0.091	1.07 ± 0.26	7.02 ± 0.40	129.07 ± 3.62
10972873	2	1008.94 ± 0.076	1.09 ± 0.19	8.78 ± 0.40	180.74 ± 3.77
10972873	2	1067.92 ± 0.085	1.27 ± 0.31	8.60 ± 0.42	140.83 ± 3.78
10972873	2	1126.19 ± 0.130	1.77 ± 0.43	7.55 ± 0.45	75.72 ± 3.50
10972873	2	1184.39 ± 0.344	3.29 ± 0.95	6.94 ± 0.61	18.81 ± 2.93
10972873	2	1243.64 ± 0.720	1.66 ± 1.12	3.93 ± 0.58	11.33 ± 2.25
10972873	2	1303.73 ± 1.197	3.71 ± 2.98	3.47 ± 0.99	2.23 ± 1.59
10972873	3	1089.29 ± 0.223	1.05 ± 0.15	10.80 ± 0.51	98.32 ± 6.46
10972873	3	1151.79 ± 0.064	1.41 ± 0.15	9.75 ± 0.37	84.67 ± 5.01
11026764	0	574.95 ± 0.147	0.48 ± 0.20	2.12 ± 0.36	8.67 ± 1.39
11026764	0	624.99 ± 0.089	0.66 ± 0.22	3.00 ± 0.32	26.39 ± 2.84
11026764	0	674.65 ± 0.108	1.03 ± 0.21	3.89 ± 0.29	46.77 ± 4.28
11026764	0	723.38 ± 0.377	0.67 ± 0.52	3.56 ± 2.58	-0.37 ± 4.24
11026764	0	772.77 ± 0.065	1.24 ± 0.14	7.30 ± 0.29	169.12 ± 27.37
11026764	0	823.16 ± 0.040	0.68 ± 0.09	7.64 ± 0.35	98.05 ± 5.46
11026764	0	873.72 ± 0.035	0.64 ± 0.08	8.70 ± 0.38	183.56 ± 6.08
11026764	0	924.14 ± 0.059	0.97 ± 0.14	7.87 ± 0.37	38.39 ± 6.16
11026764	0	974.69 ± 0.069	1.19 ± 0.18	6.02 ± 0.28	30.95 ± 4.44
11026764	0	1025.37 ± 0.118	2.02 ± 0.33	5.25 ± 0.27	17.38 ± 4.95
11026764	0	1076.39 ± 0.497	2.30 ± 0.95	3.15 ± 1.30	-0.43 ± 3.09
11026764	0	1129.53 ± 0.458	1.55 ± 3.40	2.06 ± 1.08	3.08 ± 2.01
11026764	0	1177.49 ± 0.588	3.39 ± 1.28	2.33 ± 0.33	9.27 ± 1.12
11026764	1	587.88 ± 0.101	0.41 ± 0.15	2.68 ± 0.31	21.27 ± 1.69
11026764	1	620.48 ± 0.060	0.42 ± 0.12	3.35 ± 0.29	46.52 ± 2.65
11026764	1	654.62 ± 0.094	0.42 ± 0.16	3.34 ± 0.28	45.13 ± 1.47
11026764	1	694.18 ± 0.050	0.38 ± 0.11	4.17 ± 0.29	102.10 ± 1.79
11026764	1	723.64 ± 0.219	0.53 ± 0.23	5.85 ± 2.24	-0.70 ± 4.22
11026764	1	755.15 ± 0.053	0.65 ± 0.13	6.54 ± 0.29	268.49 ± 1.89
11026764	1	799.58 ± 0.043	0.75 ± 0.10	8.80 ± 0.34	502.55 ± 2.02
11026764	1	847.44 ± 0.040	0.77 ± 0.09	9.88 ± 0.37	517.20 ± 11.43
11026764	1	893.98 ± 0.036	0.67 ± 0.08	10.66 ± 0.41	456.76 ± 6.32
11026764	1	925.81 ± 0.040	0.37 ± 0.05	7.12 ± 0.43	64.77 ± 6.00
11026764	1	954.08 ± 0.045	0.79 ± 0.11	9.83 ± 0.34	679.90 ± 2.07
11026764	1	1000.43 ± 0.069	1.48 ± 0.21	7.96 ± 0.26	—
11026764	1	1050.02 ± 0.118	2.29 ± 0.36	5.93 ± 0.23	174.39 ± 9.84
11026764	1	1099.84 ± 0.188	3.01 ± 0.55	4.62 ± 0.24	54.62 ± 1.51
11026764	1	1151.32 ± 0.345	4.02 ± 1.00	3.69 ± 0.27	21.61 ± 1.17
11026764	1	1201.07 ± 0.847	3.87 ± 2.06	2.12 ± 0.38	4.44 ± 0.73
11026764	2	669.44 ± 0.180	0.46 ± 0.24	2.18 ± 0.31	8.27 ± 3.01
11026764	2	718.93 ± 0.111	0.73 ± 0.33	4.04 ± 0.28	42.91 ± 4.30
11026764	2	766.24 ± 0.042	0.34 ± 0.04	3.99 ± 0.24	97.11 ± 4.20
11026764	2	818.75 ± 0.073	0.87 ± 0.17	6.65 ± 0.29	243.32 ± 3.83
11026764	2	868.91 ± 0.068	0.55 ± 0.12	6.84 ± 0.29	317.98 ± 4.10
11026764	2	919.94 ± 0.067	0.88 ± 0.19	7.11 ± 0.30	161.63 ± 6.25
11026764	2	970.33 ± 0.081	1.45 ± 0.21	6.72 ± 0.28	114.77 ± 3.94
11026764	2	1020.56 ± 0.147	1.68 ± 0.55	4.53 ± 0.31	46.33 ± 3.31
11026764	2	1073.63 ± 0.896	1.94 ± 0.82	3.95 ± 0.91	5.94 ± 2.48
11026764	2	1124.26 ± 0.808	4.64 ± 2.91	3.58 ± 0.88	4.80 ± 2.11
11026764	2	1172.20 ± 1.307	1.47 ± 1.82	0.38 ± 0.28	-0.94 ± 1.30
11026764	3	838.04 ± 0.275	1.19 ± 0.79	2.58 ± 0.33	14.34 ± 3.47
11026764	3	887.82 ± 0.355	1.45 ± 0.59	3.38 ± 0.33	36.41 ± 3.71
11026764	3	939.14 ± 0.200	0.79 ± 0.51	2.21 ± 0.27	10.26 ± 1.51

Continued on next page

KIC	l	ν_{nl} (μHz)	Γ_{nl} (μHz)	A_{nl} (ppm)	$\ln K$
11026764	3	991.18 \pm 0.125	7.95 \pm 0.51	4.28 \pm 0.35	-18.37 \pm 2.94
11026764	3	1041.06 \pm 0.976	2.67 \pm 2.61	1.88 \pm 0.52	3.03 \pm 2.46
11137075	0	949.02 \pm 0.082	0.52 \pm 0.17	4.70 \pm 0.53	27.36 \pm 2.50
11137075	0	1013.33 \pm 0.073	0.64 \pm 0.19	6.03 \pm 0.55	37.12 \pm 2.57
11137075	0	1078.59 \pm 0.053	0.56 \pm 0.13	7.86 \pm 0.60	105.61 \pm 3.40
11137075	0	1144.44 \pm 0.039	0.44 \pm 0.07	10.87 \pm 0.74	8.66 \pm 5.51
11137075	0	1209.71 \pm 0.056	0.70 \pm 0.16	9.73 \pm 0.63	130.12 \pm 3.41
11137075	0	1275.16 \pm 0.089	1.06 \pm 0.27	7.87 \pm 0.54	70.91 \pm 3.30
11137075	0	1341.58 \pm 0.321	2.22 \pm 1.35	5.33 \pm 1.09	5.63 \pm 2.16
11137075	0	1408.79 \pm 1.368	10.18 \pm 3.41	6.12 \pm 1.19	3.94 \pm 1.81
11137075	1	917.18 \pm 0.216	1.32 \pm 0.42	5.00 \pm 0.58	17.87 \pm 1.26
11137075	1	978.07 \pm 0.063	0.57 \pm 0.15	6.66 \pm 0.56	67.31 \pm 1.43
11137075	1	1040.72 \pm 0.047	0.50 \pm 0.11	8.47 \pm 0.63	118.98 \pm 1.73
11137075	1	1101.57 \pm 0.045	0.54 \pm 0.10	10.91 \pm 0.72	240.11 \pm 1.73
11137075	1	1142.59 \pm 0.054	0.35 \pm 0.10	5.68 \pm 0.79	9.20 \pm 5.64
11137075	1	1180.19 \pm 0.033	0.38 \pm 0.05	11.61 \pm 0.76	325.73 \pm 1.85
11137075	1	1240.81 \pm 0.069	0.88 \pm 0.16	9.51 \pm 0.57	128.65 \pm 1.71
11137075	1	1304.96 \pm 0.117	1.66 \pm 0.34	8.74 \pm 0.51	78.76 \pm 1.58
11137075	1	1370.14 \pm 0.251	2.89 \pm 0.67	7.32 \pm 0.53	36.23 \pm 1.29
11137075	1	1436.46 \pm 0.485	4.00 \pm 1.15	6.43 \pm 0.60	16.76 \pm 1.08
11137075	2	943.55 \pm 0.132	0.67 \pm 0.31	3.70 \pm 0.58	9.38 \pm 2.68
11137075	2	1007.33 \pm 0.181	1.42 \pm 0.59	5.26 \pm 0.63	23.13 \pm 2.60
11137075	2	1072.47 \pm 0.088	0.80 \pm 0.19	6.51 \pm 0.52	71.81 \pm 3.25
11137075	2	1132.47 \pm 0.098	0.56 \pm 0.17	4.23 \pm 0.50	22.59 \pm 5.64
11137075	2	1141.31 \pm 0.117	0.73 \pm 0.25	6.17 \pm 0.73	8.41 \pm 5.56
11137075	2	1204.18 \pm 0.057	0.67 \pm 0.15	8.92 \pm 0.60	126.27 \pm 3.24
11137075	2	1269.60 \pm 0.076	0.81 \pm 0.20	7.39 \pm 0.54	70.14 \pm 3.23
11137075	2	1335.63 \pm 0.579	4.65 \pm 3.07	6.29 \pm 1.28	4.81 \pm 2.13
11137075	2	1401.73 \pm 0.470	2.40 \pm 1.16	4.67 \pm 0.93	4.00 \pm 1.97
11193681	0	531.98 \pm 0.108	0.60 \pm 0.25	4.00 \pm 0.60	7.38 \pm 2.41
11193681	0	574.16 \pm 0.061	0.56 \pm 0.13	6.07 \pm 0.48	64.83 \pm 2.86
11193681	0	615.27 \pm 0.123	0.91 \pm 0.24	7.24 \pm 0.94	3.50 \pm 4.34
11193681	0	657.43 \pm 0.050	0.67 \pm 0.12	8.85 \pm 0.52	42.91 \pm 3.59
11193681	0	700.27 \pm 0.070	1.09 \pm 0.16	9.46 \pm 0.46	73.65 \pm 4.62
11193681	0	743.35 \pm 0.059	1.04 \pm 0.14	10.51 \pm 0.47	96.32 \pm 4.73
11193681	0	786.65 \pm 0.105	0.97 \pm 0.26	8.61 \pm 1.06	-0.55 \pm 4.13
11193681	0	828.92 \pm 0.153	2.12 \pm 0.38	8.96 \pm 0.61	14.66 \pm 3.68
11193681	0	872.41 \pm 0.164	2.07 \pm 0.45	7.77 \pm 0.67	6.86 \pm 3.31
11193681	0	917.46 \pm 0.612	1.36 \pm 1.17	2.76 \pm 0.98	1.84 \pm 1.74
11193681	0	959.64 \pm 1.079	2.23 \pm 2.09	2.13 \pm 1.53	-0.09 \pm 1.54
11193681	1	529.69 \pm 0.257	1.02 \pm 0.71	4.50 \pm 0.73	7.87 \pm 2.46
11193681	1	557.52 \pm 0.051	0.35 \pm 0.10	5.40 \pm 0.46	51.17 \pm 1.39
11193681	1	588.99 \pm 0.070	0.59 \pm 0.15	6.38 \pm 0.47	71.79 \pm 1.36
11193681	1	614.18 \pm 0.099	0.58 \pm 0.26	6.38 \pm 1.05	4.33 \pm 4.35
11193681	1	642.48 \pm 0.042	0.61 \pm 0.12	10.61 \pm 0.51	243.12 \pm 1.82
11193681	1	680.27 \pm 0.046	0.69 \pm 0.11	11.50 \pm 0.50	287.30 \pm 1.84
11193681	1	720.95 \pm 0.048	0.82 \pm 0.12	12.77 \pm 0.50	363.03 \pm 1.87
11193681	1	760.15 \pm 0.039	0.64 \pm 0.09	13.69 \pm 0.56	464.79 \pm 1.91
11193681	1	784.84 \pm 0.075	0.81 \pm 0.31	11.20 \pm 1.36	-1.00 \pm 4.25
11193681	1	811.27 \pm 0.066	1.22 \pm 0.17	11.53 \pm 0.42	263.20 \pm 1.75
11193681	1	851.35 \pm 0.109	1.94 \pm 0.29	9.42 \pm 0.40	117.68 \pm 1.59
11193681	1	893.84 \pm 0.152	2.46 \pm 0.41	8.23 \pm 0.39	—
11193681	1	937.49 \pm 0.160	1.53 \pm 0.40	5.39 \pm 0.41	32.33 \pm 1.26
11193681	1	980.21 \pm 0.382	2.17 \pm 1.62	3.44 \pm 0.66	0.55 \pm 0.84
11193681	2	569.17 \pm 0.148	0.44 \pm 0.24	3.76 \pm 0.53	9.28 \pm 2.83
11193681	2	611.44 \pm 0.095	0.59 \pm 0.35	5.78 \pm 0.56	17.68 \pm 4.38
11193681	2	654.33 \pm 0.161	1.39 \pm 0.44	7.38 \pm 0.56	49.85 \pm 3.14
11193681	2	696.30 \pm 0.070	0.64 \pm 0.19	9.22 \pm 0.47	104.79 \pm 3.77
11193681	2	739.13 \pm 0.079	0.97 \pm 0.21	9.42 \pm 0.46	120.68 \pm 3.57
11193681	2	782.81 \pm 0.210	1.23 \pm 0.43	8.51 \pm 1.14	9.56 \pm 4.85

Continued on next page

KIC	l	ν_{nl} (μHz)	Γ_{nl} (μHz)	A_{nl} (ppm)	$\ln K$
11193681	2	825.25 \pm 0.145	1.44 \pm 0.66	7.44 \pm 0.71	22.71 \pm 3.07
11193681	2	869.35 \pm 0.203	1.38 \pm 0.66	6.15 \pm 0.76	10.50 \pm 2.83
11193681	2	912.91 \pm 0.500	4.50 \pm 1.47	6.45 \pm 0.74	9.46 \pm 1.93
11193681	2	956.79 \pm 0.634	4.46 \pm 1.88	4.72 \pm 1.16	1.74 \pm 1.91
11395018	0	639.06 \pm 0.363	1.40 \pm 1.93	4.35 \pm 1.09	8.01 \pm 2.08
11395018	0	685.84 \pm 0.336	2.24 \pm 0.94	5.92 \pm 0.89	6.52 \pm 2.06
11395018	0	732.19 \pm 0.095	1.13 \pm 0.23	8.65 \pm 0.56	47.14 \pm 4.26
11395018	0	779.72 \pm 0.045	0.50 \pm 0.13	9.53 \pm 0.70	88.91 \pm 3.40
11395018	0	827.60 \pm 0.071	0.86 \pm 0.17	9.39 \pm 0.60	68.50 \pm 3.36
11395018	0	875.45 \pm 0.073	1.06 \pm 0.19	11.04 \pm 0.61	75.99 \pm 3.46
11395018	0	923.36 \pm 0.099	1.42 \pm 0.28	9.34 \pm 0.54	65.38 \pm 3.28
11395018	0	971.15 \pm 0.679	3.23 \pm 1.22	7.49 \pm 1.69	5.25 \pm 3.16
11395018	1	631.59 \pm 0.118	0.65 \pm 0.32	4.49 \pm 0.67	12.23 \pm 2.12
11395018	1	667.43 \pm 0.083	0.66 \pm 0.17	6.29 \pm 0.57	44.30 \pm 1.22
11395018	1	707.89 \pm 0.120	1.22 \pm 0.25	7.56 \pm 0.54	53.09 \pm 1.37
11395018	1	740.25 \pm 0.109	1.15 \pm 0.25	7.67 \pm 0.54	83.87 \pm 3.59
11395018	1	763.93 \pm 0.090	1.22 \pm 0.19	9.93 \pm 0.54	118.45 \pm 1.60
11395018	1	805.77 \pm 0.073	1.21 \pm 0.17	12.96 \pm 0.61	—
11395018	1	851.44 \pm 0.058	0.98 \pm 0.15	13.90 \pm 0.67	250.63 \pm 1.69
11395018	1	897.47 \pm 0.087	1.65 \pm 0.22	13.13 \pm 0.55	—
11395018	1	940.70 \pm 0.102	1.59 \pm 0.25	10.10 \pm 0.50	124.64 \pm 1.57
11395018	1	965.71 \pm 0.179	1.17 \pm 0.75	5.88 \pm 1.68	1.05 \pm 2.95
11395018	1	997.63 \pm 0.505	6.47 \pm 1.48	8.20 \pm 0.61	11.42 \pm 1.03
11395018	2	680.68 \pm 0.436	2.97 \pm 1.51	6.31 \pm 0.99	6.34 \pm 2.11
11395018	2	728.36 \pm 0.215	0.96 \pm 0.63	4.39 \pm 0.73	10.46 \pm 4.05
11395018	2	775.34 \pm 0.170	1.62 \pm 0.44	7.66 \pm 0.60	62.42 \pm 3.06
11395018	2	823.49 \pm 0.105	1.36 \pm 0.25	9.30 \pm 0.56	66.26 \pm 3.27
11395018	2	871.38 \pm 0.088	1.19 \pm 0.23	9.67 \pm 0.58	68.50 \pm 3.29
11395018	2	918.12 \pm 0.145	1.62 \pm 0.36	7.33 \pm 0.53	48.10 \pm 2.92
11395018	2	967.67 \pm 0.809	3.49 \pm 2.30	6.69 \pm 3.09	1.09 \pm 2.94
11414712	0	500.00 \pm 0.058	0.31 \pm 0.10	2.58 \pm 0.37	13.46 \pm 1.94
11414712	0	543.80 \pm 0.067	0.40 \pm 0.16	2.82 \pm 0.37	7.54 \pm 5.45
11414712	0	586.64 \pm 0.061	0.59 \pm 0.12	4.56 \pm 0.33	22.84 \pm 5.95
11414712	0	629.18 \pm 0.059	0.74 \pm 0.12	5.70 \pm 0.33	26.37 \pm 3.91
11414712	0	672.76 \pm 0.057	0.69 \pm 0.12	8.39 \pm 0.55	16.15 \pm 5.65
11414712	0	716.74 \pm 0.037	0.59 \pm 0.08	8.60 \pm 0.41	85.11 \pm 7.43
11414712	0	760.62 \pm 0.051	1.02 \pm 0.12	9.55 \pm 0.37	58.18 \pm 5.03
11414712	0	804.49 \pm 0.057	1.02 \pm 0.13	8.18 \pm 0.35	51.54 \pm 7.66
11414712	0	849.29 \pm 0.281	1.33 \pm 0.52	3.75 \pm 0.97	4.54 \pm 4.12
11414712	0	893.48 \pm 0.128	1.74 \pm 0.35	4.70 \pm 0.33	8.38 \pm 4.57
11414712	0	937.76 \pm 0.115	0.94 \pm 0.80	2.98 \pm 0.87	5.40 \pm 5.03
11414712	0	984.61 \pm 0.527	1.66 \pm 1.51	1.98 \pm 0.52	6.18 \pm 3.65
11414712	0	1027.11 \pm 0.386	3.63 \pm 1.17	2.70 \pm 0.29	9.57 \pm 1.12
11414712	1	513.88 \pm 0.120	0.32 \pm 0.17	2.51 \pm 0.38	9.10 \pm 1.69
11414712	1	535.48 \pm 0.176	0.32 \pm 0.19	2.15 \pm 0.40	4.79 \pm 2.43
11414712	1	561.69 \pm 0.072	0.37 \pm 0.10	4.33 \pm 0.32	69.55 \pm 1.56
11414712	1	591.94 \pm 0.053	0.34 \pm 0.08	4.65 \pm 0.32	89.28 \pm 4.65
11414712	1	615.17 \pm 0.037	0.30 \pm 0.06	5.45 \pm 0.33	158.80 \pm 2.33
11414712	1	645.59 \pm 0.034	0.35 \pm 0.06	6.52 \pm 0.33	253.34 \pm 2.25
11414712	1	674.37 \pm 0.144	0.40 \pm 0.14	6.77 \pm 0.63	38.81 \pm 5.54
11414712	1	702.97 \pm 0.043	0.64 \pm 0.10	9.27 \pm 0.40	528.40 \pm 8.66
11414712	1	739.02 \pm 0.043	0.67 \pm 0.09	10.82 \pm 0.42	628.54 \pm 13.77
11414712	1	771.13 \pm 0.044	0.58 \pm 0.08	9.30 \pm 0.37	525.74 \pm 2.14
11414712	1	794.59 \pm 0.044	0.75 \pm 0.11	9.81 \pm 0.40	145.35 \pm 10.14
11414712	1	830.71 \pm 0.067	1.29 \pm 0.25	8.69 \pm 0.29	356.64 \pm 1.90
11414712	1	871.93 \pm 0.081	1.32 \pm 0.23	7.15 \pm 0.25	270.15 \pm 1.83
11414712	1	913.42 \pm 0.124	2.08 \pm 0.38	5.74 \pm 0.23	121.88 \pm 1.61
11414712	1	946.16 \pm 0.148	1.15 \pm 0.40	3.07 \pm 0.26	44.37 \pm 3.58
11414712	1	968.19 \pm 0.135	1.24 \pm 0.36	3.28 \pm 0.24	67.31 \pm 3.95
11414712	1	1006.65 \pm 0.437	4.17 \pm 1.17	3.23 \pm 0.28	11.82 \pm 0.96

Continued on next page

KIC	l	ν_{nl} (μHz)	Γ_{nl} (μHz)	A_{nl} (ppm)	$\ln K$
11414712	2	539.99 \pm 1.028	0.72 \pm 1.01	0.72 \pm 0.54	-0.76 \pm 3.10
11414712	2	582.53 \pm 0.118	0.47 \pm 0.20	3.20 \pm 0.34	21.68 \pm 5.13
11414712	2	625.49 \pm 0.112	0.52 \pm 0.18	4.27 \pm 0.31	54.95 \pm 3.32
11414712	2	667.45 \pm 0.088	0.55 \pm 0.21	4.59 \pm 0.30	80.78 \pm 5.52
11414712	2	712.59 \pm 0.077	0.94 \pm 0.24	7.38 \pm 0.33	197.41 \pm 5.74
11414712	2	756.69 \pm 0.076	0.68 \pm 0.16	7.53 \pm 0.32	167.30 \pm 3.85
11414712	2	800.08 \pm 0.123	1.96 \pm 0.40	7.53 \pm 0.38	121.91 \pm 5.62
11414712	2	846.29 \pm 0.191	1.38 \pm 0.20	8.34 \pm 0.49	40.99 \pm 3.67
11414712	2	888.94 \pm 0.190	1.90 \pm 0.61	5.17 \pm 0.33	40.82 \pm 3.30
11414712	2	935.05 \pm 0.701	4.21 \pm 1.51	4.86 \pm 0.78	7.39 \pm 3.91
11414712	2	979.08 \pm 0.308	2.86 \pm 1.91	2.87 \pm 0.51	8.23 \pm 3.64
11414712	3	728.90 \pm 0.416	0.45 \pm 0.45	1.55 \pm 0.57	1.28 \pm 3.33
11414712	3	816.65 \pm 0.299	1.23 \pm 0.90	2.28 \pm 0.36	5.28 \pm 1.15
11414712	3	861.20 \pm 0.225	0.79 \pm 0.68	1.95 \pm 0.31	-4.00 \pm 1.30
11771760	0	426.46 \pm 0.084	0.81 \pm 0.20	8.12 \pm 0.64	51.02 \pm 2.72
11771760	0	457.89 \pm 0.189	0.60 \pm 0.40	6.86 \pm 2.44	1.53 \pm 3.85
11771760	0	489.15 \pm 0.077	1.10 \pm 0.20	11.22 \pm 0.64	43.99 \pm 4.67
11771760	0	521.74 \pm 0.085	1.24 \pm 0.20	12.50 \pm 0.69	49.51 \pm 4.84
11771760	0	554.30 \pm 0.082	0.73 \pm 0.15	14.36 \pm 1.44	3.53 \pm 4.38
11771760	0	586.64 \pm 0.137	1.24 \pm 0.32	9.20 \pm 0.93	12.74 \pm 4.16
11771760	0	619.32 \pm 0.419	1.44 \pm 0.68	9.63 \pm 4.20	-0.22 \pm 2.65
11771760	0	652.03 \pm 0.254	1.33 \pm 0.66	6.36 \pm 1.41	4.79 \pm 3.47
11771760	1	439.74 \pm 0.049	0.52 \pm 0.11	9.03 \pm 0.62	89.02 \pm 1.53
11771760	1	456.94 \pm 0.105	0.98 \pm 0.26	13.46 \pm 1.68	1.37 \pm 3.86
11771760	1	475.06 \pm 0.058	0.81 \pm 0.14	11.14 \pm 0.61	113.59 \pm 1.61
11771760	1	495.42 \pm 0.042	0.50 \pm 0.11	9.40 \pm 0.62	129.03 \pm 4.22
11771760	1	512.73 \pm 0.050	0.75 \pm 0.13	12.09 \pm 0.63	162.22 \pm 4.93
11771760	1	536.11 \pm 0.046	0.72 \pm 0.10	13.24 \pm 0.63	187.96 \pm 1.69
11771760	1	554.95 \pm 0.068	0.30 \pm 0.17	8.44 \pm 2.08	3.27 \pm 4.44
11771760	1	575.74 \pm 0.084	1.40 \pm 0.24	12.02 \pm 0.60	169.96 \pm 4.24
11771760	1	601.74 \pm 0.085	1.19 \pm 0.21	9.85 \pm 0.55	66.81 \pm 1.48
11771760	1	619.78 \pm 0.490	1.20 \pm 0.63	6.09 \pm 4.47	-0.37 \pm 2.70
11771760	1	641.17 \pm 0.154	2.06 \pm 0.42	9.58 \pm 0.64	67.29 \pm 3.63
11771760	1	669.99 \pm 0.273	3.49 \pm 0.80	9.27 \pm 0.67	18.23 \pm 1.08
11771760	2	422.48 \pm 0.065	0.56 \pm 0.17	7.54 \pm 0.67	48.37 \pm 2.61
11771760	2	454.69 \pm 0.069	0.64 \pm 0.20	8.56 \pm 0.84	19.98 \pm 4.05
11771760	2	486.41 \pm 0.072	0.73 \pm 0.18	8.44 \pm 0.67	36.52 \pm 4.52
11771760	2	518.64 \pm 0.094	1.20 \pm 0.26	10.40 \pm 0.75	38.76 \pm 4.66
11771760	2	551.32 \pm 0.084	1.03 \pm 0.19	10.40 \pm 0.68	48.61 \pm 4.37
11771760	2	583.88 \pm 0.282	2.01 \pm 0.66	8.29 \pm 1.16	11.66 \pm 4.11
11771760	2	616.83 \pm 0.547	2.54 \pm 1.06	6.88 \pm 1.72	2.38 \pm 2.69
11771760	2	649.15 \pm 0.541	3.79 \pm 1.39	8.18 \pm 1.57	3.70 \pm 3.47
12508433	0	561.73 \pm 1.138	0.99 \pm 1.31	0.34 \pm 0.35	-0.31 \pm 0.22
12508433	0	606.11 \pm 0.054	0.33 \pm 0.10	3.30 \pm 0.39	14.87 \pm 5.72
12508433	0	649.93 \pm 0.033	0.32 \pm 0.06	5.55 \pm 0.40	50.08 \pm 6.46
12508433	0	694.35 \pm 0.023	0.28 \pm 0.04	7.72 \pm 0.47	81.50 \pm 4.78
12508433	0	739.27 \pm 0.023	0.30 \pm 0.03	9.34 \pm 0.54	20.39 \pm 7.58
12508433	0	784.16 \pm 0.029	0.48 \pm 0.06	11.70 \pm 0.56	240.78 \pm 5.06
12508433	0	829.02 \pm 0.023	0.35 \pm 0.05	11.11 \pm 0.59	156.25 \pm 9.46
12508433	0	874.20 \pm 0.039	0.62 \pm 0.08	8.23 \pm 0.39	63.27 \pm 4.34
12508433	0	919.73 \pm 0.086	1.14 \pm 0.20	5.14 \pm 0.31	24.86 \pm 3.83
12508433	0	965.49 \pm 0.156	1.30 \pm 0.34	3.36 \pm 0.31	9.52 \pm 3.70
12508433	0	1011.75 \pm 0.282	2.03 \pm 0.81	3.23 \pm 0.48	4.76 \pm 3.66
12508433	1	579.21 \pm 0.120	0.32 \pm 0.13	3.22 \pm 0.39	14.28 \pm 1.96
12508433	1	598.89 \pm 0.061	0.16 \pm 0.07	2.87 \pm 0.37	11.23 \pm 4.34
12508433	1	627.12 \pm 0.032	0.26 \pm 0.04	5.23 \pm 0.38	121.51 \pm 2.05
12508433	1	657.33 \pm 0.041	0.28 \pm 0.05	4.65 \pm 0.34	80.44 \pm 5.23
12508433	1	678.99 \pm 0.035	0.29 \pm 0.05	6.66 \pm 0.41	219.27 \pm 2.25
12508433	1	713.41 \pm 0.026	0.28 \pm 0.04	8.32 \pm 0.46	237.33 \pm 5.45
12508433	1	740.55 \pm 0.021	0.25 \pm 0.01	8.45 \pm 0.49	107.75 \pm 7.68

Continued on next page

KIC	l	ν_{nl} (μHz)	Γ_{nl} (μHz)	A_{nl} (ppm)	$\ln K$
12508433	1	768.34 ± 0.022	0.27 ± 0.02	13.12 ± 0.60	983.39 ± 2.55
12508433	1	806.09 ± 0.025	0.32 ± 0.04	14.40 ± 0.68	341.16 ± 33.77
12508433	1	836.04 ± 0.019	0.25 ± 0.01	9.19 ± 0.43	423.39 ± 58.67
12508433	1	860.40 ± 0.036	0.55 ± 0.08	9.07 ± 0.41	469.30 ± 2.12
12508433	1	900.02 ± 0.040	0.48 ± 0.09	8.24 ± 0.37	409.21 ± 2.12
12508433	1	942.41 ± 0.097	1.17 ± 0.26	5.37 ± 0.28	100.35 ± 1.69
12508433	1	978.63 ± 0.154	0.95 ± 0.42	3.40 ± 0.30	32.53 ± 1.28
12508433	1	999.12 ± 0.160	0.85 ± 0.57	3.04 ± 0.32	22.70 ± 2.83
12508433	1	1037.64 ± 0.547	1.62 ± 1.02	2.53 ± 0.37	9.54 ± 0.96
12508433	2	556.92 ± 1.057	0.66 ± 0.92	0.81 ± 0.62	-0.15 ± 0.19
12508433	2	602.58 ± 0.201	0.29 ± 0.21	2.14 ± 0.57	2.04 ± 4.88
12508433	2	646.12 ± 0.084	0.34 ± 0.11	3.59 ± 0.36	27.77 ± 5.79
12508433	2	690.66 ± 0.050	0.36 ± 0.09	5.26 ± 0.35	107.81 ± 4.13
12508433	2	736.12 ± 0.031	0.29 ± 0.02	7.58 ± 0.38	174.77 ± 7.48
12508433	2	779.59 ± 0.026	0.28 ± 0.03	9.07 ± 0.44	472.95 ± 4.56
12508433	2	825.07 ± 0.039	0.48 ± 0.08	9.39 ± 0.44	408.15 ± 8.59
12508433	2	870.87 ± 0.046	0.55 ± 0.10	7.35 ± 0.37	198.95 ± 4.02
12508433	2	915.50 ± 0.099	0.91 ± 0.30	4.89 ± 0.32	63.44 ± 3.33
12508433	2	962.09 ± 0.096	0.42 ± 0.13	3.09 ± 0.29	17.61 ± 3.15
12508433	2	1007.36 ± 1.018	1.90 ± 2.00	1.97 ± 0.76	1.40 ± 3.06
12508433	3	707.13 ± 1.134	0.57 ± 0.85	0.72 ± 0.61	-1.04 ± 3.23
12508433	3	752.05 ± 0.150	0.39 ± 0.19	2.46 ± 0.35	5.68 ± 1.96
12508433	3	797.33 ± 0.057	0.30 ± 0.06	3.77 ± 0.28	50.12 ± 4.77
12508433	3	842.62 ± 0.083	0.37 ± 0.13	3.03 ± 0.28	29.26 ± 8.90
12508433	3	887.94 ± 0.117	0.51 ± 0.22	2.63 ± 0.30	19.42 ± 2.01